Feasibility study on condition-based maintenance of bolts using ultrasonic waves

Kavin Kumar Kandasamy Nanthakumar

Master of Science Thesis

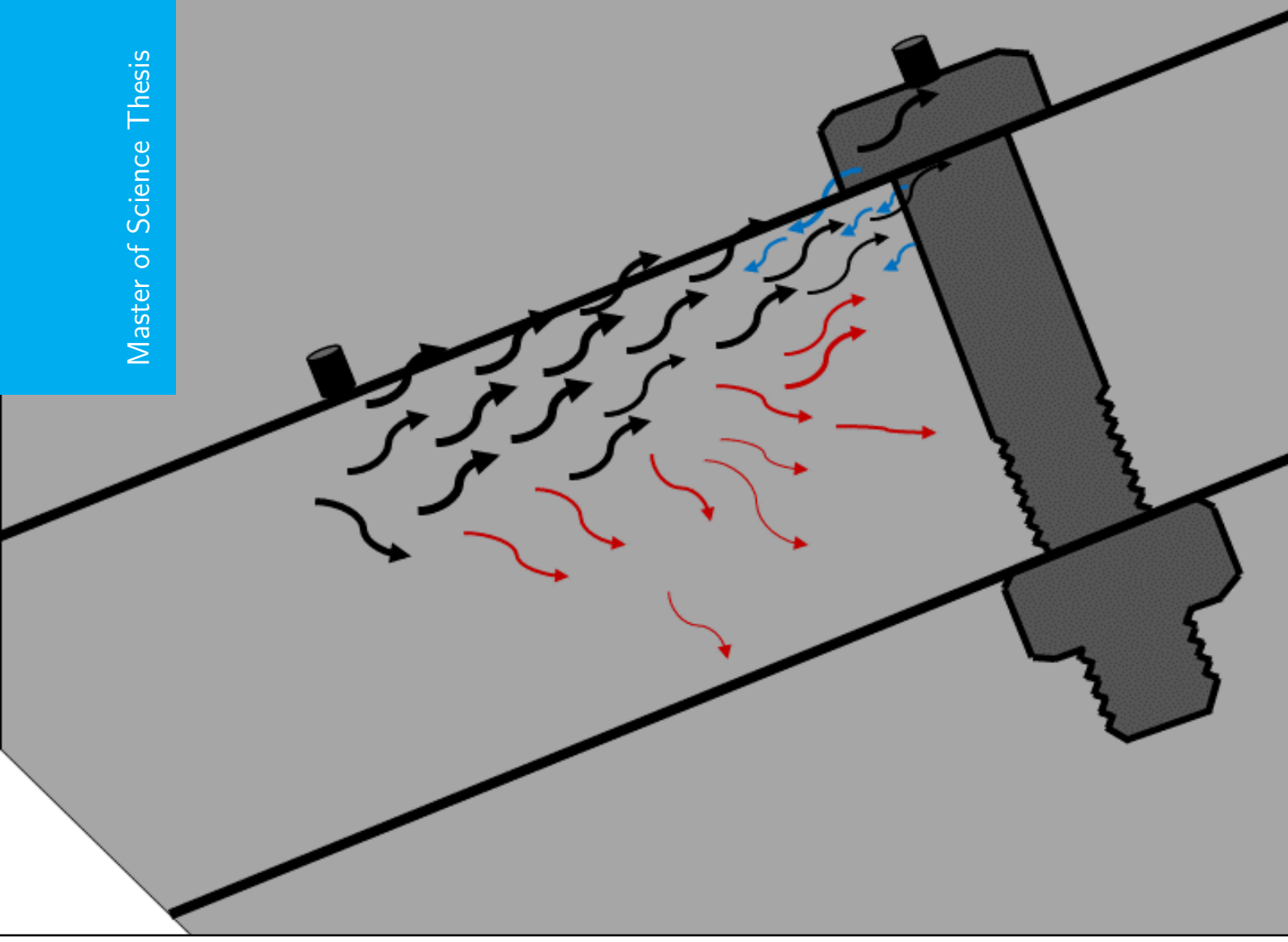

TU Delft Delft University of Technology

Feasibility study on condition-based maintenance of bolts using ultrasonic waves

Master of Science Thesis

For the degree of Master of Science in Offshore and Dredging Engineering at Delft University of Technology

Kavin Kumar Kandasamy Nanthakumar

December 15, 2021

Student number: 4994248

Thesis committee:		
	Dr. MSc. L. Pahlavan	TU Delft, Supervisor, Chair
	Dr. Ir. J. H. Den Besten	TU Delft
	Prof. Dr. MSc. C. Kassapoglou	TU Delft
	Ir. B. Scheeren	TU Delft
	MSc. F. Riccioli	TU Delft
	MSc. R. Walc	Bluewater Energy Services, External Supervisor
	Ir. A. Vollebregt	Bluewater Energy Services

TU Delft Delft University of Technology

bluewater

Abstract

The safety of offshore assets such as wind turbines, offshore cranes, and turret mooring systems partly relies on the integrity of heavy-duty bolted joints. These critical connections can be of different dimensions and exposed to monotonic and cyclic loading. Despite being small components of a structure, bolts need to be maintained appropriately to ensure structural safety and reliability. The integrity of bolted joints can be assured by checking for adequate preload. In addition, fatigue failure resulting from preload loss is of primary concern, as it can occur suddenly without any visible changes. Hence, bolts should be re-tightened periodically to ensure sufficient preload. However, in offshore conditions, this countermeasure leads to high maintenance costs while exposing the crew to unfavourable conditions and risks.

This research focuses on the feasibility of condition-based maintenance of bolts using ultrasonic waves. An energy attenuation method has been implemented for this feasibility research. The main objective is to establish a proper methodology and hypotheses for preload detection. Furthermore, along with preload detection, the feasibility of crack detection was investigated. Finally, the proposed methodology and hypotheses were validated by performing experiments and numerical simulations.

The experimental and numerical results verify the proposed methodology by showing an increasing trend in the energy and the power of the transmitted ultrasonic wave for increasing preload. Also, the feasibility of crack detection using the same setup has been positively evaluated.

The obtained results suggest that the ultrasonic waves can be employed to monitor bolts for condition-based maintenance. Additionally, a number of relevant research activities are recommended based on this study.

Table of Contents

List of Figures

List of Tables

Acknowledgements

This research was conducted as part of my master program in Offshore and Dredging Engineering at TU Delft. This thesis study was conducted by collaborating with the mechanical department of Bluewater. Bluewater owns and manages a fleet of FPSOs designed to operate in the most unrelenting environmental conditions. Bolts of different sizes are installed in these FPSOs, and it is critical to monitor and maintain these bolts to ensure their safe operation. Therefore, this thesis is framed as a result of interest in bolt monitoring.

First, I would like to thank my supervisor, Pooria Pahlavan, for giving me this opportunity and for taking the initiative to engage with Bluewater to make this research smooth and successful. The world of structural health monitoring was new to me, and he assisted me along the way by guiding and giving me some valuable feedback. His advice on professional attitudes, communication, and decision making were the most valuable life skills I learnt. I am eternally happy and grateful for his willingness to assist and support me at any time.

I want to extend my gratitude to Arjen Vollebregt and Radoslaw Walc for giving me this opportunity to work with Bluewater. Their ready availability for discussions and timely feedback on the practical applicability helped me improve this research. I am incredibly grateful for their support throughout this research period.

Furthermore, I would like to thank Filippo Riccioli for his time and effort in assisting me during this research period. Being an all-time energetic person, he kept me motivated and transferred positivity during my downtimes. I would also like to express my gratitude to Bart Scheeren and Arno Huijer for their assistance in the technical discussions during this research period. Apart from the mentioned names, I want to thank all the other people who helped me to mould this research. Additionally, I would like to thank Henk den Besten and Christos Kassapoglou for accepting the invitation to participate in the graduation committee.

Finally, I want to thank god, my parents, brother, grandparents, and friends for always being there and supporting me. I would not be the person I am today without them. Special thanks to all my friends in Delft for making this journey a memorable one. In particular, I want to thank Maha for her guidance in using overleaf to format this report better.

I hope the reader enjoys this research!

Delft, University of Technology
December 15, 2021

Kavin Kumar Kandasamy Nanthakumar

Chapter 1

Introduction

1-1 Background and motivation

Bolts are employed in various industries due to their high load-carrying capacity, reliability, and ease of deployment. Their primary function is to hold the parts together and transfer forces from one part to another [1]. Thus, despite being small components of a structure, bolts are an inevitable component that must be maintained appropriately to ensure structural safety and reliability. Based on the load transfer phenomena, bolted joints can be classified as tension joints and shear joints [2]. Figure 1-1 shows the two types of bolted joints.

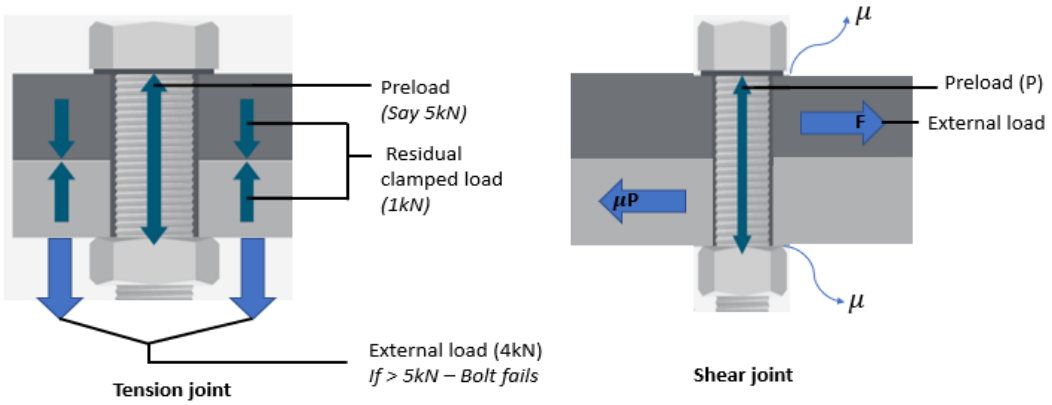

(a) *Tension joint - external load is balanced by the existing preload.* **(b)** *Shear joint - frictional resistance from the preload acts against the external load.*

Figure 1-1: *Force balance of tension and shear bolted joint [2]*

Tension joints transfer tensile force acting along the bolt axis. If the external axial load increases beyond the preload, the bolt loses its pretension, and failure happens. The shear joint predominantly transfers shear force between the clamped parts through friction [1]. Friction between the bolt head and the component is proportional to the preload [3]. The

existing preload resists the external load for both types of joints. Therefore, bolt preload is a critical design requirement for tension and shear joints.

The safety of offshore assets (e.g., wind turbines, turret mooring system, single-point mooring system, and swivel) relies on the strength of the bolted joints. These critical connections are of different dimensions and are subjected to monotonic and cyclic loading [4]. This implies that they have to withstand high dynamic stress and bending moments [5]. Figure 1-2 shows the possible location of critical bolted connections in the offshore industry.

(a) *Foundation pile attached to the turbine support structure by means of a bolted ring flange connection [6].*

(b) *Critical bolted connection in an FPSO turret swivel system [7].*

Figure 1-2: *Example of critical bolted connections in offshore structures.*

An offshore wind turbine includes hundreds of different-sized bolts varying from M12 to M72, holding the critical structural and mechanical components together [8]. In such circumstances, the failure of a single bolt can compromise the structural integrity of the entire structure. Therefore, operators and regulatory agencies are interested in the integrity of bolted connections. The integrity can be assured by checking for adequate preload of the bolt.

1-2 Impact of bolt failure

Accidents due to bolt failure have occurred in the past [4]. By thorough investigation of these accidents, bolt preload loss was reported as a significant reason for the collapse [9]. Inadequate bolt pretension and maintenance have been reported as the root cause for the failure of the tower connection in the Chinese Zuoyun wind farm [10]. A case study on the Vestas wind turbine that collapsed in December 2015 in Lemnhult, Sweden, helps to understand the effect of bolt pretension and fatigue [9]. The Swedish accident investigation authority reported that the bolts holding the first and second tower section together had suffered fatigue and could no longer withstand the normal operating loads. The loss of pretension force in the joint was found as the principal reason for fatigue [11].

The importance of bolted joints is not restricted only to the offshore and renewable energy industries. Derailment at Grayrigg in February 2007 resulted in a severe accident because of a bolt failure [12]. The main reason for the accident was the relaxation and loosening of bolted joint that connected the switch rails with the rail track. According to Kaminskaya

Figure 1-3: *The collapsed Lemnhult wind tower with the bottom part anchored to concrete base [9].*

and Lipov [13], self-loosening of bolted joints accounts for almost 20% of overall mechanical system failures. The time spent to rectify such failures can be equal to 10% of the total machine lifetime. Fatigue failure resulting from preload loss is the main concern, as it can occur rapidly without any visible changes.

1-3 Problem statement

For maintaining adequate preload, bolts need to be re-tightened periodically during the service life of the structure. However, this countermeasure leads to high maintenance costs while exposing the crew to unfavourable conditions and risks [14]. Hence, monitoring such phenomena in the field is crucial for safe and efficient condition-based maintenance. As a result, research on detecting bolt looseness and fatigue crack has gained significant attention. Bolt monitoring for condition-based maintenance can be achieved using *Structural Health Monitoring (SHM)*.

The main research question of this study is,

> *'Can preload and fatigue cracks in bolts be monitored to achieve condition-based maintenance?'*

To answer the above question, a literature study is first conducted to assess the state of the art techniques for preload and fatigue crack monitoring of bolts. Based on that, the existing knowledge gap, extended research questions and a proposed research direction are discussed.

1-4 Structural Health Monitoring

SHM is the process of gathering and analyzing data from on-board sensors to assess the structural integrity [15]. Contrary to conventional *Non-Destructive Technique (NDT)*, SHM is an integral part of the structure to facilitate continuous in-situ monitoring without compromising the structural function. SHM aims to identify and describe structural damage or degradation

at the earliest possible time in a safer, faster, and more effective way [16]. SHM can be split into four stages: (i) operational evaluation, (ii) data collection, (iii) feature extraction, and (iv) diagnostic and prognosis [15][17][18]. Figure 1-4 outlines the flow chart regarding four stages of SHM.

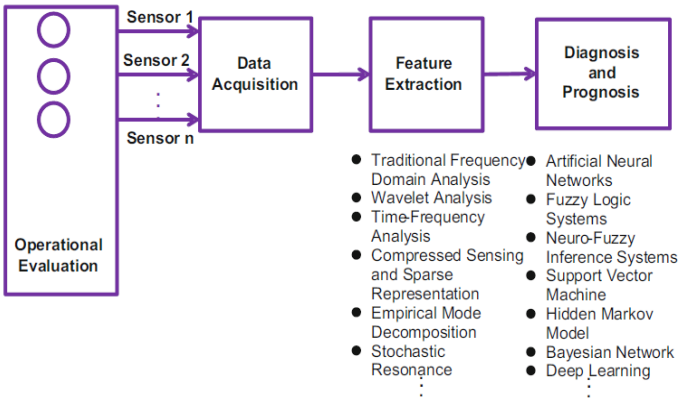

Figure 1-4: *Stages of structural health monitoring [15].*

SHM methods are broadly classified into active and passive methods [19]. When a structure response is measured for a given controlled excitation, it is of the active method (e.g., guided waves). For passive methods, damage initiation will cause the signal to be created (e.g., acoustic emission). Rytter [20] proposes a classification system with four levels of damage identification, as follows:

Level 1: Finding damage in the structure

Level 2: Finding the damage location

Level 3: Quantifying the damage severity

Level 4: Predicting the remaining structural service life

SHM assists the damage identification system in reaching level 3 and level 4.

1-5 Literature review

From the above context, it is clear that the loss of bolt pretension is of serious concern. In addition, fatigue cracks in the bolts might occur for various reasons, and early detection of them will avoid catastrophic failure of the structure. Therefore, this section focuses on state-of-the-art bolt preload monitoring and crack detection.

1-5-1 Bolt preload detection

Bolt preload detection can be broadly classified into conventional and non-conventional approaches [21].

Conventional approaches

To determine the condition of a bolted joint, conventional approaches measure the bolt axial load directly.

Using a torque wrench is one of the standard ways to check bolt preload. The torque wrench approach is based on the linear relationship between torque and preload [22][23]. The torque is checked periodically to ensure that the bolt is taut. However, there is a distinct drawback that much of the torque applied for preload check is lost due to thread friction. As a result, it is not considered a reliable method. Moreover, maintenance personnel needs to inspect the bolt pretension periodically, which exposes them to unnecessary risks. Hence using a torque wrench is an unsafe and ineffective method for condition-based maintenance.

Furthermore, load cells placed on bolts directly measure axial load. Though load cells can precisely measure the preload, they must be attached to each bolt. As a result, installing load cells for each bolt will be an expensive method of preload monitoring. *Direct tension indicator (DTI)* can also measure the bolt pretension. DTI is a protruding washer that goes under the nut or bolt head. Axial force is estimated by measuring the distance between the protruding feature and the face of the nut. The drawback of the method is that washer should be designed for every joint and periodically inspected [24].

Non-conventional approaches

Non-conventional approaches evaluate the integrity of the bolted system using secondary parameters rather than the direct bolt axial load. Several SHM methods have been investigated for condition-based maintenance of bolt pretension. Such as vibration-based approach, ultrasonic wave method and impedance-based method.

Vibration-based method

Vibration-based damage identification has been used widely in civil, mechanical, and aerospace industries [25]. Vibration signals measured from a structure with bolted joints are analysed to evaluate the bolt preload loss. Any changes in the bolted joints influence the dynamics of the structure. External excitation is imposed on the structure to check for dynamic properties like damping and stiffness changes. Changes in dynamic properties are identified through global dynamic characteristics such as natural frequency, modal shape, and modal damping [26].

Todd et al. [27] explored the effects of change in fastener clamp force on the modal properties of a constrained beam. The study found that modal properties are less sensitive to change in clamp force. Vincent Caccese et al. [28] used low-frequency modal analysis and a high-frequency transmittance function to investigate the effect of varying the preload on 16 bolts in a composite panel. The study concluded that variations in bolt preload had less impact on the fundamental frequency. Meanwhile, the change in transmittance function between two sensors for varying preload showed better results. Butner et al. [29][30] revealed how much a change in bolt preload affects the contact dynamic characteristics of a bolted joint. The study found that modal frequency decreases for the decrease in preload while modal damping

increases. Weiwei Xu [31] observed similar behaviour for a single bolted joint. The research found that modal damping was more sensitive to preload change than modal frequency. The study also found that the natural frequency and damping of the structure could determine the change in bolt tension only when the preload was below 30% of the bolt yield strength. Transverse vibration was used by Si Mohamed Sah et al. [32] to study the preload change. The result suggested that the first vibration mode was more sensitive to preload variation of a clamped structure with a single bolt.

Other than preload change, changes in contact friction, boundary condition, and structural deterioration can impact structural dynamic properties [31]. The loss of preload of a single bolt in a multi-bolted joint is a local effect and has less impact on the overall structural dynamic characteristics. Thus, the vibration-based method has low predictive and tracking capacity to preload change due to the insensitivity to local changes [33]. In addition, this method also requires baseline data from an undamaged structure to evaluate the current status. Therefore, with the current vibration-based research studies, it will be a challenge to reach damage identification levels 2 and 3.

Impedance-based method

The primary idea of the impedance-based method is to use high-frequency excitation to determine the impedance of the structure. Impedance, expressed as the ratio of the applied voltage to resultant current, is measured using an impedance analyser and piezoelectric transducers [34]. The measured electrical impedance is proportional to the mechanical impedance of the structure [35]. The damage can be detected by comparing the measured impedance to the baseline measurement. Thus, changes in impedance reflect structural changes, which link to preload variation.

Ritdumrongkul et al. [36][37] investigated the impedance change caused by bolt loosening in an aluminum bar. Observation showed that when bolts are loosened, resonance peaks shift to lower frequencies, and peak amplitude decreases. Junhua Shao et al. [38] performed experiments on M12 and M16 bolts to investigate the effect of varying bolt preload. The relationship between frequency shift and preload change was found to be linear. Linsheng Huo et al. [39] adapted the impedance-based method to a smart washer, where the peak frequency of the measured impedance was utilised to detect changes in preload. The amplitude of peak frequency is found to decrease with loss in preload.

To evaluate the structural integrity of the bolted joint, Wait et al. [40] compared the impedance method and lamb wave propagation technique. The excited lamb waves did not exhibit substantial difference between the clamped and unclamped states. However, the damage index of impedance method could identify the difference between the different preload states. Likewise, Yun-Kyu et al. [41] used impedance method and guided wave technique to test the structural integrity of bolted joint. The study explored the sensitivity of the applied techniques. In conclusion, compared to guided waves, the impedance-based method showed more sensitivity to bolt looseness.

Compared to vibration-based techniques, the high-frequency input for impedance testing improves the sensitivity of local damage identification. Although the impedance method is sensitive to bolt preload changes, it requires a high-precision impedance analyser with a

high sampling rate [21]. However, further study in the impedance-based method can lead to level 3 damage detection. Hence, the impedance-based method will lead to an expensive and complicated online monitoring system with the current research.

Ultrasonic method

High-frequency ultrasonic waves can be used to detect damage or loose bolts. Many researchers have investigated various ultrasonic wave approaches based on the acoustoelastic principle, and the principle of true contact area [42].

Ultrasonic - acoustoelastic principle

The acoustoelastic principle states that tensile stress causes elongation of the bolt as well as a change in ultrasonic velocity [43]. As a result, the ultrasonic length of the bolt increases due to pretension.

Time Of Flight- single wave method

The ultrasonic length can be calculated by multiplying the *Time Of Flight (TOF)* of a longitudinal or transverse wave with half the wave velocity. TOF can be obtained using either the pulse-echo technique or the phase shift method [44]. Bolt preload can be calculated from the ultrasonic stretch of a bolt in a stressed state [45]. Kyung-young et al. [44] estimated the bolt preload by obtaining TOF using the phase shift method. The results showed a linear relationship between the ultrasonic length and bolt load. A similar linear relationship was obtained by Jesse R. Meisterling [46] using a permanent transducer on the bolt head. Although the TOF single wave method can determine the preload with the established linear relationship, it is sensitive to various factors [42]. Moreover, a precise measuring instrument with a high sampling rate is necessary to measure the TOF in the range of nanoseconds [47]. Also, the TOF method is susceptible to environmental noise and needs to be compensated for temperature variations. Furthermore, the approach requires a baseline measurement to determine the bolt axial load, making it a challenge for continuous monitoring.

Time Of Flight- two-wave method or velocity ratio method

Johnson et al. [48] investigated the velocity ratio technique to overcome the dependency on baseline measurement. The axial force is estimated from the ratio of longitudinal to transverse wave flight time. Yasui et al. [49] used a transducer that simultaneously generated both longitudinal and a transverse wave to measure the bolt preload. Preload is estimated by measuring the ratio of time of flight of a transverse wave to a longitudinal wave in the bolt stressed state. The experiment results showed a linear relationship of axial force to the TOF ratio. Nohyu Kim et al. [50] proposed mode converted ultrasonic approach, where the TOF is determined using a spherical acoustic lens and ray analysis. The TOF ratio is computed by dividing the peak value of LL (longitudinal-longitudinal mode) by the peak value of LT (longitudinal-transverse mode). Elastic constants were also determined from ultrasonic wave velocity. Experiments used 10MHz ultrasonic waves resulted in a linear relationship between axial load and TOF ratio. But the velocity ratio method requires precise measurement of several variables such as acoustoelastic coefficients, material constants, zero stress velocities, and effective length of the bolt to calculate TOF. In addition, other effects due to residual stress and temperature change should be investigated. Similar to TOF single wave technique, the velocity ratio method demands a high-precision data collection system [51]. However, the approach can determine bolt axial load without a baseline measurement. The need for accurate TOF and material constants makes it difficult method for continuous monitoring.

Ultrasonic - Contact dynamic principle

All surfaces at the micro-level have roughness, and as a result, the asperities are distributed unevenly over the surface. Because of the presence of asperities, contact between surfaces is limited to their peaks. Thus, the real contact area is the summation of the contact area of each asperity. As discussed previously, the sensitivity of ultrasonic waves in detecting local damage is high. Therefore, when an ultrasonic wave interacts with the interface, it is partially transmitted and reflected based on the true contact area as shown in Figure 1-5. Drinkwater et al. [52] used the concept to study the aluminium-aluminium interface condition.

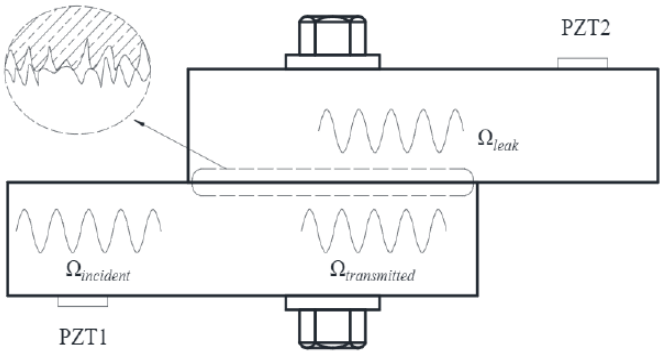

Figure 1-5: *Representation of bolted joint interface and wave transmission [42].*

Similarly, all bolted joints have partial contact at their interface. As the torque applied to the bolt increases, the true contact area increases. Contact dynamic technique is further classified into linear and nonlinear methods [53]. The linear method considers the bolted joint interface stiffness linear and ignores all the nonlinear contact effects. The Wave energy attenuation and time-reversal methods are commonly used linear contact dynamic techniques. However, when a wave interacts with an improper contact interface, contact non-linearity happens. This contact non-linearity generates second or higher-order harmonics called *Contact Acoustic Non-linearity (CAN)* [54][55]. Second-order harmonic and spectral sideband approaches are two common CAN techniques researched. Both ultrasonic excitation and vibration are simultaneously used in the sideband technique, whereas only ultrasonic excitation is used in the second harmonic method [33].

Contact dynamic linear approach - Energy attenuation method

J. Yang et al. [56][57] developed an attenuation-based diagnostic method for detecting multi-level bolt looseness on a thermal protection panel of a space vehicle. Figure 1-6 shows the protection panel considered for the study. Ultrasonic waves are sent from a bracket-mounted washer embedded with a sensor and received on the other side of the bracket. The research utilised contact area changes to assess the looseness of a panel and bracket. Changes in contact area for varying preload affected the power spectrum and wave energy of the transmitted signal. The data was collected for three different torque values. The dissipation of wave energy from the bracket to the panel was observed to increase with increasing preload. The dissipation reduced the energy and power spectrum of the received waveform at the other end of the bracket for increasing preload. But the methodology and experiment design followed are specific to the particular application of thermal protection panel. Doyle et al. [58] observed that the transmitted signal phase shift was linear to the varying bolt torque level.

However, the phase difference between the waves for different torque levels were significantly less. Additionally, phase shift detection requires an in-depth investigation of the involved geometry, wave speed, effect of temperature change, and sensor placement.

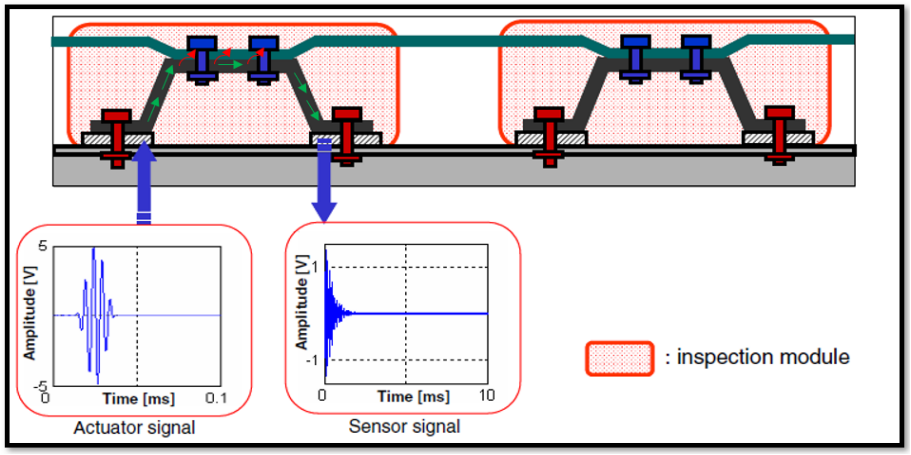

Figure 1-6: *Protection panel prototype used for bolt loosening study by J Yang et al. [57].*

Meanwhile, Wang et al. [59] used the transmitted energy to detect bolt preload in a lap joint. The study showed that for M12 and M16 bolts, transmitted energy increases for increasing torque value. However, a saturation was found to occur after a particular torque value, as shown in Figure 1-7(a).

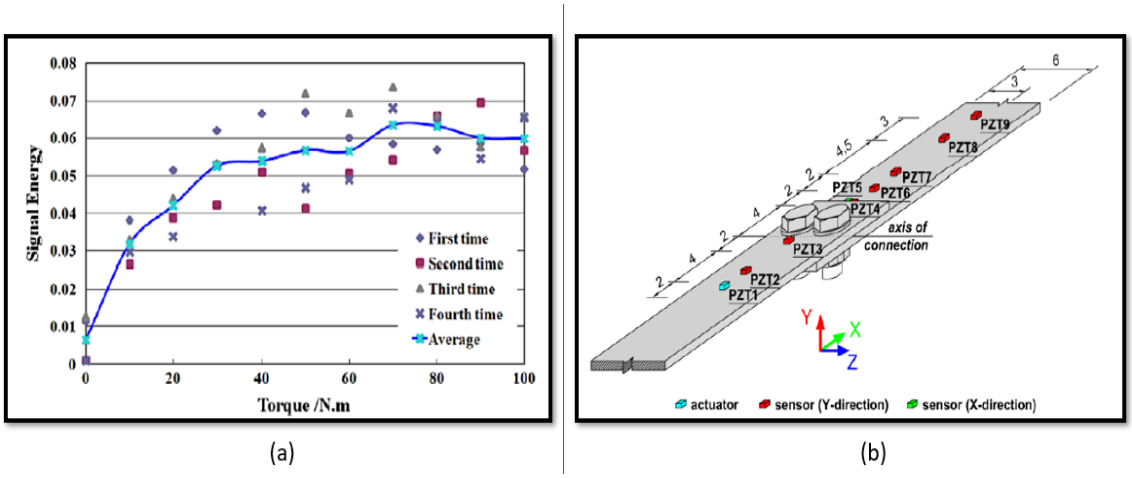

Figure 1-7: *(a) Signal energy variations for different torque level [59]. (b) Sensor arrangement considered for the experimental investigation by R Kedra et al. [60].*

Experimental investigation of ultrasonic wave propagation on a bolted (M12) lap joint was performed by Kedra et al. [60]. Figure 1-7(b) shows the sensors arrangement considered for the experimental investigation. Only sensor nine from the considered experimental setup showed an increasing trend for transmitted energy with increased preload. Hence, accurate sensor positioning, excitation frequency, and proper time window selection need to be further investigated to improve the diagnostic possibilities. Y Heyue et al. [61] used two annular disc washers with a machined concave and convex surface along with piezoelectric sensors.

Based on the preload, the contact between the machined surface changed and accordingly, the transmitted energy changed. A linear relationship was found between the preload and the transmitted energy.

Contact dynamic linear approach - Time reversal method

The guided waves used in wave energy attenuation are complex because of several aspects such as wave reflections, mode conversion, dispersion, and scattering. Thus, a time-reversal wave-based technique was introduced by Fink et al. [62] for monitoring the condition of bolted joints. A time-reversal method reverses the received signal and sends it back to the source location to reconstruct the input signal. The refocused peak amplitude was used as the tightness indicator for preload detection by Parvasi et al. [21]. The proposed tightness index rises in accordance with the bolt torque. The time-reversal procedure is depicted in Figure 1-8. A similar result was seen in Wang Tao et al. [63] investigation, where the plates of different surface roughness were employed. The study revealed that the trend for preload change is more evident for plates with high roughness. Similar to the energy attenuation method, the saturation phenomenon was more evident for low surface roughness. In addition, the time-reversal technique depends on linear reciprocity. The presence of any non-linearity such as crack can make the approach subject to error. For the time-reversal technique, the sensors are also required to act as actuators [21]. Hence time reversal technique is quite complex for online monitoring than the energy attenuation method.

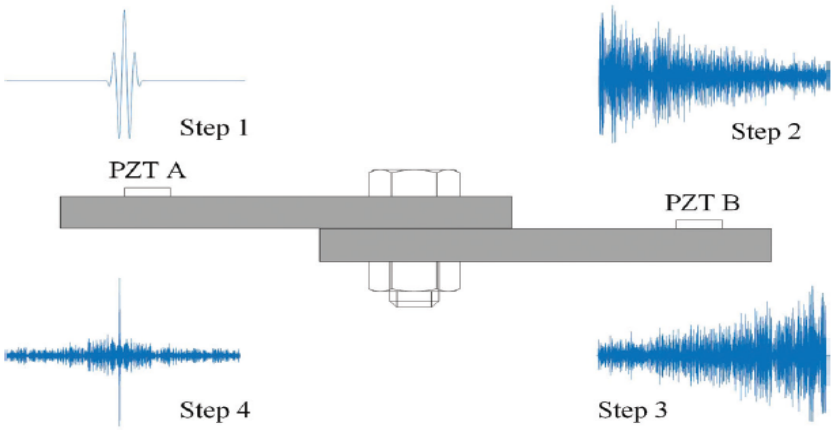

Figure 1-8: *Time reversal wave transmission procedure [64].*

Contact dynamic nonlinear approach - Second-harmonic method

When the excited acoustic wave wavelength exceeds the interface gap distance, the wave tends to open and close the gap locally. As a result, contact non-linearity happens. This non-linearity generates second-order harmonics in the frequency spectrum [65][66]. Amerini et al. [53] estimated the bolt pretension from the non-linearity index based on power spectral density. The study found that the spectral amplitude difference between the carrier frequency and the second harmonic reduces when the bolt loosens. However, the investigation did not observe any apparent change in damage index when the applied torque exceeds 6 Nm for the M10 bolt. Thus, it can be difficult for a second-harmonic method to detect the early bolt looseness. Similarly, Yi Yang et al. [67] studied the influence of the second harmonic generated by guided waves. The study showed better results for the antisymmetric mode than

the symmetric mode of guided waves. Non-linearity from measuring instruments, material, and other damage can affect the second harmonic magnitude. Moreover, second-harmonic peak amplitude is small, making it difficult to differentiate from other nonlinear effects.

Contact dynamic nonlinear approach - Sideband method

Contact non-linearity in the sideband method occurs due to both low-frequency vibration and high-frequency ultrasonic wave excitation. Opening and closing of the contact interface happen due to vibration. Due to this, the high-frequency ultrasonic signal will partly decouple during the opening period and remains unaffected during the closing period of vibration. Amplitude modulated signal is received due to this contact non-linearity [53]. The damage index for detecting bolt looseness was calculated by taking the mean of the magnitude of left and right sidebands. The damage index value tends to reduce for increasing preload [68]. Also, Meyer et al. [69] found that sidebands are sensitive to various other factors such as impact amplitude, impact location, exciting frequency, and sensor location. The drawback of the sideband method is the need for a shaker or impact hammer to generate low-frequency vibration in addition to piezoelectric transducers [33]. With the proposed experimental setup, online monitoring using the sideband method becomes more complex and expensive.

1-5-2 Numerical simulation

The wave propagation in bolted structures is complex due to several aspects such as dispersion, boundary reflections, and attenuation of waves. The *Finite Element Method (FEM)* can be applied to study wave propagation in complex geometries. Also, simulations from the FEM can provide insights to check results for different experimental setups, source frequencies, and sensor positions.

Clayton et al. [70] developed a three-dimensional finite element model for guided wave propagation in bolted joints. The study modelled the contact region of the lap joint as different linear models representing different bolt preload to reduce the computational cost. However, the method was employed only to detect tight or loose states and found it challenging to implement for different preload levels. Doyle et al. [71] examined the use of FEM software (ABAQUS) to model bolted joint interfaces. Results suggested that the linear model with contact properties available in the software does not properly replicate the effect of surface roughness. Later, J Bao et al. [72] used 2D contact elements to model the bolted joint interface for transient wave propagation analysis in ANSYS. Still, the results could not properly implement the effect of surface roughness on wave transmission. Parvasi et al. [21] performed a numerical analysis for the time-reversal technique in ABAQUS. The bolted joint interface is improved by adding a randomly generated surface height value to the appropriate in-contact surface nodes. The true contact area is generated from the plastic deformation of the fluctuating random nodes for different preload in the quasi-static analysis. However, the mesh size considered for the model was in the order of 1.8mm, which is much larger than the actual micro-asperities on rough surfaces.

Moreover, the usage of commercial FEM programs requires 6 to 10 nodes per wavelength of the exciting wave, resulting in a large number of nodes and a correspondingly high computational cost [73]. Hence, a higher-order *Spectral Finite Element Method (SEM)* can be preferred to investigate high-frequency wave propagation phenomena. Furthermore, the tech-

nique reduces computational time by using higher-order shape functions like Legendre-Gauss Lobatto-Lagrange-polynomial [74].

1-5-3 Bolt crack detection

Bolt crack detection can be broadly classified into conventional and non-conventional approaches as discussed below:

Conventional approaches

Liquid penetrant, magnetic particle, and ultrasonic testing are the NDT techniques used for crack detection in bolts, welds, and other structural surfaces. Ultrasonic and magnetic particle testing is preferred for crack detection in fasteners [75][76]. However, maintenance personnel must visit the site periodically to check for cracks present in bolts. Thus, the conventional methods cannot be implemented for continuous monitoring of cracks. For a detailed information on conventional NDT techniques Willcox et al. [77] can be referred.

Non-conventional approaches

Similar to preload monitoring, an impedance-based method can be used to detect cracks in bolts. Initiation of cracks changes the mechanical impedance of the structure, which can be utilised to detect cracks. As discussed earlier, implementing an impedance-based method for online monitoring is complex due to the need for a highly precise impedance analyser with a high sampling rate.

However, the ultrasonic technique is more sensitive to local damage like cracks and contact variation. Furthermore, the SHM using ultrasonics can be accomplished utilising an active or passive approach. For the active ultrasonic approach, the high-frequency signal is used as a source to check for the change in the received signal to detect cracks. M Suh et al. [78] used the delay in the rayleigh waves caused by the thread tip diffraction to detect cracks in the bolt thread root. Similarly, phased array ultrasonic crack detection for bolts was investigated by M. Moles et al. [79]. The investigation used a small jig at the bolt head to hold the scanner, which generated the S-scan image. By interpreting the generated S-scan image presence of cracks can be detected.

Nonlinear ultrasonic features can also detect cracks by identifying new signal components in the frequency spectrum. Mevissen et al. [80] used non-linear ultrasonic method to detect cracks in turbine blade. The nonlinear parameters were observed to change with crack size. Results indicated that the proposed technique could detect in-service cracks. However, active ultrasonic crack detection requires a pulsing system with a sensor array, increasing the complexity of online monitoring.

Acoustic Emission (AE), on the other hand, is a well-known passive technique. Damage or cracks cause the structure to release energy in the form of elastic waves. Collecting these waveforms makes it possible to deduce valuable information about the damage [81][82]. Furthermore, the AE features from the waveform gives information about the crack growth

phenomenon. As a result, this research study focuses on the acoustic emission approach for crack detection.

Acoustic Emission approach

The AE technique can be used to detect and track cracks [81][83]. When a crack begins to grow, strain energy is released in the form of elastic waves. The primary emission of acoustic waves is due to crack tip movement. Acoustic emission is also produced due to secondary activity caused by crack face friction between the asperities. Therefore, the crack can be detected by analysing the characteristics of the produced acoustic wave [81][82][83]. As discussed in Chapter 2-1-4, signal features such as counts (hit rates), amplitude, energy, and rise time can be used as characteristics of the waveform. Clustering the AE signals can help in a more detailed analysis of the crack.

Additionally, the AE method enables tracking of the crack growth rate. Several studies have been carried out for crack rate prediction using AE. Traditionally crack growth rate can be estimated using the Paris law as expressed below [84],

$$\frac{\mathrm{d}a}{\mathrm{d}n} = C(\Delta K)^m \tag{1-1}$$

where a is the crack length, n is the number of cycles, ΔK - stress intensity factor range, and C and m are the material constants.

The log-log plot derived from the Paris law shows the relation between crack growth rate and stress intensity factor range. The crack propagation curve is classified into three regions: region I represent crack initiation, region II represents stable crack growth, and region III is an unstable crack growth to failure. Figure 1-10 shows the relation between crack growth rate and stress intensity factor.

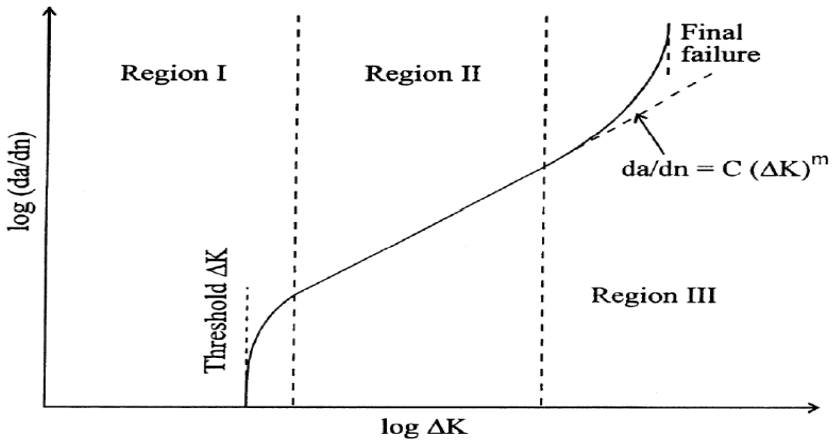

Figure 1-9: *Relation between crack growth rate and stress intensity factor [84].*

Furthermore, an equation similar to Paris law establishes the relation between AE count rate and stress intensity factor range [83][85].

$$\frac{d\eta}{dn} = B(\Delta K)^p \tag{1-2}$$

where η is the number of counts/hits, n is the number of cycles, ΔK is the stress intensity factor range, and B and p are constants.

Similarly, a relationship between the AE energy rate and the crack growth rate is established [82, 86].

$$\frac{\mathrm{d}a}{\mathrm{d}N} = D\left(\frac{\mathrm{d}U}{\mathrm{d}N}\right)^q \tag{1-3}$$

with D = C/(B_e^q) , q = m/p, $\frac{\mathrm{d}a}{\mathrm{d}N}$ the crack growth rate, and $\frac{\mathrm{d}U}{\mathrm{d}N}$ the AE absolute energy rate

Jianguo et al. [86] conducted a fatigue test on compact tension specimens made of ASTM572G50 to determine the relationship between AE absolute energy rate and count rate to crack growth rate. The experiment results in Figure 1-10 show the relationship between AE absolute energy and AE counts corresponding to crack growth rate. Keshtgar et al. [87] examined the capability of the acoustic emission technique to detect crack growth during a high cycle fatigue test. The experiment was conducted on an aluminum alloy. The results indicated that a proposed averaging index called AE intensity is linearly related to crack growth. Urbahs et al. [88] performed a bench fatigue test on a helicopter tail boom bolted joint. Using the AE parameters (amplitude, count, and energy) from the acoustic emission, the bolt fracture was predicted 26 to 44 flight hours before the collapse. Using acoustic emission, Pascoe et al. [89] investigated the fatigue crack growth within a single load cycle. The results suggested that the crack growth might occur during both loading and unloading of a double cantilever beam. It was also observed that the strain energy release rate must exceed a crack growth threshold for cracks growth to occur.

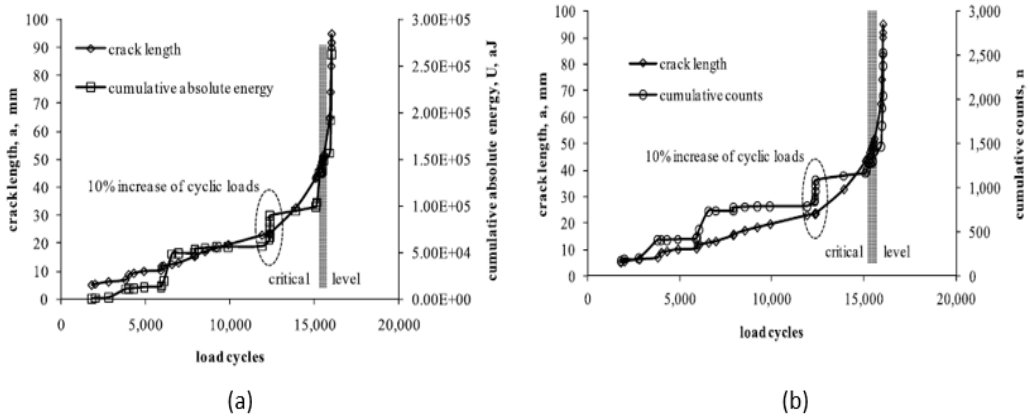

Figure 1-10: *(a) Relation between crack length and AE cumulative absolute energy versus load cycle (b) Relation between crack length and AE cumulative counts versus load cycle [86].*

From the above studies, it is clear that the AE features can be utilised to determine the crack growth rate. Thus, by utilising acoustic emission to detect and track a crack, the longevity of the bolt could be extended. However, most investigations are confined only to Mode 1 fatigue cracks in a plate under a constant amplitude load cycle. More experiments on bolts and multiaxial fatigue need to be investigated for bolt fatigue crack tracking. Even though AE tracking can predict crack propagation and remaining lifetime, further studies need to be done. Considering the time limit, the crack tracking part will not be further explored in this study. Hence, this feasibility study is limited to crack detection alone.

1-5-4 Literature review conclusion

Preload detection

Significant research has been conducted on detecting the loss of bolt preload. This literature study examined both conventional and non-conventional preload and crack detection approaches. The ultrasonic technique was found to be more sensitive to local changes caused by bolt preload than vibration and impedance-based approaches. The contact dynamic approach has demonstrated the most promising results with simple theory among the ultrasonic methods discussed. Considering the accuracy, cost, and feasibility, the energy attenuation method can be more appropriate for continuous bolt preload monitoring. Therefore, the energy attenuation method is preferred for this feasibility study.

Crack detection

Numerous research has been reported on crack detection and tracking in bolts. From the presented crack detection approaches, the AE technique is preferred for this feasibility study. As discussed in Section 1-5-3, it can be understood that further investigation is necessary to develop a reliable crack tracking approach. Therefore, based on the scope of this feasibility study, only the crack detection part using AE will be investigated.

1-6 Knowledge gap

1-6-1 Preload monitoring

Experimental setup

Most research investigations on the energy attenuation method have used a flat lap joint fastened by a single bolt, with an actuator and sensors mounted on the top and bottom plates (as shown in Figure 1-5 and Figure 1-7). Since the positions of sensors were on the plate, change in the true contact area between the plates due to preload variation was the influencing parameter. However, the change in preload of an individual bolt is a local effect. Thus, the setup investigated in the previous studies cannot track individual bolt preload in multi-bolted joints. Additionally, the sensor configuration utilised in previous research results in significant signal attenuation and scattering, as the ultrasonic wave must travel through thick plates to assess large size bolts. Also, the experiments conducted were only on bolt sizes of range M2 to M16.

Signal processing

The response received by the sensor comprises the source signal along with complicated interference patterns due to scattering, reflections, dispersion and mode conversion. The previous studies took the entire recorded signal for analysis and have not sufficiently examined the appropriate time window selection and signal processing methodology. Additionally, the conducted research so far seems predominantly baseline-dependent and requires signals from the intact situation for comparison to determine the present preload.

To bridge knowledge gap for preload monitoring

A feasible preload detection methodology that tracks individual bolts regardless of the dimension needs to be investigated. Further exploration of optimal sensor position, excitation frequency, proper time window selection, and signal processing methodology is also required to detect preload loss in a multi-bolted joint.

1-6-2 Numerical simulation

In most previous studies, the commercial FEM was adopted to perform numerical analysis of the wave propagation phenomena in bolted joints. However, there is still a knowledge gap in implementing the influence of interface surface roughness on the transfer of ultrasonic waves in FEM. As discussed in Section 1-5-2, SEM will be preferred for this feasibility study. As a result, the feasibility of adopting SEM for numerical analysis of wave propagation in bolted joints, including the effect of the interface, is yet to be investigated.

1-6-3 Crack detection

As mentioned in Section 1-5-3, numerous research studies illustrate the feasibility of using AE technique for crack detection. However, it is realised that the optimal sensor position

is required to collect acoustic emission signals to detect cracks effectively. Furthermore, no research has been found on integrating preload and crack detection utilising the same experimental configuration. Therefore, an experimental setup with optimal sensor positions to detect preload loss and crack must be examined.

1-7 Research question

Given the existing state of the art and knowledge gaps, the main research question is modified as,

> *'Can ultrasonic waves be utilized for monitoring of individual bolts in a multi-bolted joint independent of its size and length ?'*

The research question is answered with the help of the following sub-questions that are clustered according to chapters,

1-7-1 Background knowledge

- What causes the bolt to lose its preload?
- Which location of the bolt is highly prone to fatigue cracks?
- What are ultrasonic waves, and what parameters can be extracted from them?

1-7-2 Analytical framework and methodology

- Which sensor position and experimental setup would be appropriate for preload monitoring of each bolt in a multi-bolted joint?
- What methodology and hypotheses can be used to monitor preload in bolts?
- Which part of the collected signal can be chosen to verify the hypothesis?

1-7-3 Experiment results and hypothesis verification

- What is the influence of the source frequency?
- Can the proposed methodology and hypothesis be applicable for bolts independent of its dimension?
- Can the experimental setup proposed for preload monitoring be also utilised for crack detection in bolts?

1-7-4 Numerical simulation

- How can the change in interface conditions for varying preload be implemented in the SEM to study wave propagation?
- Can the proposed methodology and hypothesis be extended for the passive preload monitoring?

1-8 Research direction

The main research question can be addressed using the proposed research approach as shown in Figure 1-11. First, an analytical framework with a proposed experimental setup is formulated for wave propagation in the bolted joints. Furthermore, the methodology and hypothesis for preload monitoring are introduced. The proposed methodology and hypothesis will be verified with a small-scale experimental setup. Then, with the observations from the small-scale experiments (M12), the same methodology and hypothesis will be tested for different source frequencies in a large size (M64) bolt. Finally, a crack is simulated to investigate if the same experimental setup can detect cracks effectively in bolts.

The SEM model will be utilised for numerical simulation to provide better insights about the wave propagation in the bolted joints. Furthermore, the idea of introducing an interface layer is investigated to simulate the change in wave transmission for varying preload. Thus, the proposed hypothesis and methodology will be verified with experimental observations and numerical simulations.

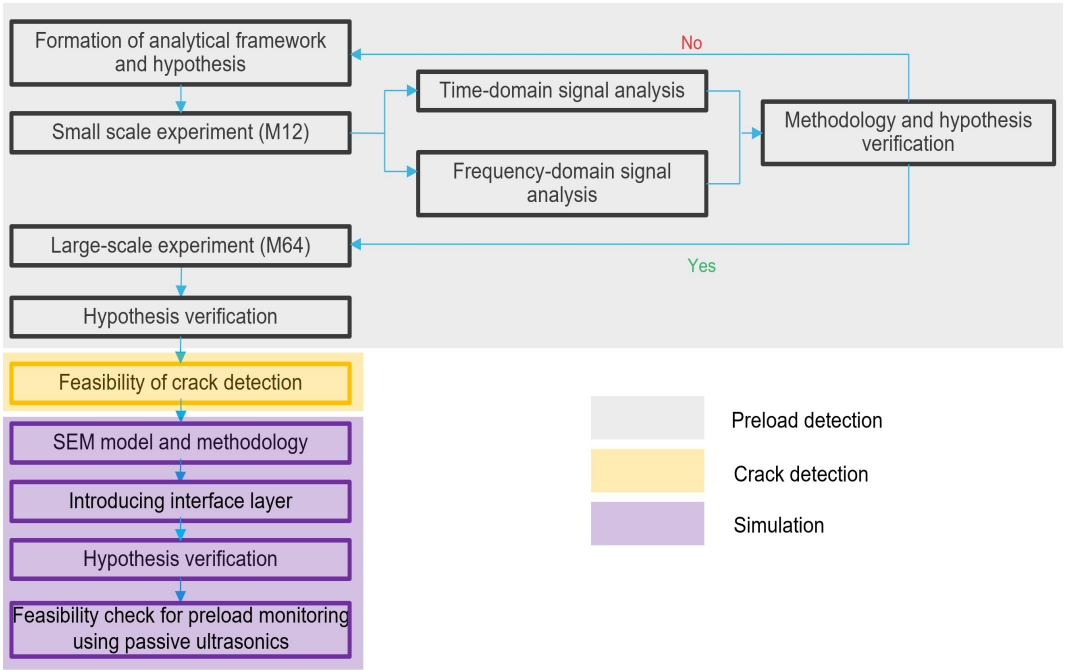

Figure 1-11: *Proposed research direction.*

1-9 Report outline

The thesis report is structured in the following way.

Figure 1-12: *Report outline.*

Chapter 2

Background knowledge

This chapter presents the theoretical background on the topics of pretension loss, bolt fatigue, and ultrasonic waves. This chapter aims to answer the following research sub-questions,

- What causes the bolt to lose its preload?
- Which location of the bolt is highly prone to fatigue cracks?
- What are ultrasonic waves, and what parameters can be extracted from them?

2-1 Preloaded bolts

Mechanical properties of bolts are indicated by their class property. Based on that, bolts of classes 8.8 and 10.9 are allowed to pretension [5].

2-1-1 Tightening method

Bolts can be pretensioned in the following ways [90]

- Torque method
- Combined method (torque + rotating head/nut over an additional angle)
- HRC tightening method
- Direct tensioning indicator method
- Hydraulic bolt tensioner

The above-mentioned tightening procedures have different reliability. Thus the tightening procedure selection will influence the final attained pretension. The present study focuses on monitoring bolt preload independent of the tightening procedure. For a detailed review of tightening methods, Berenbak [90] and Nijgh [91] can be referred.

2-1-2 Pretension loss

Regardless of bolt size, loss of pretension in all preloaded bolts is inevitable. Three phases of pretension loss are recognized: an initial loss, short-term relaxation, and long-term relaxation [91]. Figure 2-1 shows the change of bolt preload over time.

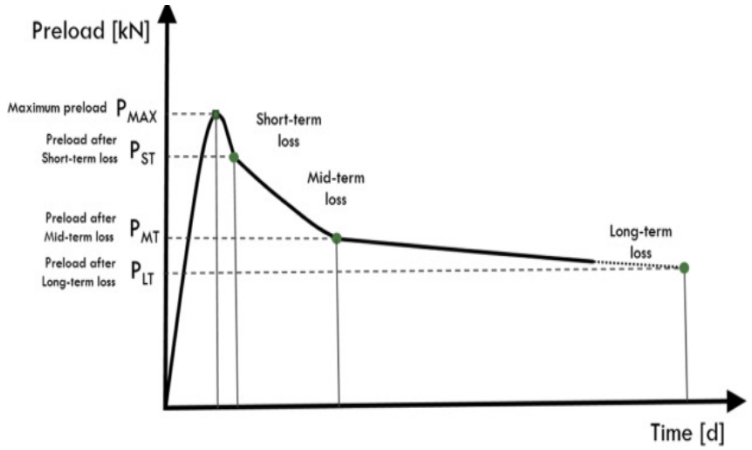

Figure 2-1: *Initial, short-term and long-term preload loss over time [92].*

Initial loss of pretension often happens immediately after bolt tightening. The loss can be reduced by selecting a highly reliable tightening procedure. Loss due to elastic interaction between bolts is unavoidable, as it is difficult to pretension all the bolts simultaneously. The amount of elastic interaction between bolts is directly related to the joint size and bolt spacing [91].

Within the initial 12 hours of preloading, short-term relaxation takes place. The short-term loss is due to several reasons such as bolt bending, non-parallelism of joint, geometric variance, and embedment [93]. By proper installation, all the former reasons could be avoided. Embedment is the plastic deformation of the surface at the interface. Embedding loss usually accounts for only 10% of the total preload loss [94]. This deformation starts immediately after tightening and extends until a perfect fit between the interface surfaces is obtained [95]. Vibrations, stress relaxation, and thermal effects have been reported as driving causes for long-term relaxation [92].

An early study on bolt preload loss due to dynamic axial load is reported by Goodier et al. [96]. They monitored the loss of preload in a bolt of 3/4 in. loaded in the range of 2.2kN to 26.69kN. The study showed that the maximum rotation of nut detected was 2 degrees in 500 cycles. Later, Gerhard H Junker [97] demonstrated that pretension loss occurs when a mating thread or the bearing surface overcomes the static friction. The investigation used DIN 933 M10 bolts subjected to vibration. The investigation showed complete preload loss within 200-500 cycles. In addition, the loosening rate was also observed to be independent of loading frequency and dependent on the amplitude of relative motion per cycle. A study by Junker [97] concluded that the most severe loading that may cause self-loosening in a bolted joint is transverse vibration. Jiang et al. [98] conducted a study on M12 bolts subjecting them to a cyclic displacement. The study suggested that the relative displacement of the two clamped parts is crucial. Also, observed that the self-loosening resistance increased with

clamp force.

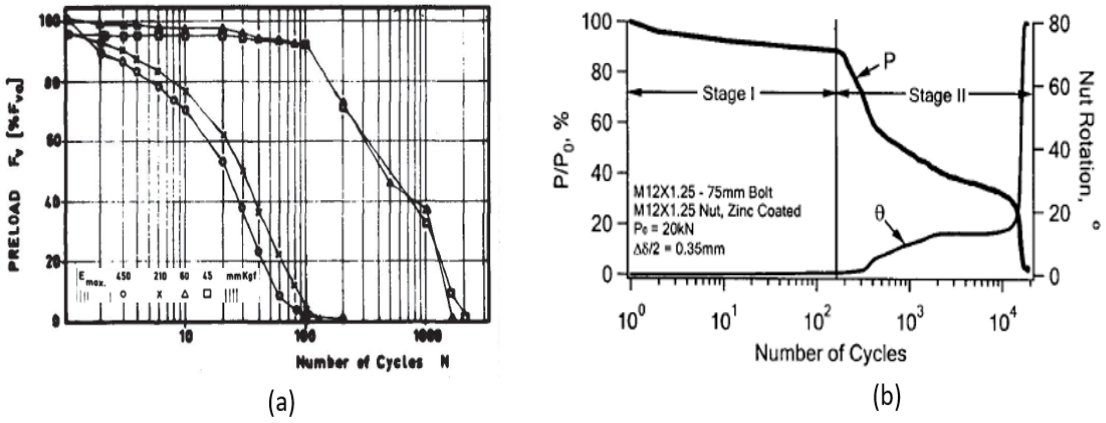

Figure 2-2: *(a) Graph from Junker experiments showing preload percentage vs. the number of cycles, plotted for the different transverse load. Preload decreases as the number of cycles increase for each transverse load [97]. (b)Self loosening sequence showing gradual preload relaxation followed by rapid loosening owing to transverse cyclic load [98].*

Despite extensive research on bolted joint loosening, it is evident that preload loss is inevitable regardless of bolt type, dimension, or mating plate surface treatment [93]. Among several causes leading to bolt relaxation, vibration may cause complete loss of pretension. However, the other reasons stated before may be responsible for a limited amount of bolt relaxation [91][97]. Although appropriate pre-tensioning might eliminate the initial preload loss, monitoring and maintaining proper preload during service remains critical.

2-1-3 Fatigue in preloaded bolts

Bolt fatigue occurs when cyclic load cause progressive, localized, and irreversible damage to the bolt thread or shank. After significant fluctuations, this damage may grow into cracks and eventually lead to fracture [99]. The fatigue failure typically occurs in three stages: crack initiation, crack propagation, and final fracture. A large portion of fatigue life, roughly between 85 to 90% of a total lifetime, exists in the crack initiation stage [100]. Thus, if it is possible to detect the crack during its initiation or propagation stage, the collapse of the joint and structure can be avoided.

Location of fatigue cracks in bolts

Fatigue cracks often occur in joints because of notches, eccentricity in load transmission, corrosion and fretting damage [3]. Figure 2-3(a) depicts possible crack locations in bolt.

Notable stress concentration spots for preloaded tension joints are thread roots, thread run-out, and radius under the bolt head [101]. In addition, the load between the bolt thread and the contact face of the nut is not uniform. As a result, the first six threads take up almost the entire load, where only the first thread undergoes one-third of the total load [102]. Crack initiation in bolt thread for tension joint is shown in Figure 2-3(b). An experimental study by

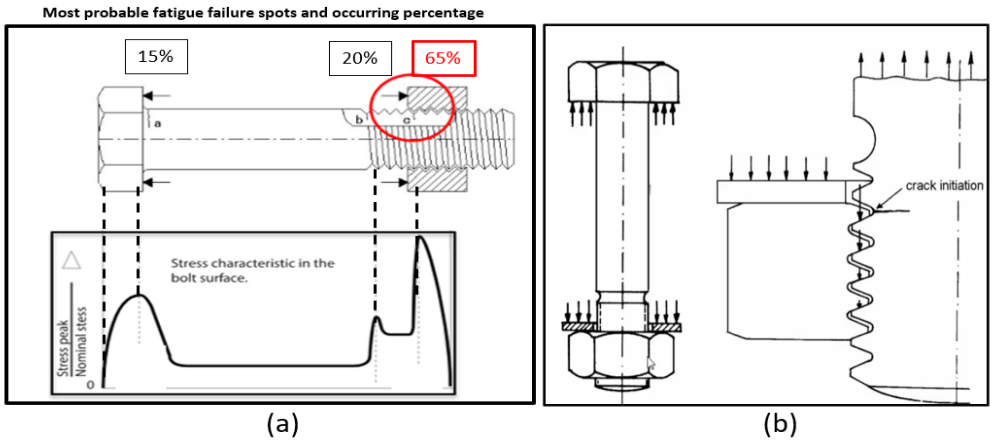

Figure 2-3: *(a) Most probable fatigue failure spots in bolts and their stress characteristic [3] (b) Crack initiation in the first thread of the bolted joint in tension [101]*

Hashimura et al. [103] did not show any crack nucleation at the thread root for the bolts that loosened within $10^2 - 10^3$ vibration cycles. Meanwhile, a crack was observed at the thread root for bolts that loosened between $10^4 - 10^6$ cycles, indicating that high cycle fatigue can occur along with bolt preload loss.

Due to the intense load transmission from the bolt shank, high-stress concentration will occur at the holes in shear joints without preload. On the other hand, preloaded shear joints will not have any stress concentration at the holes. However, fretting occurs at cross-section of the plate due to micro-movements of contact surfaces [100].

Effect of preload on fatigue

The fatigue life of bolts is influenced by various factors, such as the load acting on the bolt, component material, thread pitch, and level of preload present in the bolt. Cracks propagate due to cyclic stress amplitude acting on the joint. As the preload is increased, the stress range amplitude decreases and the mean stress increases. However, the fatigue life is more sensitive to stress amplitude than the mean stress [104]. The fatigue life of the bolt should be unaffected if the applied load does not exceed the pretension load [105]. Therefore a reduction of design preload can result in increased fatigue damage and stress amplitude range [11]. Thus, by maintaining proper preload, fatigue life can be improved greatly.

Cracks may not be apparent at the early stage of fatigue life since the bolt head, and nut hides the fatigue initiation spots. Therefore, monitoring the bolt preload and crack during service is crucial to avoid a catastrophic failure. For this, structural health monitoring serves the purpose.

2-1-4 Ultrasonic waves

Among various available methods, ultrasonic detection is one of the commonly preferred methods for SHM [59]. Furthermore, ultrasonic SHM is often preferred due to its high sensitivity and accuracy, as well as due to its ability to scan large areas at a low-cost [106].

Wave propagation is caused by a pressure difference due to a localized disturbance in a medium. Waves with frequencies greater than 20 kHz are referred to as ultrasonic waves, and they propagate in solids as elastic waves. Acoustic emissions generated by crack and corrosion are also referred to as elastic waves in principle [15]. Ultrasonic waves can propagate through solids in longitudinal and shear modes. Moreover, ultrasonic waves can propagate as surface waves at the interface between two mediums and as lamb waves in a thin medium. The particle displacement in the propagating medium depends on the wave mode, as reported in Figure 2-4.

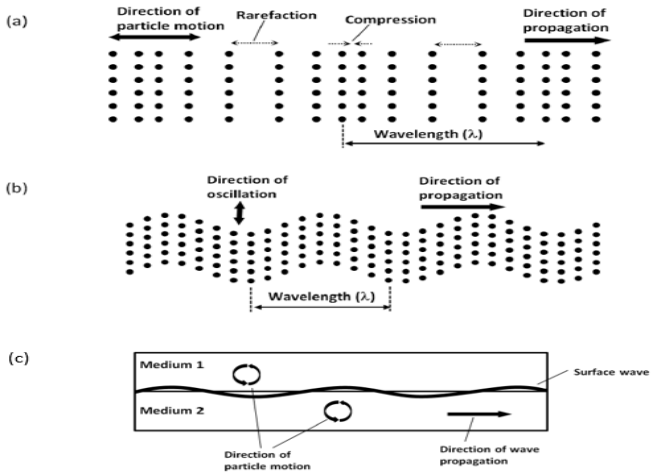

Figure 2-4: *Representation of a) Longitudinal wave b)Shear wave c) Surface wave [107].*

In longitudinal waves, the particle oscillation is the same direction as the wave propagation. On the other hand, in traverse waves or shear waves, the particle oscillation is perpendicular to the wave propagation direction. The surface waves will propagate along a flat or curved surface of a thick solid and penetrate maximum up to a depth of one wavelength. Lamb waves propagate in a thin medium and disperse into several modes at high frequencies [106][107].

Wave attenuation and transmission

Propagating waves lose their intensity due to geometric spreading and material attenuation [108]. Geometric spreading depends on the expansion of wavefront generated. The spreading loss follows a spherical spread rule for body waves from a point source. Equation 2-1 shows the expression to calculate geometric spread loss due to spherical spread rule in decibels [109].

$$SL_b = 20 \log_{10} \left(\frac{r}{x} \right) \tag{2-1}$$

where r is the source sphere radius, and x is the distance travelled from the source.

Meanwhile, the spreading loss for surface waves and guided waves from a point source follows the cylindrical spread rule. Equation 2-2 shows the expression to calculate geometric spread loss due to cylindrical spread rule in decibels [109].

$$SL_s = 20 \log_{10} \left(\sqrt{\frac{r}{x}} \right) \tag{2-2}$$

Material attenuation is a combined result of scattering, wave mode conversion, and energy dissipation. In addition, ultrasonic transmission loss at boundaries is related to acoustic impedance. Wave behaviour is predominantly determined by the media in which the wave propagates. Each medium has its specific acoustic impedance. The transmission and reflection of waves at the interface depend on the acoustic impedance of the two mediums. When an incoming wave travels from a medium of high impedance to a low impedance, wave amplitude increases and vice versa. Acoustic impedance of a medium can be calculated as follows:

$$Z = \rho C \tag{2-3}$$

in this equation, Z denotes the acoustic impedance, ρ is the density of the medium, and C is the wave velocity in the medium.

Wave parameter

The ultrasonic waves can be generated and received by piezoelectric transducers. The collected waves are generally post-processed using advanced signal processing to extract the required information. Characteristics of the received waveform can be defined using various wave parameters such as time of arrival, peak amplitude, energy, hits, and rise time. Figure 2-5 shows an elastic wave with several features in the time-domain. The arrival time specifies the start of a wave where the signal first crosses the threshold. Peak amplitude is the highest absolute signal value measured in a hit. Rise time is the time taken to reach peak amplitude from the arrival time. Energy is calculated by adding the squared sample values of a hit and multiplied by sampling time.

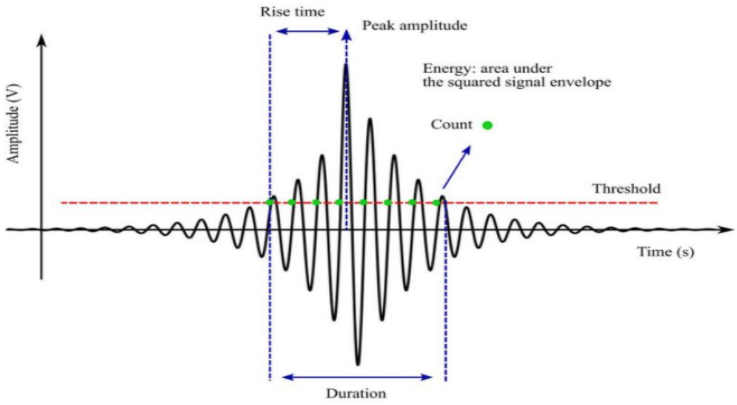

Figure 2-5: *Elastic wave and its features [110].*

2-2 Chapter highlights

From the background knowledge, it is clear that the loss of pretension is ineluctable, and transverse vibration acts to be a severe loading for bolt self-loosening. Moreover, the first thread of the bolt that engages with the nut is prone to crack most of the time. The influence of fatigue was found to increase when the drop in preload increases. Hence, it is clear that monitoring pretension and fatigue cracks in bolts can avoid a catastrophic failure of a structure. In addition, SHM using ultrasonic waves can assist in getting the status of the bolts in service. Following this, Chapter 3 will discuss the analytical framework and methodology proposed for this research study.

Chapter 3

Analytical framework and methodology

In evaluating the feasibility of bolt monitoring using ultrasonics, it is essential to understand the propagation of ultrasonic waves in the bolted joint and its interface. An analytical framework for the propagation and transmission of ultrasonic waves is presented. An experimental setup with various source and sensor positions is proposed. Finally, the methodology and hypothesis proposed based on the analytical framework are discussed. This chapter aims to answer the following research sub-questions,

- Which sensor position and experimental setup would be appropriate for preload monitoring of each bolt in a multi-bolted joint?
- What methodology and hypotheses can be used to monitor preload in bolts?
- Which part of the collected signal can be chosen to verify the hypothesis?

3-1 Introduction

The principle of the chosen preload detection method for this feasibility study is based on the change of true contact area. As discussed in Chapter 1-6-1, the experimental setup adopted in earlier studies has limitations, and to overcome these limitations and bridge the knowledge gap, an experimental setup is proposed. Figure 3-1 shows the preliminary experimental setup considered for the analytical framework. The sensor is on the bolt end, and the actuator is near the plate/nut interface. In addition, a reference sensor is placed in between the actuator and the interface to ensure that the methodology is independent of baseline measurement. The proposed sensor and actuator positions for the analytical framework is expected to have better sensitivity for the preload change as it considers the local contact area changes due to preload variation. The static preload analysis performed also supports the proposed sensor position. Appendix A gives a brief discussion on the static preload analysis performed.

3-2 Analytical framework

An analytical framework for preload and crack detection in bolts[1] is presented below with a representative scheme of the corresponding experimental setup as shown in Figure 3-1 and Figure 3-2.

3-2-1 Analytical framework for preload detection

Preload detection in bolts is estimated by ultrasonic wave propagation through the plate, plate-nut interface, nut, and bolt. An analytical framework including transmission, reflections, and scattering of the ultrasonic wave is proposed. Figure 3-1 illustrates that a source signal(S) from the actuator travels through the plates (W_1 and W_2), through the plate-nut interface (T), and then through the nut and bolt (W_3) to finally reach the measuring sensor. Before reaching the measuring sensor, the signal is generally subjected to scattering, dispersion, mode conversion and multiple reflections.

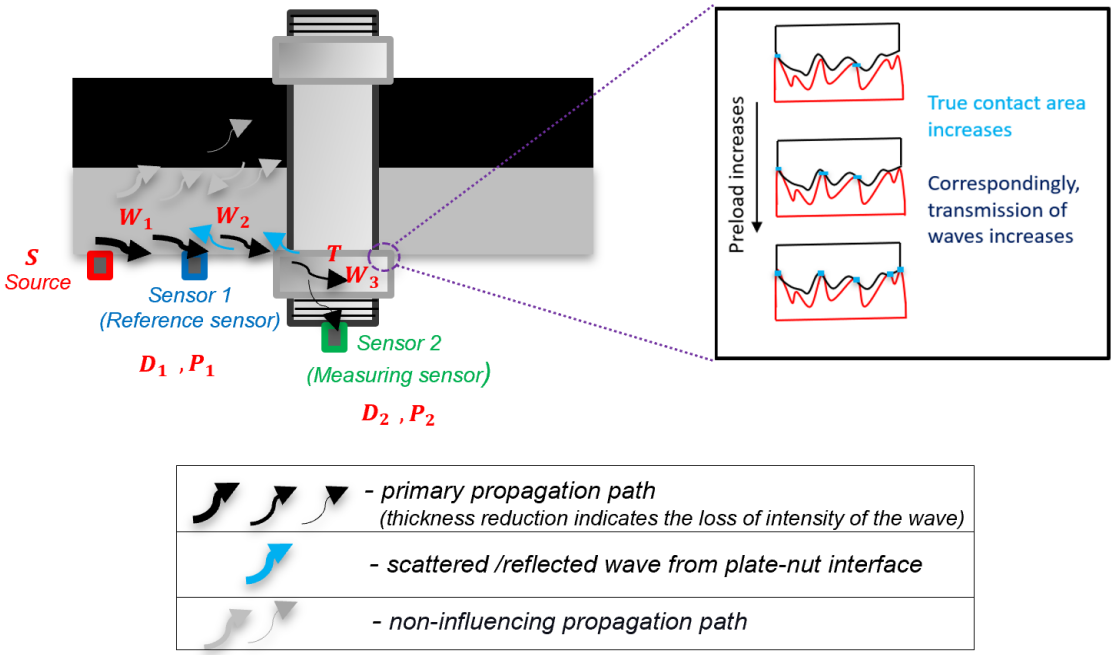

Figure 3-1: *Representation of wave propagation path for preload detection.*

The reference sensor collects information about the propagating source signal (S), including the reflections from the plate-nut interface and other boundaries. Convolution of various propagation functions, wave reflections, and background noise expresses the recorded $\mathbf{P_1}$ (reference sensor signal) and $\mathbf{P_2}$ (measuring sensor signal) signals.

[1] From here the term bolts in this thesis refers to stud bolts.

$$\mathbf{P_1} = D_1(\omega_c)\, W_1(l_s, l_{z1}, m_1, \omega_c)\, S(\omega_c) + P_1^R + P_n + N_E \tag{3-1}$$

$$\mathbf{P_2} = D_2(\omega_c)\, W_3(l_i, l_{z2}, m_2, \omega_c)\, T(l_i, F, m_1, m_2, \omega_c)\, W_2(l_{z1}, l_i, m_1, \omega_c)\, W_1(l_s, l_{z1}, m_1, \omega_c)\, S(\omega_c) + P_2^R + P_n + N_E \tag{3-2}$$

Wherein,

$\mathbf{P_1}$ and $\mathbf{P_2}$ are the signals received by the reference and measuring sensors respectively
m_1 and m_2 represents the influence of plate and bolt material (bolt and nut material properties are assumed to be same),
l_s, l_{z1}, and l_{z2} are the position of source and sensors (reference and measuring) in space,
l_i(Ra) is the location of plate-nut interface asperities which depends on the surface roughness of plate and nut,
ω_c is the centre frequency of the propagating wave,
F represents the bolt preload,
Ra is surface roughness of the plate and nut,
S is the source signal,
W_1 represents wave propagation function of the plate between the actuator and reference sensor,
W_2 represents wave propagation function of the plate between the reference sensor and plate-nut interface,
W_3 represents wave propagation function of the nut (W_{nut}) and bolt (W_{bolt}) between the plate-nut interface and measuring sensor, ($W_3 = W_{nut} + W_{bolt} + T_{thread}$, whereas, T_{thread} is transmission between nut and bolt thread which is assumed as constant for all preload.)
D_1, D_2 are the propagation function of sensors (reference and measuring) including the couplant,
P_1^R and P_2^R represents the reflected wave components from the plate-nut interface and bolt top edge,
P_n represents all neglected paths, reflections and mode conversions of the transmitted response,
N_E depicts the background noise, and
T depicts the transmission co-efficient at the plate-nut interface.

The analytical framework expresses the response received by the reference and measuring sensors. The response of reference and measuring sensors are collected for different preload states. Then, following the methodology outlined in Section 3-3-1, the bolt preload can be estimated by comparing the output of the sensors. Similar to preload detection, an analytical framework for crack detection is presented in the following section.

3-2-2 Analytical framework for crack detection

This section describes an analytical framework for crack detection using the same experimental setup proposed for preload detection. As discussed in Chapter 2, the first thread that engages with nut is highly prone to cracks in preloaded bolts. Thus, acoustic emission from the first engaged bolt thread crack is considered for the analytical framework. Figure 3-2 depicts the two different wave propagation paths for the acoustic emission to reach the sensors. In the primary wave propagation path, acoustic emission propagates through the bolt and nut with reflections (W_{c2}, W_{c1} and P_{n}) to reach sensors (1 and 2). Similarly, the wave travels through the plates and interfaces (plate-nut and plate-plate) in the secondary wave propagation path before reaching sensors (2 and 1). Due to transmission loss across multiple interfaces, the signal received through the secondary wave propagation path will have lower intensity than the primary. Hence only the primary wave propagating path is considered for the analytical framework. The elastic waves propagating through the primary path reach sensor 2 first and then transmit through the plate-nut interface to reach sensor 1. The received signals can be used to detect the crack initiation or propagation in bolts. The received acoustic wave by sensors 1 and 2 are expressed as,

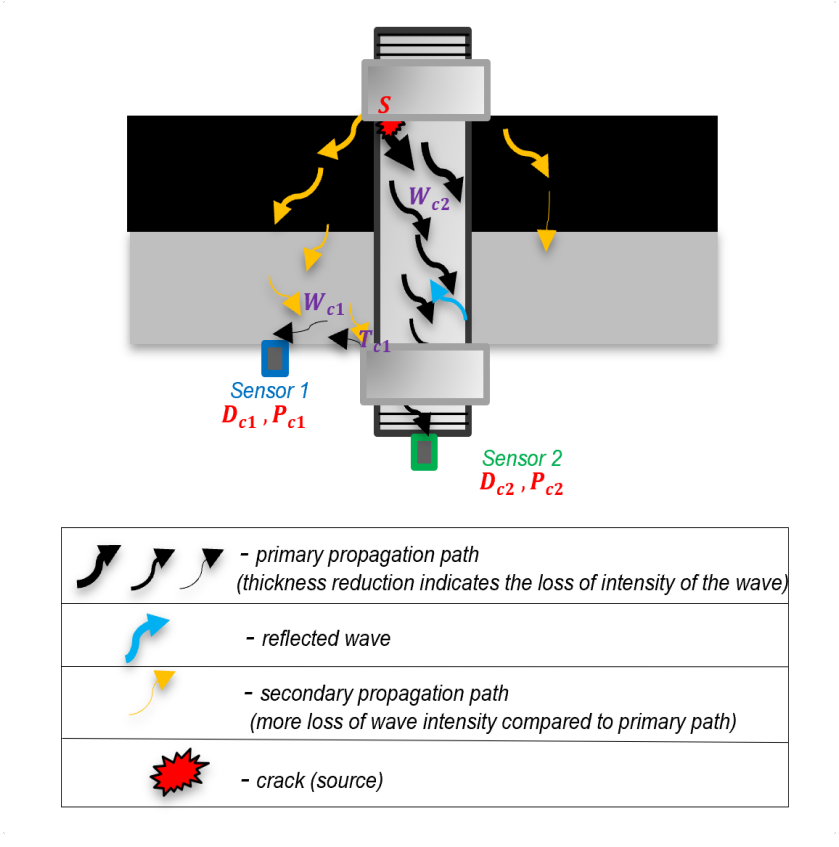

Figure 3-2: *Representation of wave propagation path for crack detection.*

$$\mathbf{P_{c2}} = D_{c2}(\omega)\, W_{c2}(l_s, l_{z2}, m_2, \omega)\, S(\omega) + P_{\mathrm{n}} + N_E \tag{3-3}$$

$$\mathbf{P_{c1}} = D_{c1}(\omega)\, W_{c1}(l_i, l_{z1}, m_1, \omega)\, T_{c1}(l_i, F, m_1, m_2, \omega)\, W_{c3}(l_s, l_i, m_2, \omega)\, S(\omega) + P_{\mathrm{n}} + N_E \tag{3-4}$$

Wherein,

$\mathbf{P_{c1}}$ and $\mathbf{P_{c2}}$ are the signals received by the sensors 1 and 2,
m_1 and m_2 represents the influence of plate and bolt material (bolt and nut material properties are assumed to be same),
l_s, l_{z1}, and l_{z2} are the position of crack and sensors (1 and 2) in space,
l_i(Ra) is the location of plate-nut interface asperities which depends on the surface roughness of plate and nut,
ω is the frequency of the acoustic wave from the crack,
F represents the bolt preload,
S is the acoustic signal released from the crack,
W_{c1} represents wave propagation function of the plate,
W_{c2} represents wave propagation function of the bolt and nut in combination (based on l_{z2}),
W_{c3} represents wave propagation function of the bolt and nut in combination (based on l_i),
D_1, D_2 are the transfer function of sensors 1 and 2 including the couplant,
P_{n} represents all neglected paths, reflections and mode conversions of the transmitted response,
N_E depicts the background noise, and
T_{c1} depicts the transmission co-efficient at the plate-nut-bolt interface.

3-3 Methodology

The preload and crack detection methodologies are described in detail using the analytical framework discussed before.

3-3-1 Methodology for preload detection

Experimental setup - The experimental setup as shown in Figure 3-1 will be used for preload detection.
Source signal (S) - Hanning windowed five cycle burst signal with a specific centre frequency is used as a source signal in the experiments. A waveform generator generates the source pulse. Five cycle burst signal is preferred for an optimal combination of signal length and bandwidth to limit the amount of dispersion. Figure 3-3 shows the effect of the number of burst cycles on frequency bandwidth.

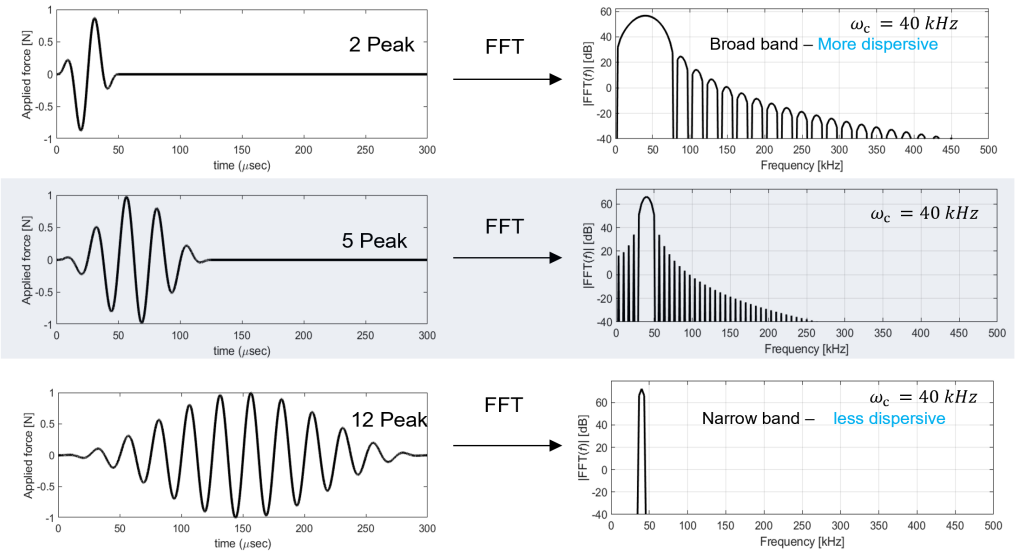

Figure 3-3: *Signal length increases in time-domain with number of peaks, but the frequency spectrum is getting narrower for increasing peaks in time domain.*

Reference sensor signal ($\mathbf{P_1}$) - Source (S) propagating from the transducer is collected by the reference sensor before reaching the measuring sensor. As discussed in Section 3-2-1, the reference sensor signal is expected to have components such as the propagating source, reflections, dispersion and random noise. Figure 3-4 depicts a reference sensor signal from an experiment that comprises the relevant components outlined in an analytical framework. The reference sensor signals are not expected to change with preload variations.

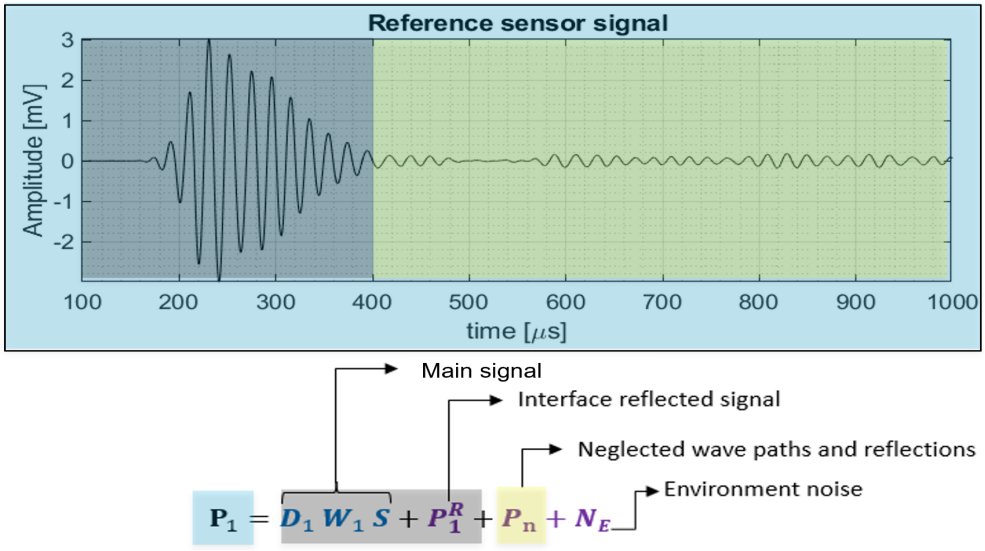

Figure 3-4: *Sample of reference sensor signal from an experiment.*

Measuring sensor signal ($\mathbf{P_2}$) - Source (S) propagating through the plate and plate-nut interface, finally reaches the measuring sensor at the end of the bolt. The received response includes components as discussed in the analytical framework Section 3-2-1. Figure 3-5 illustrates a sample of measuring sensor signal from an experiment with distinct components. Variations in preload are expected to cause changes in measuring sensor signals as the transmission coefficient (T) changes.

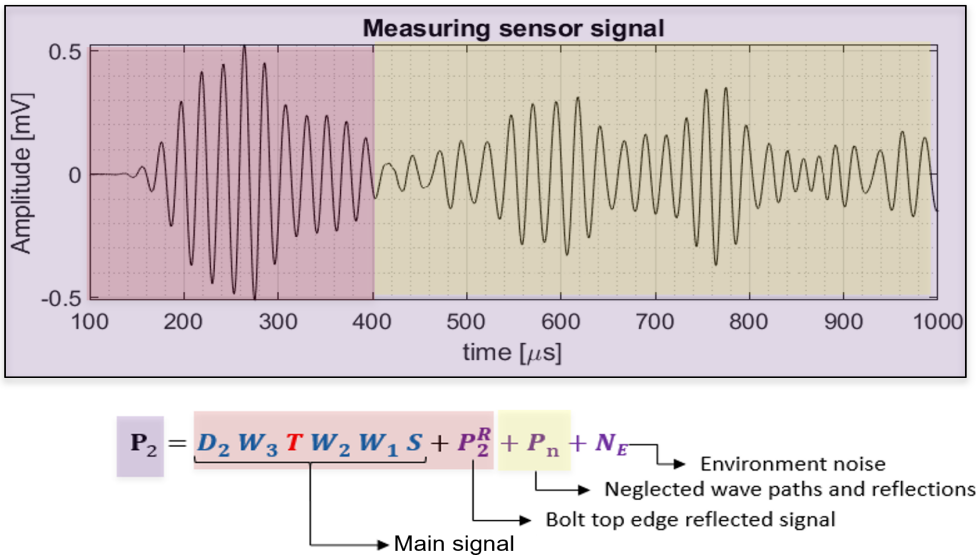

Figure 3-5: *Sample of measuring sensor signal from an experiment.*

Simplification of the analytical framework - The reference and measuring sensor responses are collected to determine the bolt preload state. However, the complete recorded signal duration is not necessary for preload detection. Instead, the initial part of the transient response containing the source wave is utilised to determine bolt preload. Based on the assumption, the signal component that contains all the neglected paths and reflections with complex interference (P_{n}) are excluded from the obtained analytical expression. Furthermore, it also assumed that the ambient noise (N_E) is random and uncorrelated with propagating signal. Therefore, the random noise can be reduced, for example, an averaging technique as shown in the Equation 3-5.

$$P_{1_{avg}}(t) = \frac{1}{N} \sum_{n=\langle N \rangle} P_{1_n}(t) \tag{3-5}$$

whereas $P_{1_{avg}}$ is the averaged reference sensor signal, and N represents the total number of signals collected for averaging.

Therefore the Equation 3-3 and 3-2 reduces to,

$$\mathbf{P_1} = D_1(\omega_c)\, W_1(l_s, l_{z1}, m_1, \omega_c)\, S(\omega_c) + P_1^R \tag{3-6}$$

$$\mathbf{P_2} = D_2(\omega_c)\, W_3(l_i, l_{z2}, m_2, \omega_c)\, T(l_i, F, m_1, m_2, \omega_c)\, W_2(l_{z1}, l_i, m_1, \omega_c) \\ W_1(l_s, l_{z1}, m_1, \omega_c)\, S(\omega_c) + P_2^R \tag{3-7}$$

The reduced expression for P_1 and P_2 can be further simplified to express the measuring sensor signal as a transformation of the reference sensor signal. By careful calibration of the sensors the reference and measuring sensor transfer functions can be considered identical (D_1 D_2). Also, the interface and bolt edge reflected signals in the initial wave packet is assumed to have negligible variations for preload changes. Hence the reflected wave components P_1^R and P_2^R are neglected from the analytical expression. The simplified formulation is given as,

$$\frac{\mathbf{P}_2}{\mathbf{P}_1} = W_2(l_{z1}, m_1, \omega_c)\, T(F, Ra, m_1, m_2, \omega_c)\, W_3(l_{z2}, m_2, \omega_c) \tag{3-8}$$

From the simplified expression, it is clear that the wave collected by the measuring sensor is estimated by the convolution of the reference sensor signal, propagation functions and transmission coefficient at the interface. Positioning the reference sensor near the plate-nut interface minimizes the influence of propagation functions (W_2 and W_3).

$$\frac{\mathbf{P}_2}{\mathbf{P}_1} \propto T(\omega_c, F, Ra, m_1, m_2) \tag{3-9}$$

Finally, the measuring sensor signal ($\mathbf{P_2}$) is expressed as a transformation of the reference sensor signal ($\mathbf{P_1}$) with the transmission coefficient (T). Transmission coefficient, in turn, depends on the preload present in the bolt, source centre frequency, and surface roughness of the plate and nut.

Extracting the first envelope of reference signal - The initial part of the reference sensor signal is used to estimate bolt preload as shown in Equation 3-6. The selection of the initial part of the signal is achieved with the proposed Algorithm 1. The Algorithm selects the first wave packet by enveloping the signal using the Hilbert transform, identifying the maximum envelope peak, and detecting local maxima changes. The length of the excited source signal is $100\mu s$, and it reaches a maximum peak at $50\mu s$. The change in local maxima after the maximum peak in the reference sensor signal is examined for each time point (t) and (t+$25\mu s$). Furthermore, the time point at which the local maxima changes is considered the end of the first wave packet. Figure 3-6 shows the sample output for Algorithm 1 utilising sample signals from the experiment as described in Chapter 5.

Algorithm 1 : For extracting the first wave packet of reference sensor signal

Input : Reference sensor signal ($\mathbf{P}_2 = D_2W_3TW_2W_1S + P_2^R + P_n$)
Output: Selection of initial part of the input ($\mathbf{P}_2 = D_2W_3TW_2W_1S + P_2^R$)

$ref \leftarrow$ reference sensor signal
$y \leftarrow$ envelope of ref
$[peaks, loc] \leftarrow$ all peaks and its location of y
$peak_{max} \leftarrow$ the maximum value of $peaks$
$pos_{max} \leftarrow$ index of $peak_{max}$ in loc
for $i \leftarrow loc(pos_{max})$ *to* $loc(end)$ **do**
  if $y(i) < y(i{+}25\mu s)$ **then** ▷ locate change in local maxima
$end_{envelop} = i$ ▷ change in local maxima is taken as end of 1^{st} envelope
    break
  end if
end for

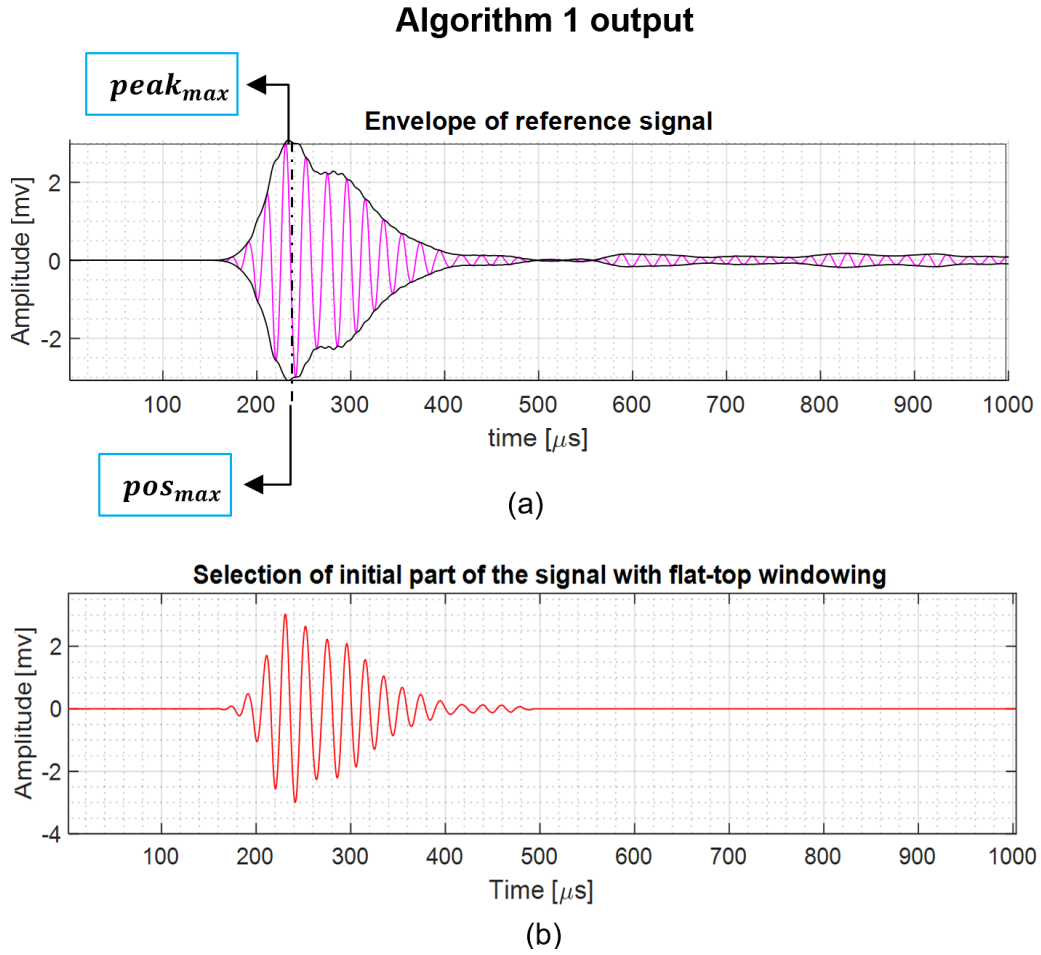

Figure 3-6: *Algorithm 1 output: (a) The reference sensor signal with envelope pointing the maximum peak position. (b)The extracted first wave packet of the reference sensor signal.*

Selecting the main wave packet - The source wave passes the reference sensor and gets transmitted to the measuring sensor. The first wave packet of the reference sensor signal is cross-correlated with the measuring sensor signal to identify the source wave in the measuring sensor output. The cross-correlation is then normalised with the maximum auto-correlation value of Algorithm 1 output. Finally, the normalised cross-correlation value is enveloped using Hilbert transform to detect the maximum peak and lag time. Algorithm 2 describes the outline of selecting the wave packet of the measuring sensor signal using cross-correlation. Figure 3-7 shows the sample output of Algorithm 2 utilising experimentally obtained signals. Auto-correlation and cross-correlation of the signals are expressed in the Equation 3-10 and 3-11.

$$C_{11}(\tau) = \int_0^t S_1(t-\tau) * S_1(t)dt \tag{3-10}$$

$$C_{21}(\tau) = \int_0^t S_1(t-\tau) * S_2(t)dt \tag{3-11}$$

where, s_1 is the windowed reference sensor signal, s_2 is the measuring sensor signal, C_{11} is the auto-correlation of s_1, C_{12} is the cross-correlation of s_2 and s_1.

The following Algorithm was implemented in MATLAB.

Algorithm 2 : For selecting the wave packet of the measuring sensor signal

Input : Extracted reference sensor signal(output of Algorithm 1) and measuring sensor signal

Output: Selection of main wave packet of the measuring sensor signal

1: $s_1 \leftarrow$ windowed reference sensor signal
2: $s_2 \leftarrow$ measuring sensor signal
3: $[c_{11}] \leftarrow$ the auto-correlation of s_1
4: $[c_{12}, lag] \leftarrow$ the cross-correlation of s_2 with s_1
5: $c_{nor} = \frac{C_{12.}}{\max(\text{abs}(C_{11}))}$
6: $c_{env} \leftarrow$ envelope of c_{nor}
7: $[peaks, lag_{loc}] \leftarrow$ all peaks and corresponding lag location of c_{env}
8: $peak_{max} \leftarrow$ the maximum value of $peaks$
9: $pos_{max} \leftarrow$ position of $peak_{max}$ in lag_{loc}
10: $end_{envelop} = pos_{max} + a$ ▷ a - is the width of selected part of reference sensor signal
11: $start_{envelop} = pretriggertime + end_{envelop}$ - a

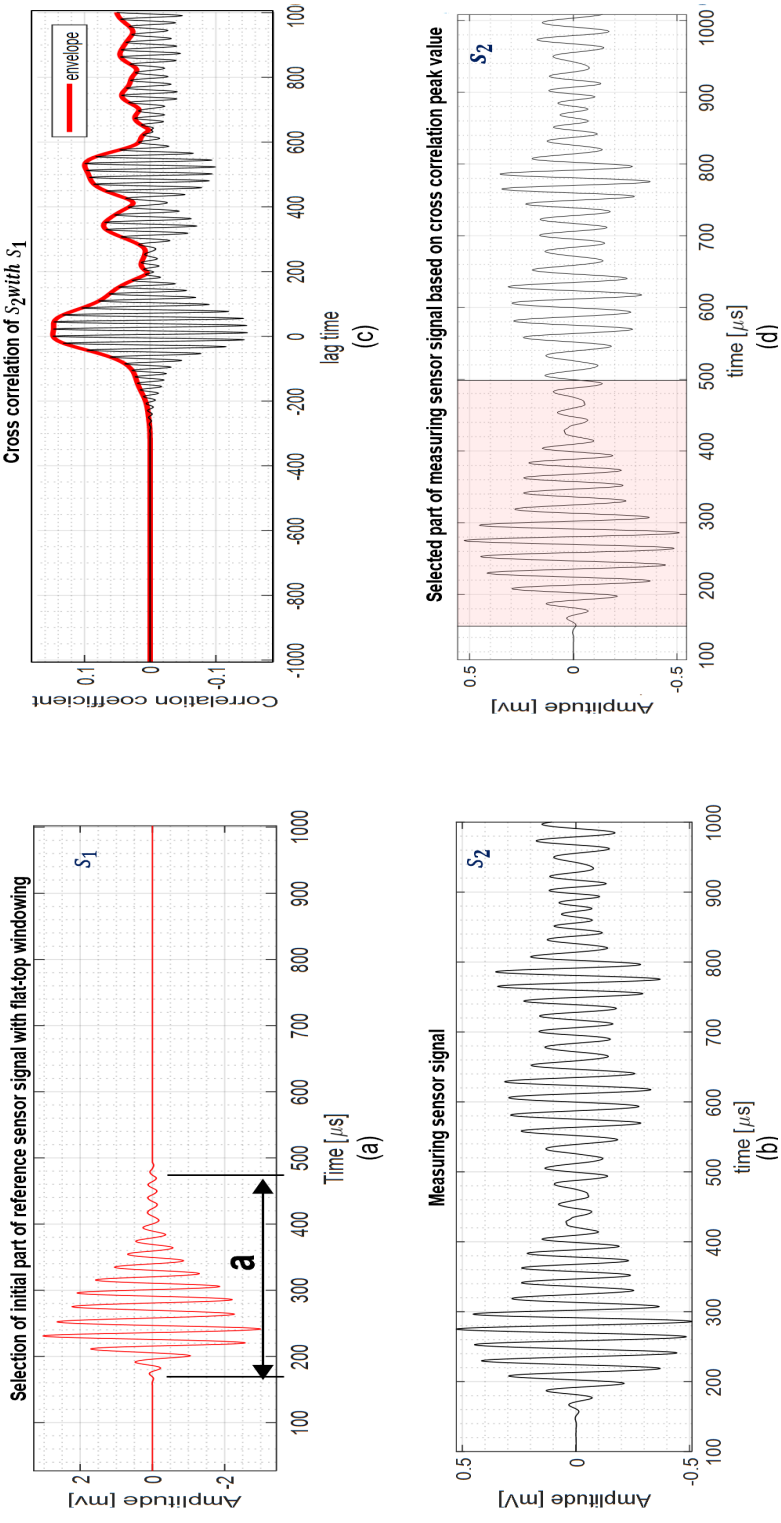

Figure 3-7: *Algorithm 2 output: (a) The final output of extracted first wave packet of the reference sensor signal (s_1). (b) The measuring sensor signal (s_2). (c) Normalised cross-correlation value for s_1 and s_2 plotted against the lag time. Cross correlation signal is enveloped using Hilbert transform to detect the peak value. (d) Selected wave packet of the measuring sensor signal using Algorithm 2.*

Hypothesis for preload detection - The signals are collected by the reference and measuring sensors for different preloads. The proposed methodology is followed to select the wave packet of the sensor responses. From the analytical framework, it is clear that the measuring sensor signal is the convolution of the reference sensor signal and transmission co-efficient. As the bolt preload increases, the interface contact area increases. Therefore, the signal transmission is expected to increase with the increase in preload. Hence the hypothesis proposed for the feasibility study is,

Hypothesis 1: Transmitted wave energy increases as preload increases.
Hypothesis 2: The power of fundamental frequency increases as preload increases.

The validity of the proposed hypothesis is verified by performing experiments as discussed in Chapter 4

3-3-2 Methodology for crack detection

This study examines crack detection feasibility with the same experimental setup of preload detection. As discussed in Chapter 2-1-3, the most prominent fatigue crack location in preloaded bolts is the first engaging thread of bolt with nut. For this feasibility study, artificial cracks will be simulated at the first engaging thread instead of fatigue tests to generate the elastic waves similar to the acoustic emission from cracks. The amplitude of the received signal depends on the location and orientation of the sensor relative to the acoustic source. Hence to check for the maximum propagation path, artificial cracks will be simulated on the opposite end of the bolt sensor position. As per the proposed analytical framework in Section 3-2-2, sensors will collect the acoustic wave generated by the simulated crack after propagating through the bolt, nut and plates. Therefore, crack detection feasibility will be investigated by initiating artificial cracks and collecting the corresponding signals. Since only the feasibility of the crack detection is checked, no further signal processing will be performed for the received signal.

3-4 Chapter highlights

An analytical framework was established for bolt preload and crack detection. The methodology for preload detection described the wave packet selection Algorithm for reference and measuring sensor signals. The proposed hypothesis states that as the preload increases, the energy and power of the received signal increase. Finally, to check for the feasibility of crack detection, simulated cracks are proposed in the first engaging thread of bolt and nut. The validity of the proposed methodology and hypothesis is checked by the experiments described in Chapter 4.

Chapter 4

Experiments

Experiments were conducted to evaluate the feasibility of utilising ultrasonic waves to detect bolt preload and cracks. Small (M12 bolt) and large (M64 bolt) scale experiments were conducted to assess the validity of the proposed methodology and hypothesis. In this chapter, the experimental setup is outlined first, followed by the experimental procedure.

4-1 Experiment setup

4-1-1 Small-scale geometry

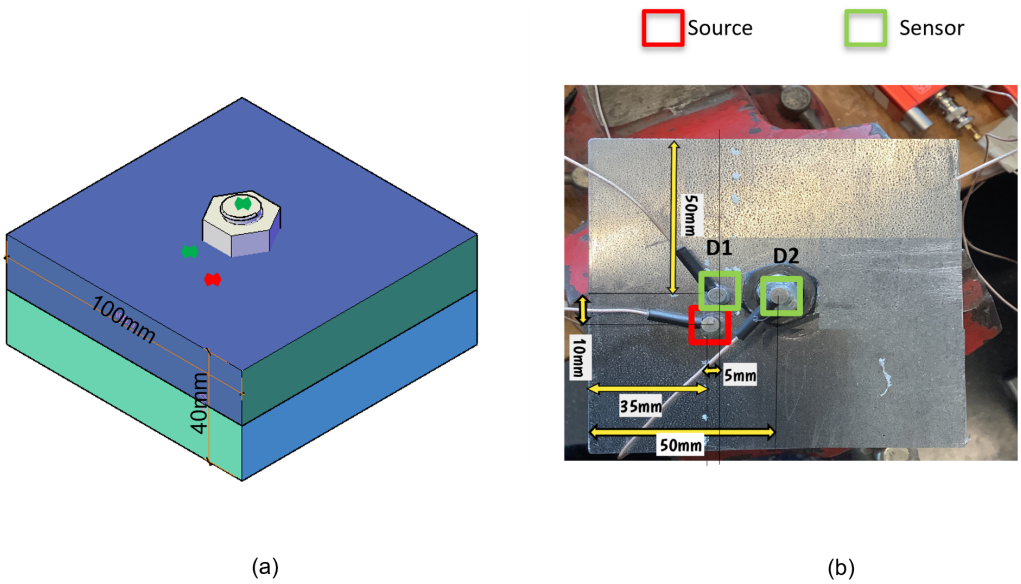

(a) (b)

Figure 4-1: *(a) small-scale experiment setup model. (b) Actual experiment setup with actuator and sensor positions.*

The preliminary setup outlined in Chapter 3 was further extended for the small-scale experiments. Bolts of minimum size M12 and grade 8.8 or 10.9 are allowed for pretensioning [5]. Hence for the small-scale experiments, plates with dimension 100mm×100mm×20mm were fastened with an M12 bolt of grade 8.8 and length 75mm. Figure 4-1 shows the setup used for the small-scale experiment. Both plate and bolt material was chosen as steel. A strain gauge with a full Wheatstone bridge circuit was attached to the bolt shank to have precise and controlled bolt pretension.

4-1-2 Large-scale geometry

After analysing the observations from the small-scale experiments (discussed later in Chapter 5-1-4), experiments were conducted on a larger bolt of size M64 connecting two flanges. The sensor positions were maintained the same as in small-scale experiments. Figure 4-2 shows the geometry considered for the large-scale experiments and the corresponding sensor positions. The experimental setup considered consists of twelve bolts. However, experiments were conducted only on two bolts (bolt 1 and bolt 7). Since the proposed methodology and hypotheses depend on the local changes in the contact area of the plate-nut interface, the same sensor setup can be replicated to all bolts in future for preload tracking without any interference in its result. Hence, only two diagonally opposite bolts (1 and 7) were preloaded to have an even pressure distribution over the flange for this feasibility study.

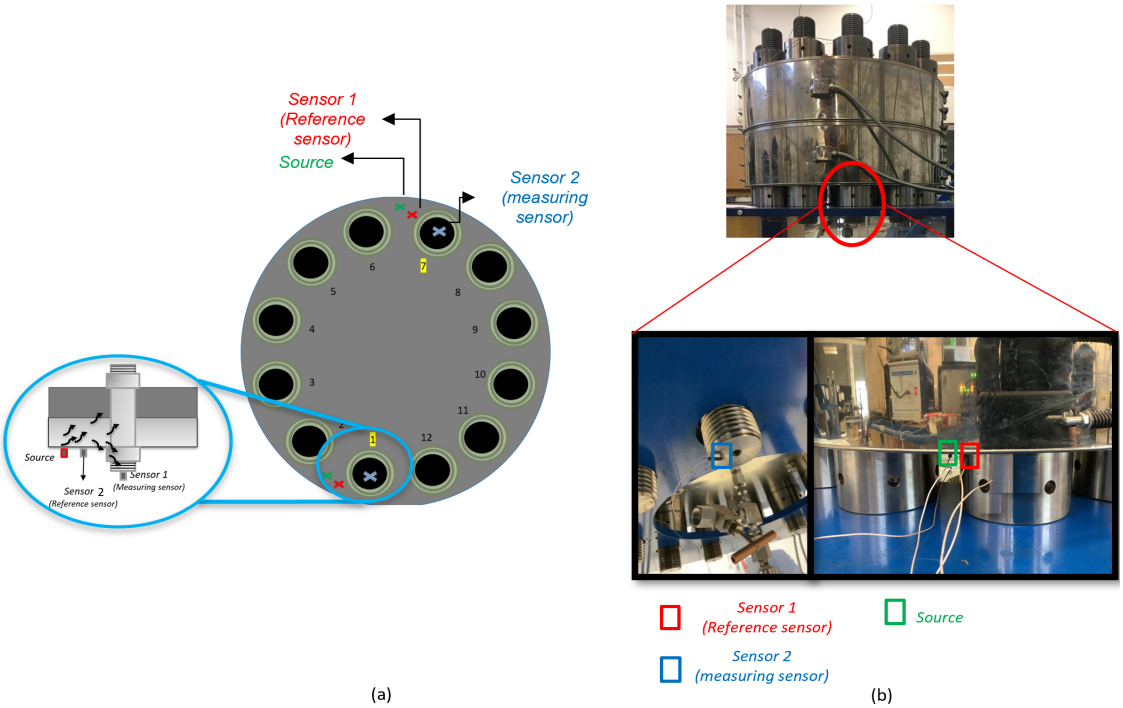

Figure 4-2: *(a) large-scale experiment setup model. (b) Actual experiment setup with actuator and sensor positions.*

4-1-3 Experiment layout

Figure 4-3 shows the experimental layout followed for both small- and large-scale experiments. Resonant Acoustic Emission (AE) sensors were used for this feasibility experiments. The small-scale experiments used VS600-Z1 transducers, whereas VS600-Z1 and R-6α transducers were used for the large-scale experiments. With a hot-glue couplant, the transducers were attached to the geometry (adhesive mount). All the resonant transducers used in the experiments could function as actuators and sensors. A voltage pulse (five-peak gaussian signal) was transmitted from the signal generator through a power amplifier. The power amplifier amplified the generated burst signal 50 times and transmitted it to the actuator. The sensor received the structural response for the given pulse. The 40dB Vallen AEP-5H preamplifier was used to amplify the response. The amplified signals were then collected by the Vallen AMSY-6 Data Acquisition System (DAQ). The collected signals were further processed in MATLAB.

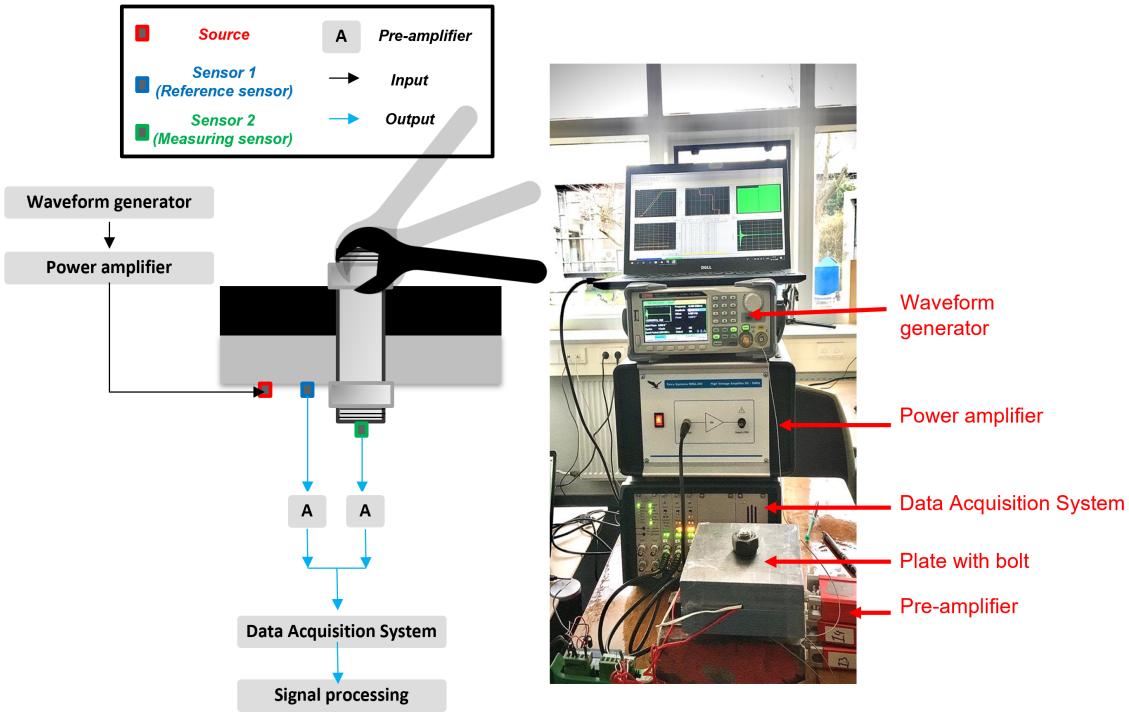

Figure 4-3: *Schematic experiment layout for small- and large-scale experiments. Actual experimental layout for small-scale experiment.*

4-2 Experiment procedure

4-2-1 Preload detection

As discussed in Chapter 1, bolts can be in tension or shear joints with various external loads acting on them. However, this feasibility study was conducted in a laboratory environment without any external loads acting on the bolts. Hence only the bolt preload was changed, and the corresponding responses for the given pulse were recorded. The experimental procedure for small- and large-scale experiments are described below.

Small-scale experiment

In small-scale experiments, bolt (M12) was tensioned from 1kN to 50kN in four steps (1kN, 10kN, 20kN, and 30kN). To examine the effect of source centre frequency, source signals of 50kHz (low), 150kHz (medium), and 600kHz (high) centre frequency were generated and sent to the actuator. For each bolt pretension, the source signal of different frequencies was sent from the signal generator, and the DAQ collected their corresponding response from the sensors. Since the received response of the sensor has the possibility of having random noises, the averaging technique was used as expressed in Equation 3-5 to reduce it. Hence, 30 burst signals were generated for each centre frequency, and the corresponding responses were recorded to minimise the random noise. Thus, each bolt preload is associated with the responses for three different source centre frequencies, as shown in the Table 4-1. Figure 4-4 shows the representation of the experimental procedure.

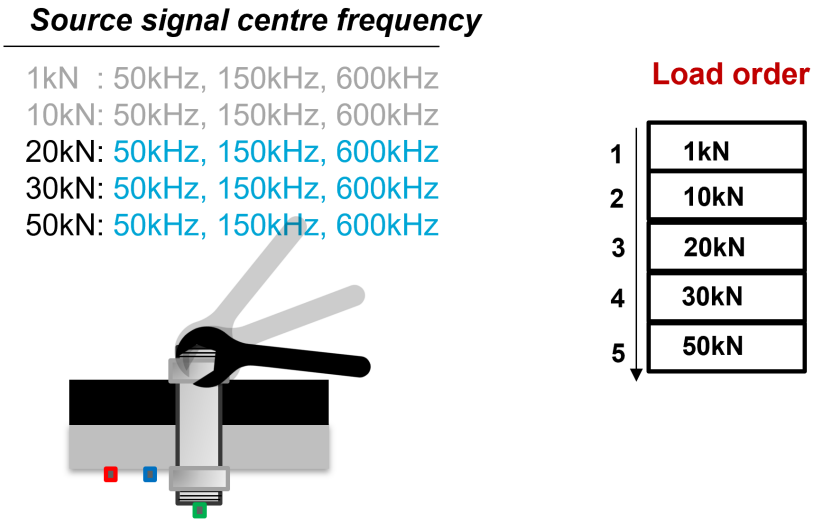

Figure 4-4: *Representation of collection of responses for different source centre frequency for each preload and load order used in the experiments.*

Small-scale experiment	
Load	Frequency
1kN	600kHz
10kN	150kHz
20kN	50kHz
30kN	
50kN	
Sensor used:	VS600-Z1

Table 4-1: *Preloads and the source frequencies used in the small-scale experiments.*

Large-scale experiment

For large-scale experiments, bolts of size M64 were tensioned from 300kN to 1800kN in steps of 300kN. A hydraulic tensioner (HTT2327) was used to pretension the bolts precisely. As shown in Table 4-2 sources of different centre frequencies were sent for each preload, and the corresponding responses were collected in DAQ. Three experiments were conducted in two bolts to check for the feasibility of preload detection. The methodology proposed in Chapter 3-3-1 depends on the true contact area at the micro surface level. Therefore, the influence of plastic deformation of these micro surface roughness during the load repeatability needs to be checked. Hence, the load was increased in steps of 300kN till 1800kN first and then repeated randomly to assess the repeatability of sensor responses. Figure 4-5 shows the experimental procedure, and the load repeatability order followed in Experiment 1 (Bolt 1 - using VS600-Z1 sensor). The same approach was used for bolt 1 with R-6α and bolt 7 with VS600-Z1.

Large-scale experiment				
Bolt 1			Bolt 7	
	Sensor: VS600-Z1	Sensor: R-6α		Sensor: VS600-Z1
Load	Frequency	Frequency	Load	Frequency
300kN	25kHz	15kHz	300kN	25kHz
600kN	40kHz	25kHz	600kN	40kHz
900kN	60kHz	40kHz	900kN	60kHz
1200kN	80kHz	60kHz	1200kN	80kHz
1500kN	100kHz	80kHz	1500kN	100kHz
1800kN			1800kN	
	Experiment 1	Experiment 2		Experiment 3

Table 4-2: *Preloads and the source frequencies used in the large-scale experiments.*

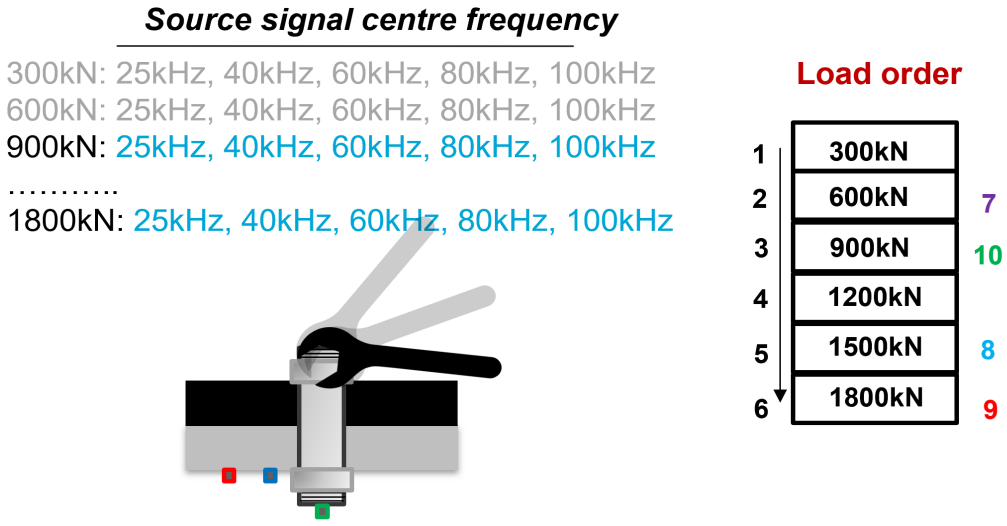

Figure 4-5: *Representation of experiment 1 collection of responses for different source centre frequency for each preload and the load order used in the experiments to check the repeatability.*

Data Acquisition System (DAQ) settings

Vallen AMSY-6 DAQ was used for the collection of transient recordings and acoustic emissions. The sampling rate set for all the experiments were 10MHz. To avoid the aliasing effect, the sampling rate should be two times greater than the frequency of interest. Therefore, the source centre frequency determines the minimum sampling rate required. The maximum frequency used in the feasibility experiments was 600kHz, and the selected sampling frequency was sufficient to record the signals. The threshold for all the sensors was set to 35dB in all experiments. The pre-triggered time for small-scale experiments was 400 μs and 200 μs for large-scale experiments. The response was measured for 1500 μs in all experiments.

4-2-2 Crack detection

The same experimental setup was used for the detection of cracks in bolts. As discussed in Section 3-3-2, artificial cracks were simulated on the first engaging thread of bolt and nut. Pencil-Lead Breaks (PLB), also known as Hsu-Nielsen source, is a well-known technique that has been used as a method to generate reproducible AE signals artificially [111][112]. Hence considering the objective and the time limit, cracks were simulated near the engaging thread using a PLB. Figure 4-6 shows the simulated crack at the bolt thread.

Figure 4-6: *Simulated crack at bolt thread using Hsu-Nielsen source.*

Chapter 5

Experimental results and hypothesis verification

Experiments were conducted as described in Chapter 4. The corresponding experimental results, observations, and hypothesis verification are presented in this chapter.

5-1 Small-scale experiment results

Small-scale experiments were conducted following the experiment procedure and DAQ settings as discussed in Chapter 4-2-1.

5-1-1 Influence of source frequency

Signals were obtained for three different source frequencies for each preload as mentioned in Table 4-1. Figure 5-1 shows the received response of the measuring sensor signal for the preload of 50kN and source centre frequencies 600kHz (in higher frequency regime) and 50kHz (in lower frequency regime). The measured response for the source signal at 600kHz showed high interference. The source with 150kHz exhibited similar high interference. Therefore, component separation from the sensor response gets complicated due to the high interference pattern. Furthermore, the shorter wavelength of the high-frequency burst signal increases the influence of reflection components in the wave packets. For these reasons, the proposed methodology and algorithm will not be applied to high-frequency source signals.

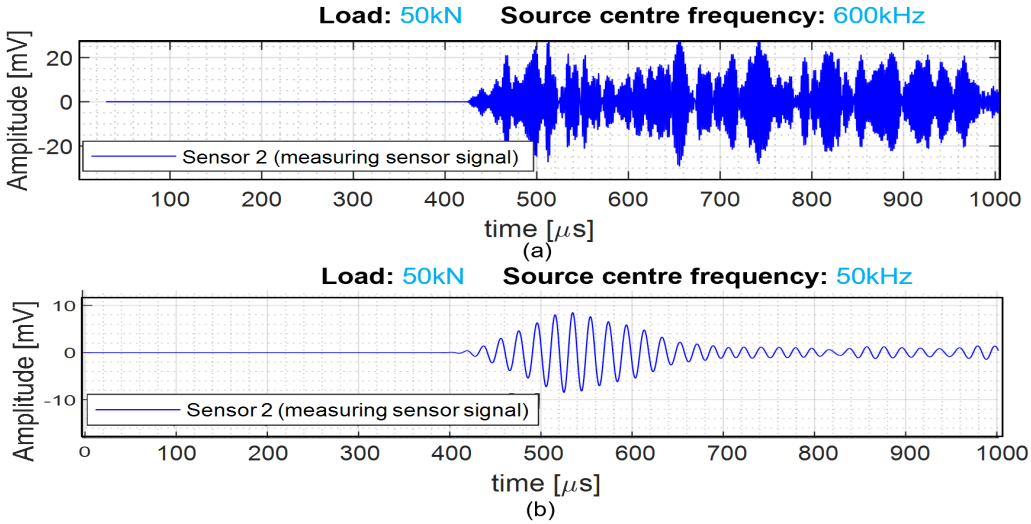

Figure 5-1: *(a) Measuring sensor response for a source of centre frequency 600kHz with high interference and (b) Measuring sensor response for a source of centre frequency 50kHz.*

As an answer to research subquestion,

- What is the influence of the source frequency ?

The interference in the sensor response increases with an increase in source frequency. With increased interference, identifying components in the measured response becomes complicated. Hence the proposed methodology and hypothesis in Chapter 3 seems to have better applicability to low-frequency sources.

5-1-2 Sensor response for different preload levels

Considering the influence of source frequency, signals collected by the reference and measuring sensor for the source of 50kHz under different preload were further processed. Following the algorithm outlined in Chapter 3-3-1, the envelope was selected from the reference and measuring sensor responses. Figure 5-2 shows the algorithm output for sensor responses under various preload levels. The reference sensor measurements show minor variations for preload changes. This minor variation was due to the reflected and scattered components from the plat-nut interface in the wave packet of the sensor response. However, these minor variations for varying preload are negligible, and the reference sensor signal can be considered constant for all preload. Meanwhile, the preload changes cause significant variations in the measuring sensor signals. The variation in the measuring sensor signal is due to the change in the interface true contact area with preload.

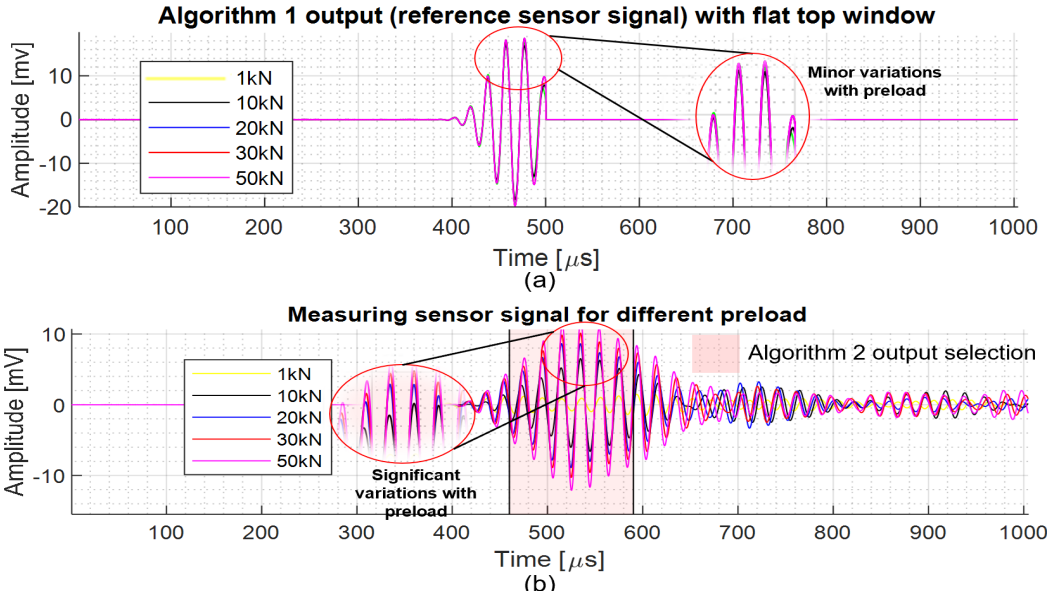

Figure 5-2: *(a)Reference sensor signal with algorithm 1 output. (b) Measuring sensor signal with algorithm 2 output.*

5-1-3 Hypothesis verification

To verify the hypothesis proposed in Chapter 3-3-1, time and frequency domain signal analyses were performed on the obtained algorithm output.

Time-domain analysis for 1^{st} hypothesis verification

According to the proposed first hypothesis, the energy of the transmitted signal increases with preload as the true contact area increases. Therefore, the energy of the extracted envelope of reference and measuring sensor signals are determined for all preloads. Energy is calculated as the square of the voltage response of the sensors. The energy ratio of the measuring sensor signal to the reference sensor signal is then obtained to have a baseline free methodology. Figure 5-3 shows the part of the signal taken for the calculation of energy ratio.

The derived result of the analytical framework from Chapter 3-3-1 can be utilised to verify the proposed hypothesis. Equation 5-3 shows the proportionality of the energy ratio to the transmission coefficient.

$$\frac{\mathbf{P}_2}{\mathbf{P}_1} \propto T\left(\omega_c, F, Ra, m_1, m_2\right) \tag{5-1}$$

Given source centre frequency, surface roughness, bolt and plate material, the ratio is dependent on the preload level.

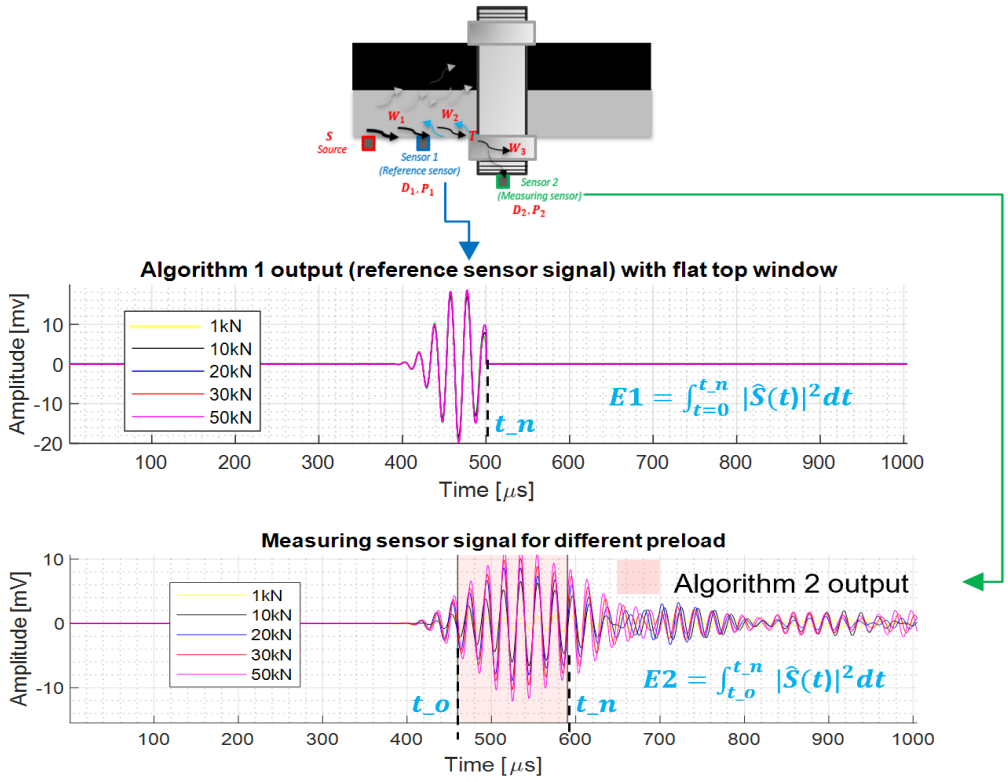

Figure 5-3: *Selected part of the reference and measuring sensor signal for calculation of energy.*

$$\frac{\mathbf{P}_2}{\mathbf{P}_1} \propto T\,(F) \tag{5-2}$$

The energy ratio between the measured and reference sensor response can be determined from time-domain analysis. Then the Equation 5-2 can be written as,

$$\frac{\mathbf{E}_2}{\mathbf{E}_1} \propto T\,(F) \tag{5-3}$$

whereas, $\mathbf{E}_1$ and $\mathbf{E}_2$ are the calculated energy (mV^2) of the selected part of the reference and measuring sensor response.

Figure 5-4 shows that the energy ratio increases with preload. This supports the proposed hypothesis 1 that the preload can be estimated with an established relationship (trend) between the energy ratio and preload.

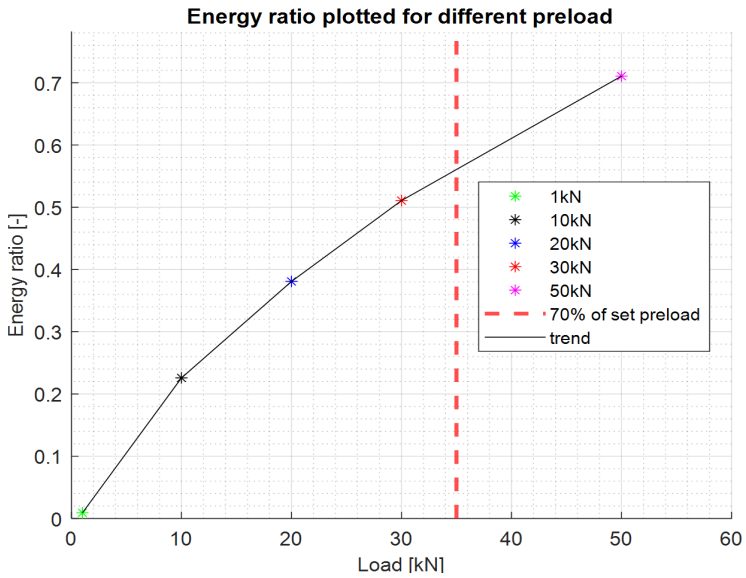

Figure 5-4: *Energy ratio plotted for different preload..*

Verification for time-window selection

The development of the algorithm in Chapter 3-3-1 was based on the assumption that the initial part of the recorded response represents the direct arrival of source signal and is not strongly influenced by mode conversion and other reflections.

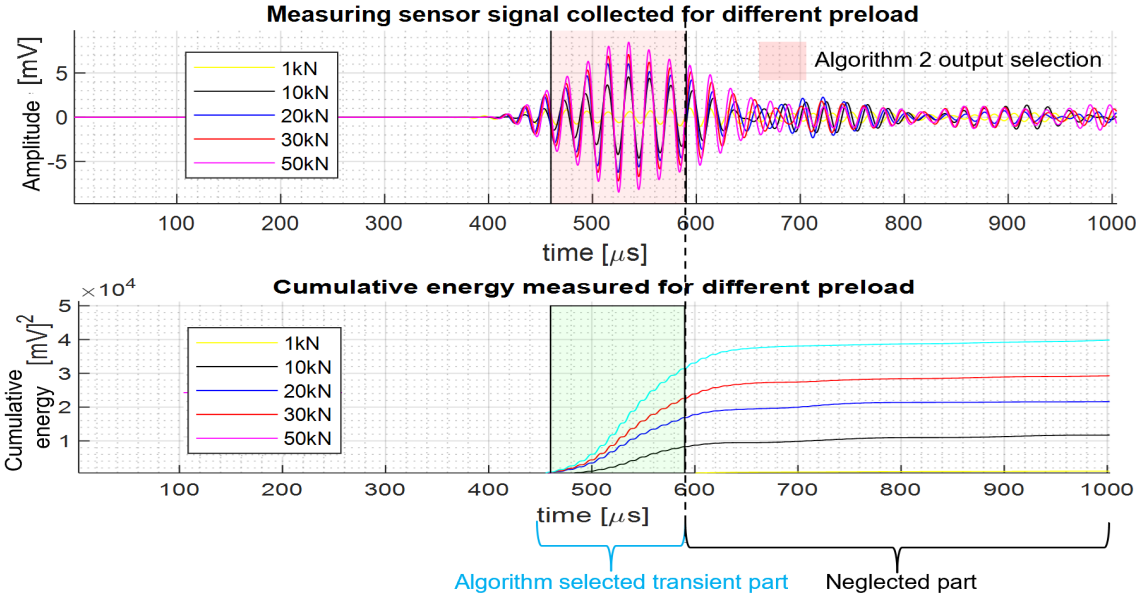

Figure 5-5: *Cumulative energy plotted for different preload to differentiate the algortihm selected transient response from the total response.*

To verify the considered assumption for time-window selection, the cumulative energy was calculated for the measuring sensor response collected for different preloads. Figure 5-5 shows that the energy from the selected part of the transient response is enough to distinguish the preload as the cumulative energy tends to reach a stable state after that. Hence the assumption considered in the analytical approach is validated, and the algorithm for selecting the measuring sensor signal will be used for other conducted experiments.

Time-frequency-domain analysis for 2^{nd} hypothesis verification

The second proposed hypothesis states that the power of the fundamental frequency increases with preload. The hypothesis is verified in the time-frequency domain. Figure 5-6 shows the outline followed for the time-frequency domain analysis.

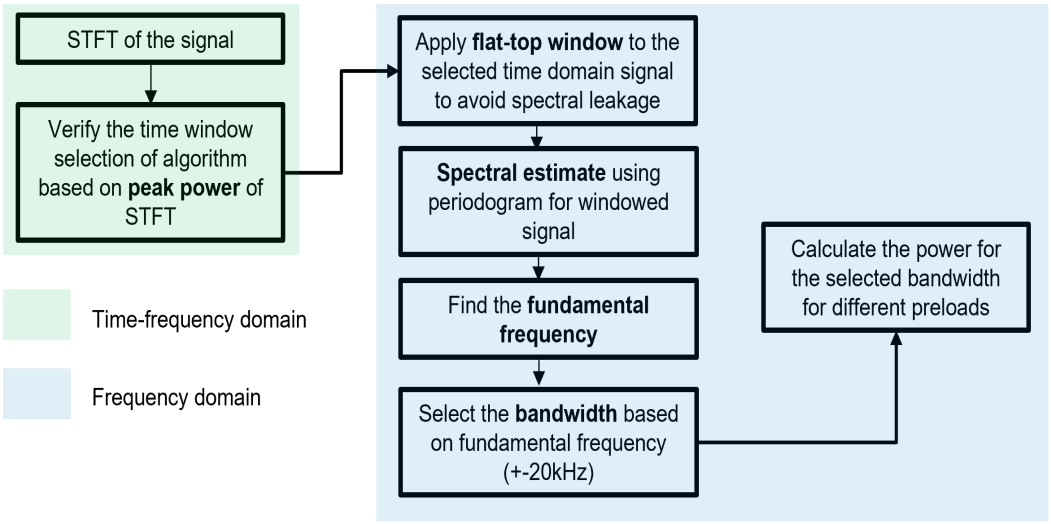

Figure 5-6: *Outline followed for the frequency domain analysis.*

Time-frequency domain analysis for time-window selection

First, the measuring sensor response in the time domain was transferred to the time-frequency domain using Short Term Fourier Transform (STFT). Then, STFT was used to examine the peak power of the signal. For STFT, a flat-top[1] window with a size of 512[2] samples and overlap of 80% was used to achieve an optimum frequency and temporal resolution. The minimum frequency that can be determined from the preferred STFT window setting was 20kHz. It was observed that the peak power of the measuring sensor signal for all preloads were within the selected part of the signal. Hence, only the output of algorithm 2 was taken

[1]Flat-top window is preferred here since the amplitude accuracy is importnat

[2]Window size was chosen based on minimum frequency to be detected $x = (f_s) / (f_{\min})$, whereas f_s is the sampling rate (10MHz) and $f_{\min}$ is the minimum frequency to be detected (20kHz)

for further frequency domain analysis instead of the entire signal. Figure 5-7 shows recorded signals for different preloads.

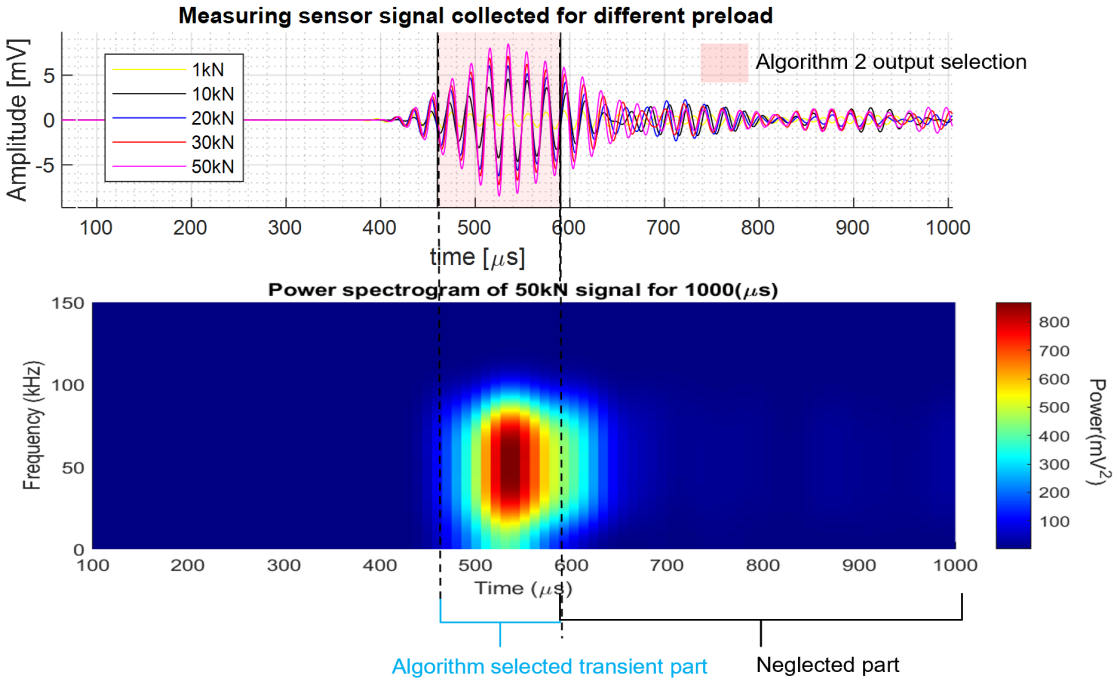

Figure 5-7: *STFT of the signal to examine the peak power time window selection.*

Frequency domain analysis for power spectral estimate

A flat-top window was applied to the algorithm selected part of the reference and measuring sensor signal to avoid spectral leakage as shown in Equation 5-4. Non-parametric estimate of the spectral density of the signal was calculated using the periodogram. The expression for calculating periodogram is shown in the Equation 5-5

$$s_w(t) = s(t).w(t) \tag{5-4}$$

whereas, $s_w(t)$ is the windowed signal, $s(t)$ is the actual signal and $w(t)$ is the flat-top window.

$$S_x(f) = |S(f)|^2.(2/(f_s.N)) \tag{5-5}$$

$$S(f) = \sum_{n=0}^{N-1} s_w(n) \cdot e^{-i2\pi k \frac{n}{N}} \tag{5-6}$$

whereas, $S_x(f)$ is the periodogram[3] (mV^2/Hz), f_s is the sampling frequency, S(f) is the discrete fourier transform of the windowed signal, n and k are time and frequency index, and N is the number of samples considered.

[3]To express in decibel(dB/Hz) - 10 .log .S$_x(f)$

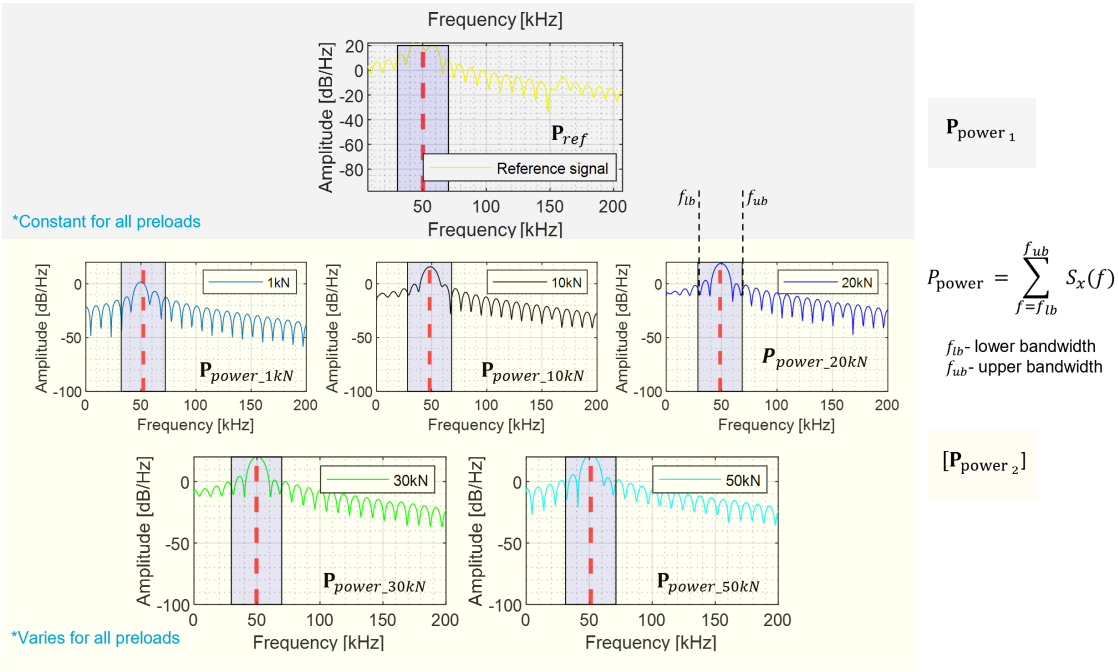

Figure 5-8: *Selection of fundamental frequency and bandwidth in periodogram plotted in decibel scale.*

The fundamental frequency was determined by detecting the peak of the obtained periodogram. In order to consider the dispersion of waves around the fundamental frequency, a bandwidth of +/- 20kHz was selected for calculating the power. Then, similar to the Equation 5-3 the power ratio was calculated by dividing the power of the selected bandwidth of the measuring sensor signal by the reference sensor signal.

$$\frac{\mathbf{P}_{power_2}}{\mathbf{P}_{power_1}} \propto T\,(F) \tag{5-7}$$

whereas, P_{power_2} is the power obtained from the bandwidth of measuring sensor signal, P_{power_1} is the power obtained from the bandwidth of reference sensor signal.

Figure 5-9 shows the increasing trend of power ratio with an increase in preload. Therefore, the proposed second hypothesis seems valid that the preload can be estimated with the established relationship (trend) between the power ratio and preload.

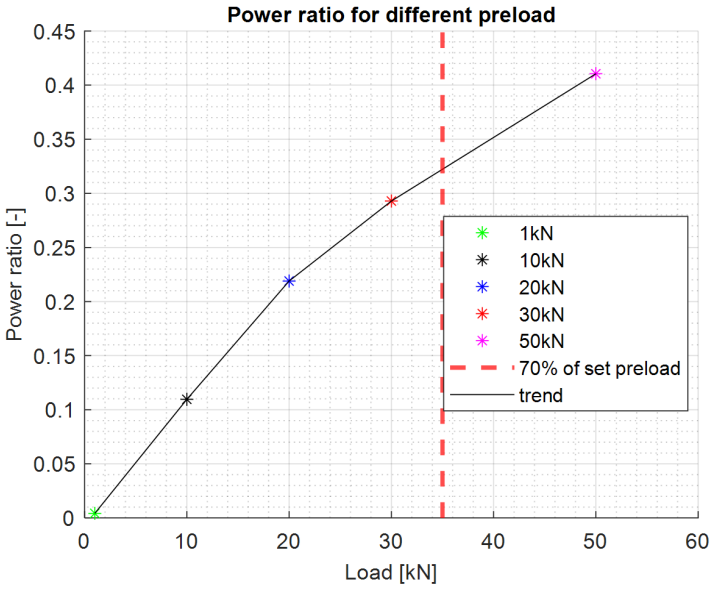

Figure 5-9: *Power ratio plotted for different preload.*

5-1-4 Small-scale experiment observations

- **Source frequency -** Source signal of lower frequency (50kHz) showed less interference and better results than higher frequency source signals (150kHz and 600kHz).
- **Experimental setup -** Experimental setup with proposed sensor positions were able to collect the responses properly for different preloads. As expected, the reference sensor signals for different preloads were constant, and the measuring sensor signals varied proportionally to the preload level. Thus, a baseline-free methodology can be established using the proposed setup.
- **Analytical framework and methodology -** Signal analysis was done for the sensor responses based on the proposed analytical framework and methodology. In addition, the simplifications and the assumptions employed for the selection of signal envelope in the proposed algorithms in Chapter 3-3-1 were checked and verified.
- **Hypotheses verification -** Proposed hypotheses 1 and 2 are verified by obtaining increasing trend energy and power ratio plots. Hence the same methodology, sensor positions and hypotheses will be used for the large-scale experiment verification.

5-2 Large-scale experiment results

As an answer to research subquestion,

- Can the proposed methodology and hypothesis be applicable for bolts independent of its dimension?

Based on the small-scale experiment observations, the large-scale experiments were designed and conducted as discussed in Chapter 4. Three experiments were conducted on two bolts (M64) of the considered setup. Results and the hypotheses verification for the three experiments conducted are discussed in this section. The procedure for the hypotheses verification is the same as followed in Section 5-1-3. Hence only the relevant results are discussed in this section.

5-2-1 Bolt 1 - VS600-Z1

Experiments were conducted for five different source frequencies using a resonant sensor VS600-Z1 as shown in Table 4-2. Figure 5-10 shows the trend obtained for hypothesis 1 (energy ratio trend) for different source frequencies. A similar trend was also seen for hypothesis 2. The experiments collected sensor responses for different source frequencies for every individual preload. Therefore, all the parameters except the source centre frequency were constant for each preload. However, only the source frequency of 40kHz showed a proper increasing trend and verified both the proposed hypotheses. A possible reason for other frequencies not providing a proper trend could be the use of resonant frequency sensors.

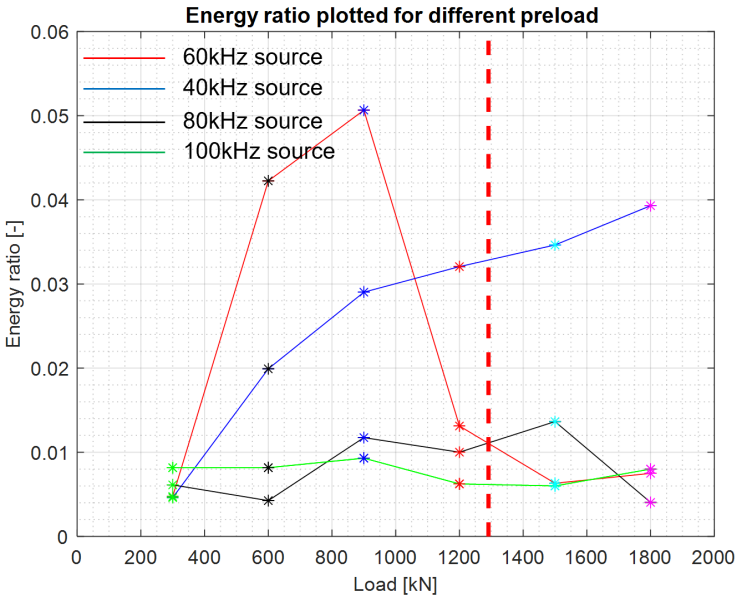

Figure 5-10: *Energy ratio plotted for each preload of bolt 1 - VS600 for different source centre frequencies.*

Even though the VS600-Z1 sensor gave better results for the 50kHz source in the small-scale experiment and the 40kHz source in bolt 1 of a large-scale experiment, the applicability of the sensor for other source frequencies were an issue. However, the validity of the proposed hypotheses for the 40kHz source confirms that the true contact area of the plate-nut interface increases with preload. Figure 5-11 shows the sensor signal collected for 40kHz source frequency for different preloads.

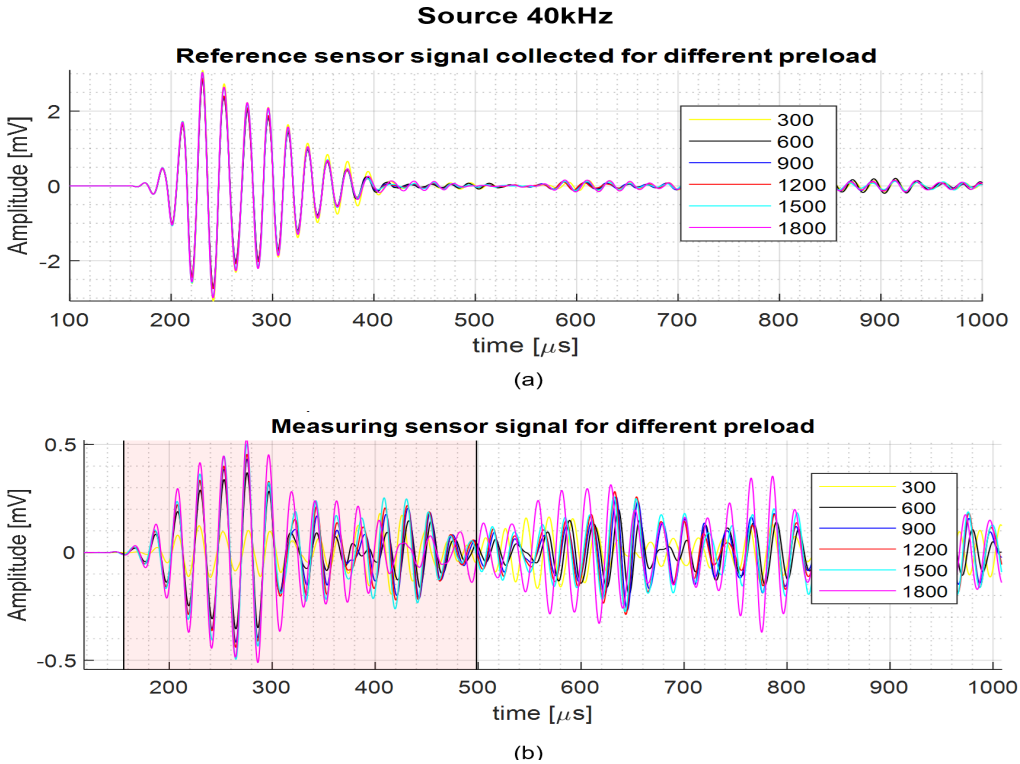

Figure 5-11: *(a) Reference sensor response in different preload levels for 40kHz source signal (b) Measuring sensor response in different preload levels with algorithm selected envelope for 40kHz source signal.*

The sample experimental signals shown in Chapter 3-3-1 to explain the algorithm 1 and 2 are corresponding to bolt 1 -VS600-Z1 sensor responses for 40kHz. The energy and power ratio obtained for the 40kHz source signal are shown in Figure 5-12 and 5-13 with repeatability check.

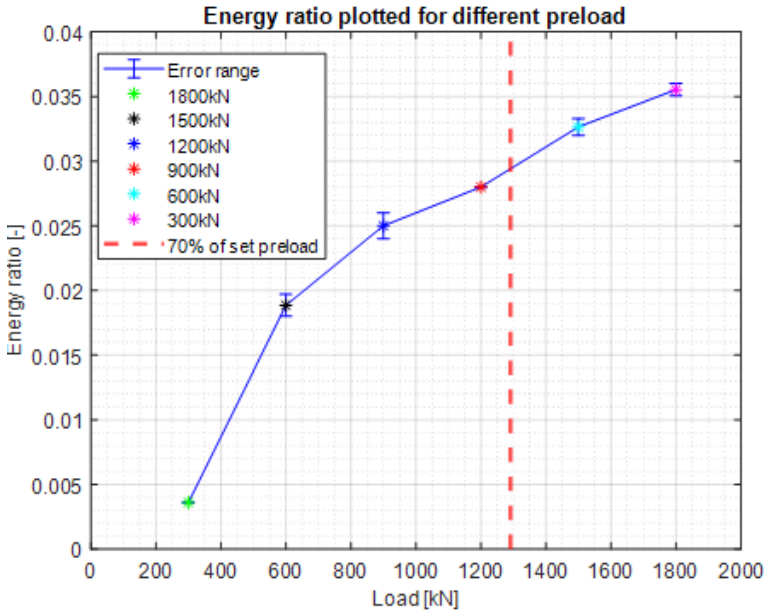

Figure 5-12: *Energy ratio plotted for bolt 1 - VS600 using 40kHz as source centre frequency.*

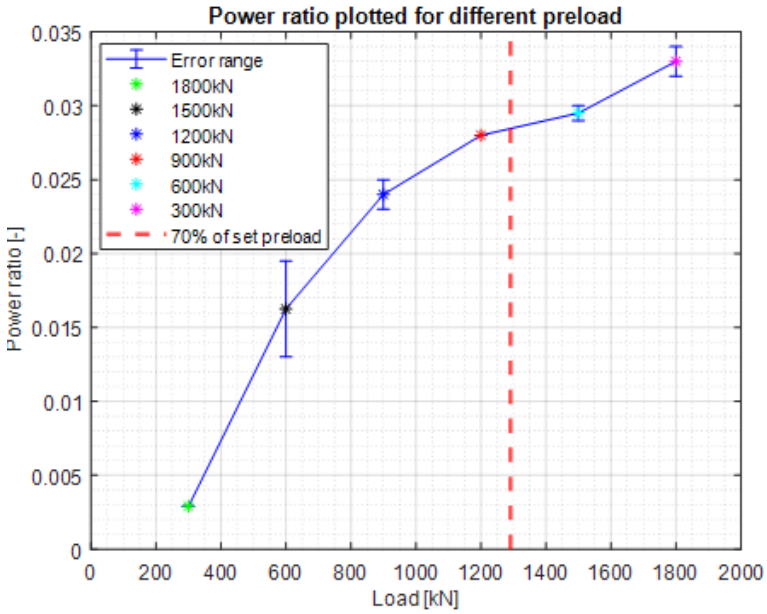

Figure 5-13: *Power ratio plotted for bolt 1 - VS600 using 40kHz as source centre frequency.*

5-2-2 Bolt 1 - R6α

Similar to Section 5-2-1 experiments were conducted for five different source frequencies as shown in Table 4-2. R6α also being a resonant sensor at 60kHz showed proper trend and verified both hypotheses 1 and 2 only for the source of 60kHz. Figure 5-14 shows the reference and measuring sensor response collected for 60kHz source in different preload levels. The obtained energy and power ratio plots are shown in Figure 5-15 and Figure 5-16.

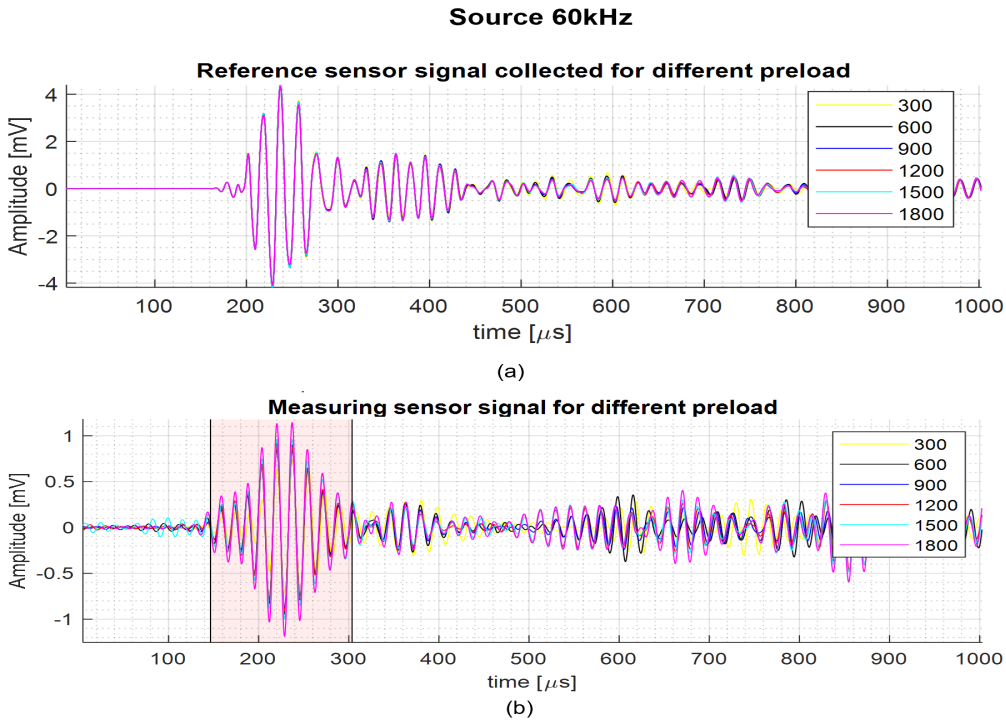

Figure 5-14: *(a) Reference sensor response in different preload levels for 60kHz source signal (b) Measuring sensor response in different preload levels with algorithm selected envelope for 60kHz source signal.*

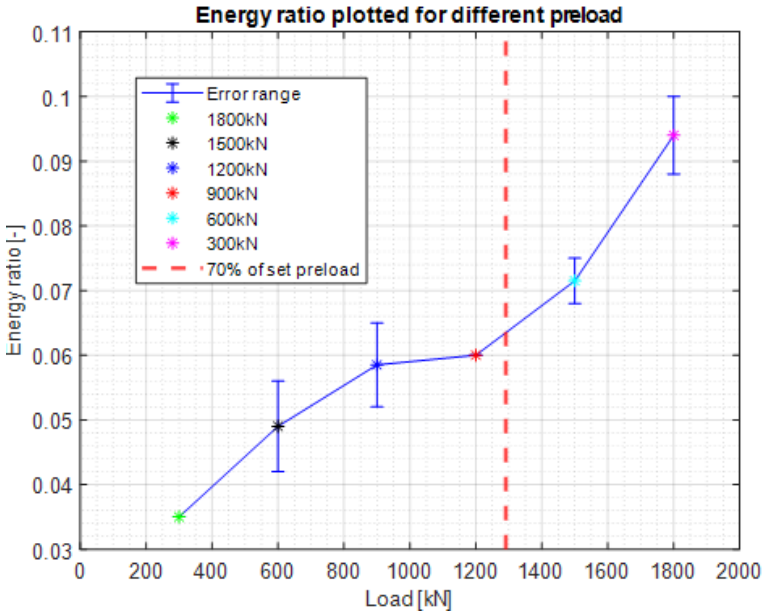

Figure 5-15: *Energy ratio plotted for bolt 1 - R6α using 60kHz as source centre frequency.*

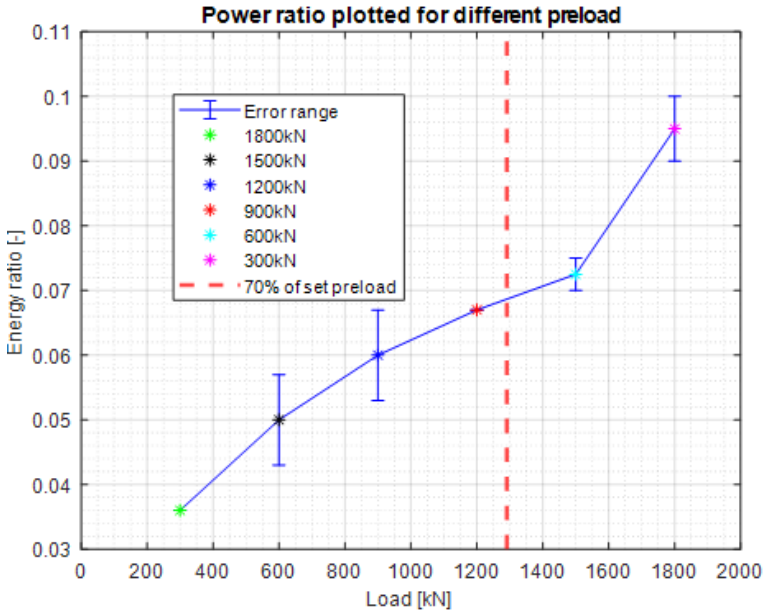

Figure 5-16: *Power ratio plotted for bolt 1 - R6α using 60kHz as source centre frequency..*

5-2-3 Bolt 7 - VS600-Z1

For bolt 7, the higher source frequencies 150kHz and 600kHz were also checked to ensure the small-scale experiment observations. The observation for high frequency showed high interference pattern similar to the small-scale experiments. Figure 5-17 shows the measuring sensor response collected for 150kHz at 1800kN. However, among other source frequencies, results with a proper trend for hypotheses 1 and 2 were obtained only for 60kHz. Figure 5-18 shows the sensor responses collected for 60kHz source in different preload levels. The obtained energy and power ratio plots are shown in Figure 5-19 and Figure 5-20.

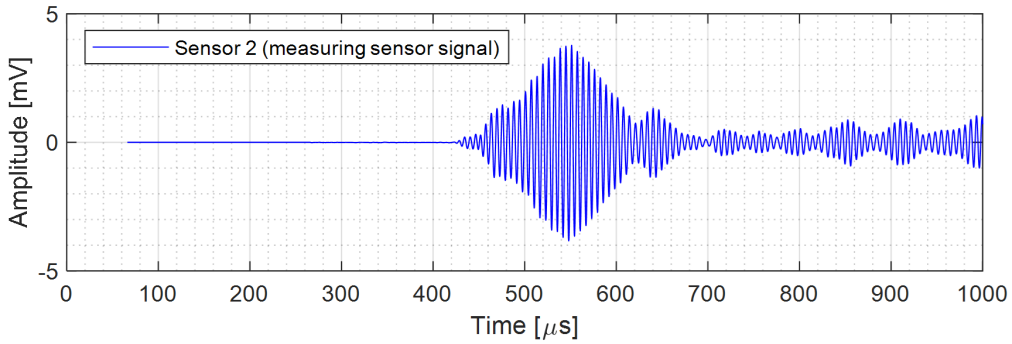

Figure 5-17: *High interference pattern is observed in the measuring sensor response collected for 150kHz at 1800kN.*

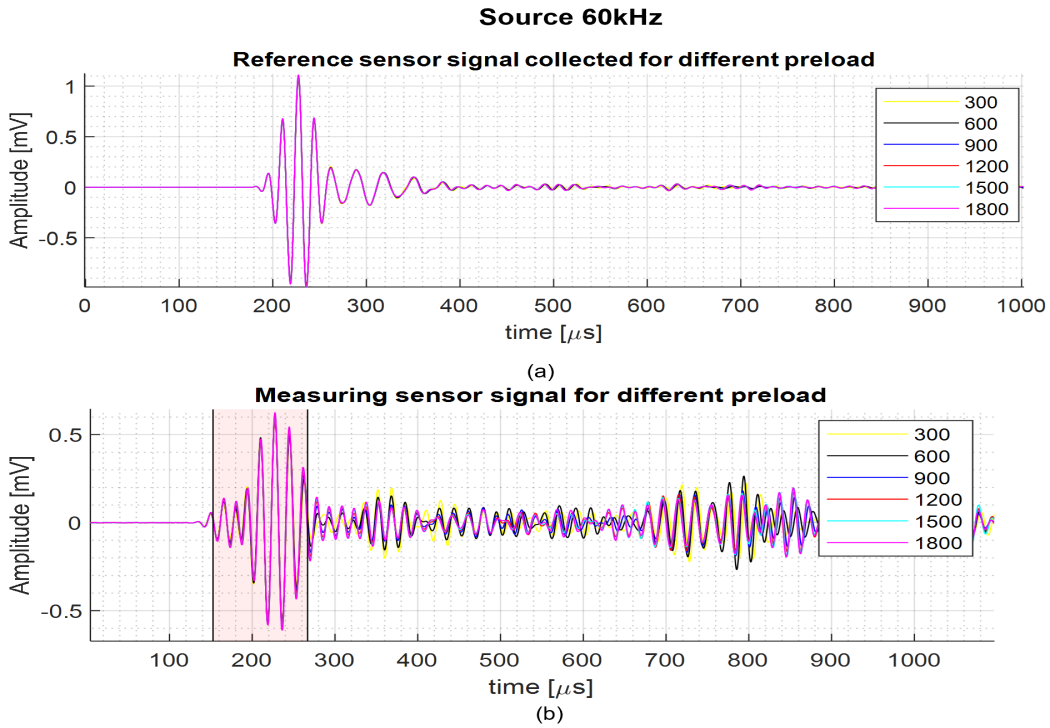

Figure 5-18: *(a) Reference sensor response in different preload levels for 60kHz source signal (b) Measuring sensor response in different preload levels with algorithm selected envelope for 60kHz source signal.*

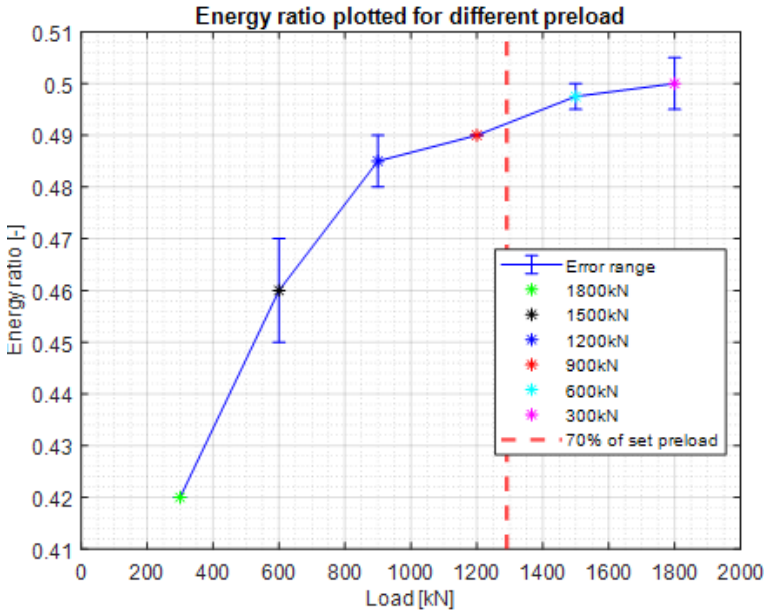

Figure 5-19: *Energy ratio plotted for bolt 7 - VS600 using 60kHz as source centre frequency.*

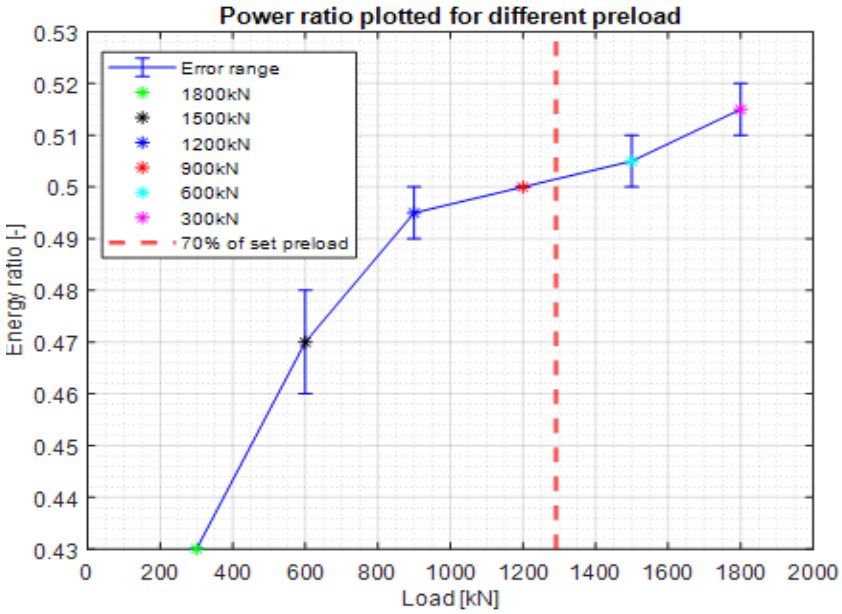

Figure 5-20: *Power ratio plotted for bolt 7 - VS600 using 60kHz as source centre frequency.*

5-2-4 Large-scale experiment observations

- **Source frequency observation:** Higher frequencies showed a similar interference pattern in sensor response as in small-scale experiments. However, only a certain frequency in each experiment was able to verify the hypotheses. Different source frequencies were tested for each preload. Thus, the parameters such as sensor position, couplant, preload and the contact asperities at the interface are constant for all source frequencies tested. The obtained results seem that the proposed methodology and hypotheses are valid. However, using a resonant sensor is expected to have a strong influence on the final result and hypothesis verification. Table 5-1 shows an overview of all experiment results conducted with M64 bolts.
- **Experimental setup -** Experimental setup were the same as followed for the small-scale experiments. Similar to small-scale experiment observations, reference sensor responses had no changes for varying preload and meanwhile, measuring sensor responses varied proportionally to the preload change.
- **Methodology and hypothesis verification:** Proposed hypotheses are verified by following the same methodology as of small-scale experiments. The validity of the methodology and hypotheses on M64 bolts. However, further experiments and research on sensor and source frequency response are needed.

Bolt 1	
VS600-Z1	
Load	Frequency
300kN	25kHz
600kN	40kHz
900kN	60kHz
1200kN	80kHz
1500kN	100kHz
1800kN	

Bolt 1	
R-6α	
Load	Frequency
300kN	15kHz
600kN	25kHz
900kN	40kHz
1200kN	60kHz
1500kN	80kHz
1800kN	

Bolt 7	
VS600-Z1	
Load	Frequency
300kN	25kHz
600kN	40kHz
900kN	60kHz
1200kN	80kHz
1500kN	100kHz
1800kN	

Table 5-1: Overview of large-scale experiment results (Green: Proposed hypothesis validated Red: Not validated)

5-3 Crack detection

To answer the following research subquestion,

- Can the experimental setup proposed for preload monitoring be also utilized for crack detection in bolts?

The Hsu-Nielsen source was used to simulate cracks in the first engaging thread of bolt and nut for crack detection. The elastic wave generated from the simulated crack propagated through the bolt, nut and plate to reach the measuring and reference sensors. As discussed in the Chapter 3-2-2 for the simulated cracks, the elastic waves propagate through the primary path reached sensor 2 first. And then, the acoustic wave gets transmitted through the plate-nut interface and reached sensor 1. To check the loss of the elastic waves, sensor responses were collected for multiple simulated cracks at different preload levels. The sample responses of sensors 1 and 2 for the simulated crack is shown in Figure 5-21. As expected, the response received by sensor 2 was better compared to sensor 1 response. Since the elastic waves need to transfer through an interface to reach sensor 1, there is a considerable loss of wave intensity. All the simulated cracks were tested on the bolt thread of the opposite end of the sensors. Cracks on the thread of the sensor side might have a stronger response than the conducted experiments. However, the simulated cracks were tested to check for the loss of elastic waves for a maximum possible propagation path. Figure 5-22 shows the peak amplitude of a hit for the simulated cracks at preload levels of 300kN, 900kN and 1800kN. It is observed that the sensor 2 peak value is high compared to sensor 1. Moreover, it can be observed that due to the influence of the plate-nut interface for each preload, the peak amplitude of sensor 1 gets varied.

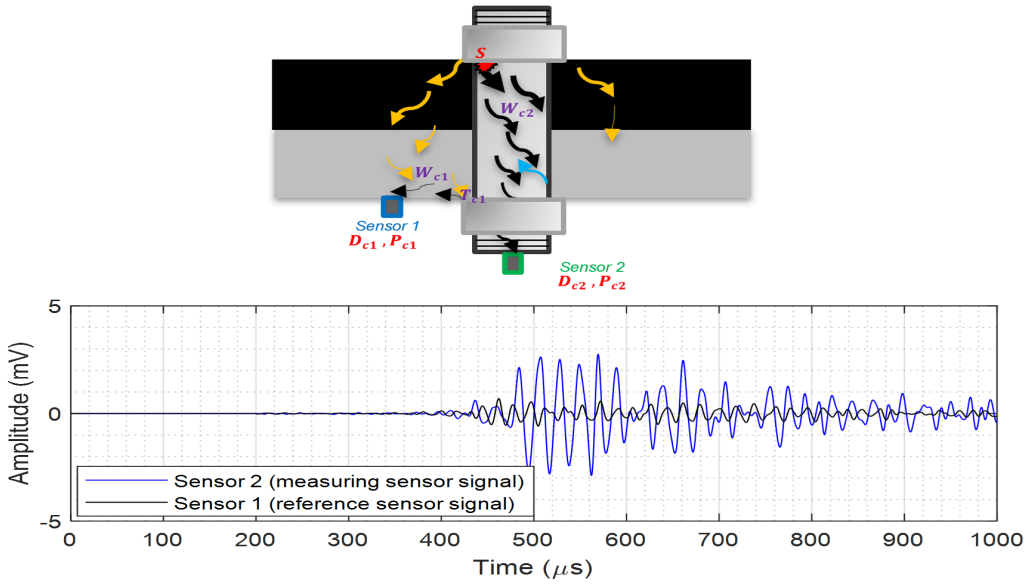

Figure 5-21: *Sample of simulated crack responses by the sensor 1 and sensor 2.*

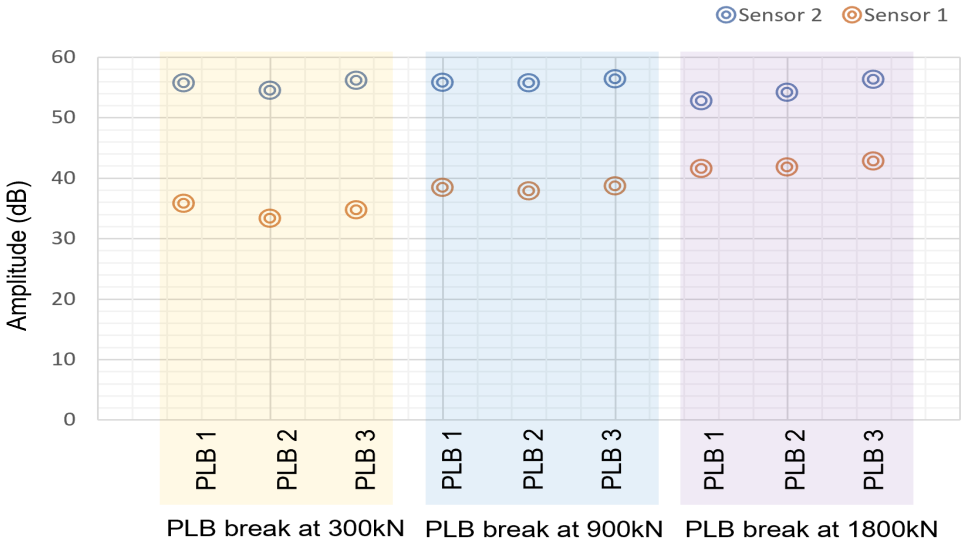

Figure 5-22: *Peak amplitude of simulated cracks at preload levels of 300kN, 900kN and 1800kN.*

5-3-1 Crack detection observation

From the experimental observation for crack detection, it is clear that both the sensors were able to detect the simulated cracks. However, considering the loss of elastic wave at the plate-nut interface, the response of the sensor attached to the bolt end (sensor 2) can be preferred to be taken for crack detection study. Limited to the scope of this feasibility study, the possibility of crack detection using the same experimental setup is confirmed.

Chapter 6

Numerical simulation

The experiment results showed that the proposed hypotheses are valid and can be used to estimate bolt preload. However, the experiment results did not show the validity of the hypotheses for all the source frequencies. The main objectives of the numerical simulations in this chapter are to additionally check the validity of the hypothesis independent of sensors and coupling, understand the wave propagation and reflections better, and check the feasibility of passive preload monitoring. To achieve the mentioned objectives, the methodology for numerical simulation is established first. Once the model and method are formulated, the simulation will be flexible, take less time, and be cost-efficient compared to performing multiple experiments.

6-1 Introduction

The equation of motion following the general theory of elasticity is given by,

$$\rho\{\ddot{\mathrm{u}}\} + \nabla \cdot \{[T]\} = \{\mathrm{f}\} \tag{6-1}$$

whereas u is the deformation, ρ is the specific mass, ∇ is the divergence operator, T is the stress tensor and f is the external body force. Finite element methods can be used to solve this wave equation numerically. As discussed in Chapter 1-5-2, SEM is considered in this research for performing the numerical simulation. In SEM, the domain is discretised into elements, each having collocation points of Gauss-Lobatto-Legendre (GLL) nodes. The number of GLL points is determined by the polynomial order used. This research uses a higher-order Lagrange interpolation polynomial as a basis function that passes through local Gauss-Lobatto integration points defined per element [18][113]. The orthogonality of the basis function results in the diagonal mass matrix, which is a significant advantage of this method in simulation of ultrasonic waves with small element sizes [74]. The equation of motion is reduced to the algebraic Equation 6-2 by finite element discretisation.

$$[\mathrm{M}]\{\ddot{\mathrm{u}}_i\} + [\mathrm{K}]\{\mathrm{u_i}\} = \{\mathrm{f_{v,i}}\} \tag{6-2}$$

For time discretization, an explicit Newmark scheme is used. Komatitsch and Tromp [113], Pahlavan [18], and Gopalakrishnan [74] may be consulted for a more detailed description of the spectral element technique.

6-2 Methodology

Figure 6-1 shows the methodology followed to perform the numerical simulations. Initially, a 2D model representing the experimental setup is defined. Then, the corresponding material properties are assigned. Next, the interface layer with varying properties is introduced to include the influence of surface roughness. Finally, the mesh convergence is checked before running the required simulations.

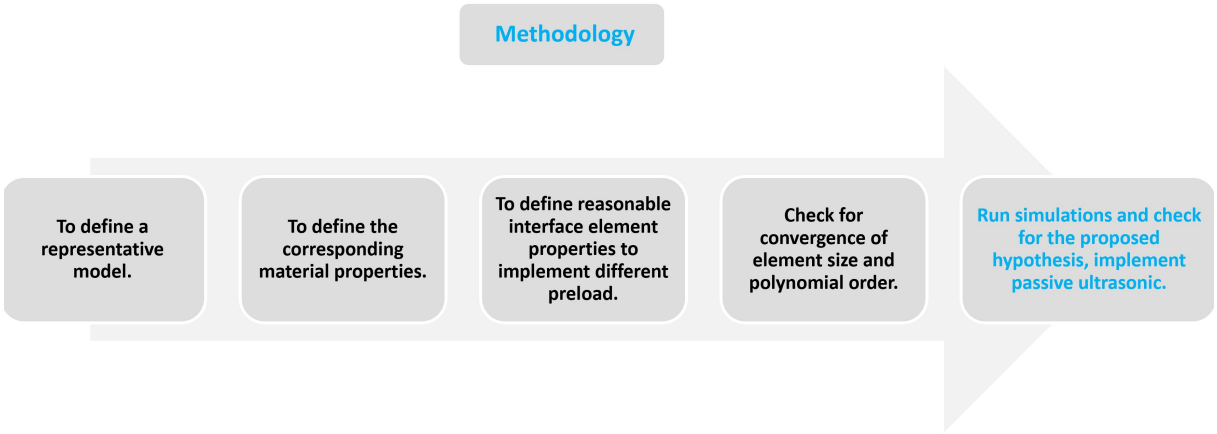

Figure 6-1: *Methodology for numerical simulation.*

6-2-1 Model description

For the sake of computational efficiency, a 2D model in analogy with the large scale experiment setup as described in Chapter 4-2-1 is created. Plane strain conditions are assumed for the modelled 2D geometry. Figure 6-2 shows the model. A rectangular domain of dimension 600mm $\times$ 680mm is considered. The domain height was determined by the length of the M64 bolt considered. Source and a reference sensor are positioned on the plate near the interface, and another sensor (measuring sensor) is on the bolt top end. The material properties considered for the plate, bolt and nut are given in Table 6-1.

Component	Material	Young's modulus [$\times 10^9$ N/m2]	Poisson ratio [−]	Density [kg/m3]
Plate	A316	193	0.27	8000
Nut	carbon steel	210	0.3	7800
Bolt	carbon steel	200	0.3	7800

Table 6-1: Material properties used in the analysis

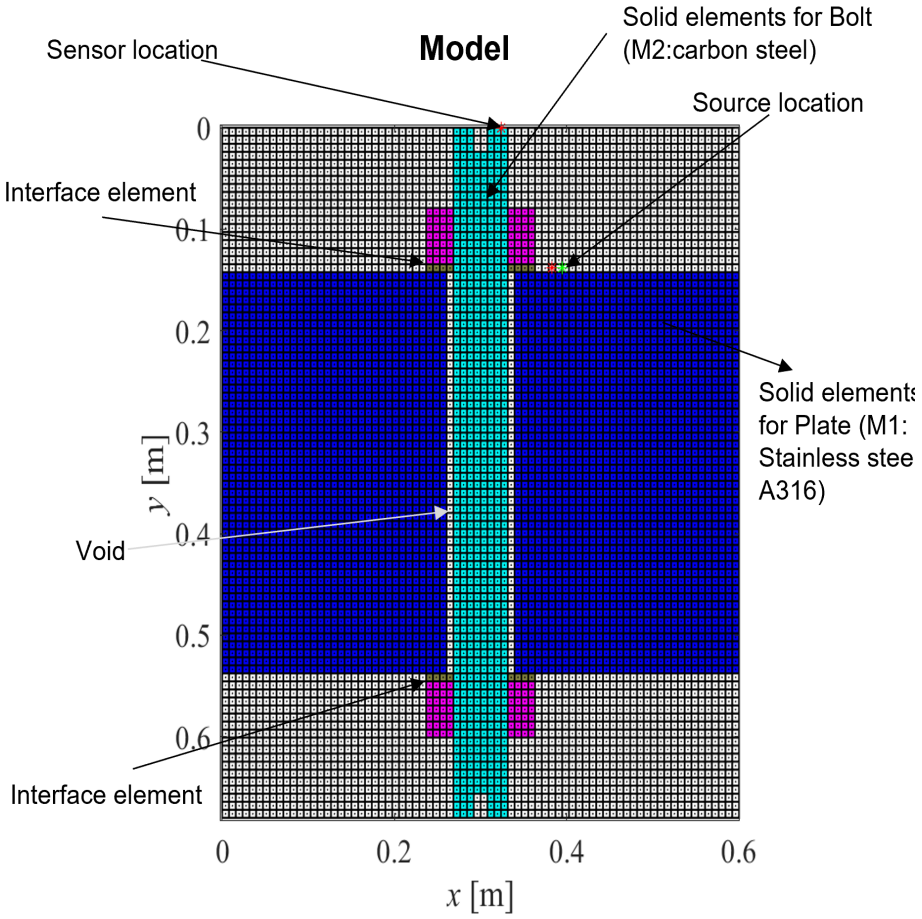

Figure 6-2: *Model considered for numerical simulation.*

6-2-2 Interface element

This section answers the research subquestion,

- How can the change in interface conditions for varying preload be implemented in the Spectral Finite Element Method (SEM) to study wave propagation?

As discussed in Chapter 1-6-2, the implementation of interface conditions in the simulation is necessary to study the wave propagation. Figure 6-3 shows the actual representation of the interface contact area. As the preload increases, the true contact area increases and correspondingly, the transmission of waves increases.

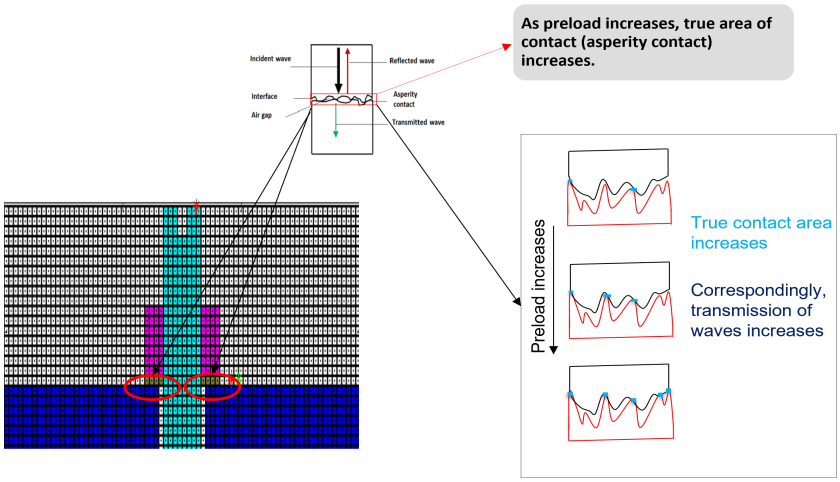

Figure 6-3: *Actual representation of interface element.*

To implement the interface layer into the simulation model, the research of Kendall et al. [114] was used as the basis. The study attempted to determine the true contact area between two stationary contacts using the ultrasonic technique. Figure 6-4 shows the experimental setup used by Kendall et al. [114]. The ultrasonic wave was sent through one body, and transmitted intensity through the interface was measured at the other end.

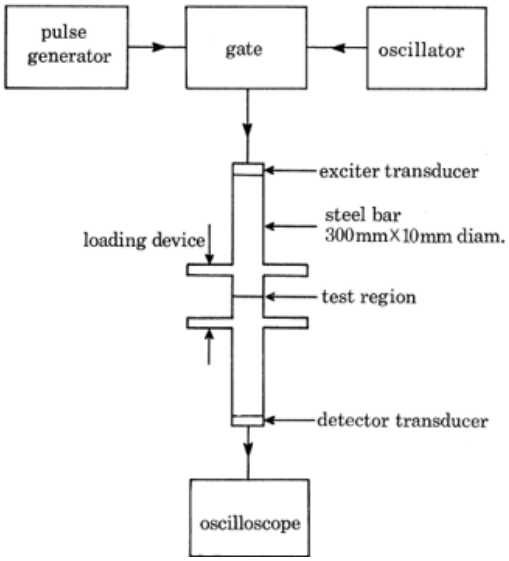

Figure 6-4: *Schematic representation of the experimental setup used for determining the interfacial stiffness[114].*

The study found that the transmitted pulse is proportional to the elastic stiffness of the interface. Figure 6-5 shows the variation of interface stiffness with load.

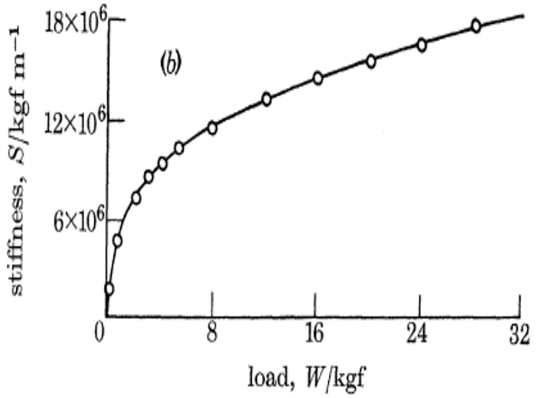

Figure 6-5: *Interface stiffness of the steel bar increases as the load applied increases [114].*

An expression derived for the single contact interface stiffness by Kendall et al. is given in Equation 6-3. The interface stiffness of single contact is proportional to the contact radius and Young's modulus of the material.

$$S = k.E.a \tag{6-3}$$

whereas S is the interface stiffness, k lies between $\pi/2\,(1-v^2)$ and $2/\,(1-v^2)$, E is the Young's modulus and a is the contact radius.

Similar studies were also performed by other researchers [52][115]. This knowledge can be extended and used in numerical simulations. The interface stiffness is used as a variable parameter to represent the change in preload. Meanwhile, wave transmission and reflection are generally influenced by the acoustic impedance of the material. Thus, this research proposes a novel approach of adjusting the acoustic impedance of interface elements from the estimated interface Young's modulus (change in E changes the interface element stiffness). The approach for defining an interface layer is initially described analytically and later numerically verified.

Analytical approach

For the analytical approach, a normal incidence of the wave is considered. The wave is assumed to transmit from the plate to the nut through the interface layer. The material properties of the plate and nut are considered as mentioned in Table 6-1. The property of the interface layer is considered the same as a nut. While Young's modulus of the interface layer is varied from 5 % of E_{nut} to 60 % of E_{nut} to change the wave transmission analogous to the preload change. The transmission of the wave across the materials with different acoustic impedance is determined using Equation 6-4. Figure 6-6 shows the schematic representation of the assumed wave propagation and the outline of the approach. For analytical calculation,

only the effect of material property is considered. The influence of thickness is not taken into consideration.

$$T = \frac{2 * Z_1}{(Z_{m1} + Z_{m2})} \tag{6-4}$$

whereas T is the transmission coefficient, Z_{m1} is the acoustic impedance of the material the wave propagates from, and Z_{m2} is the acoustic impedance of the material the wave propagates.

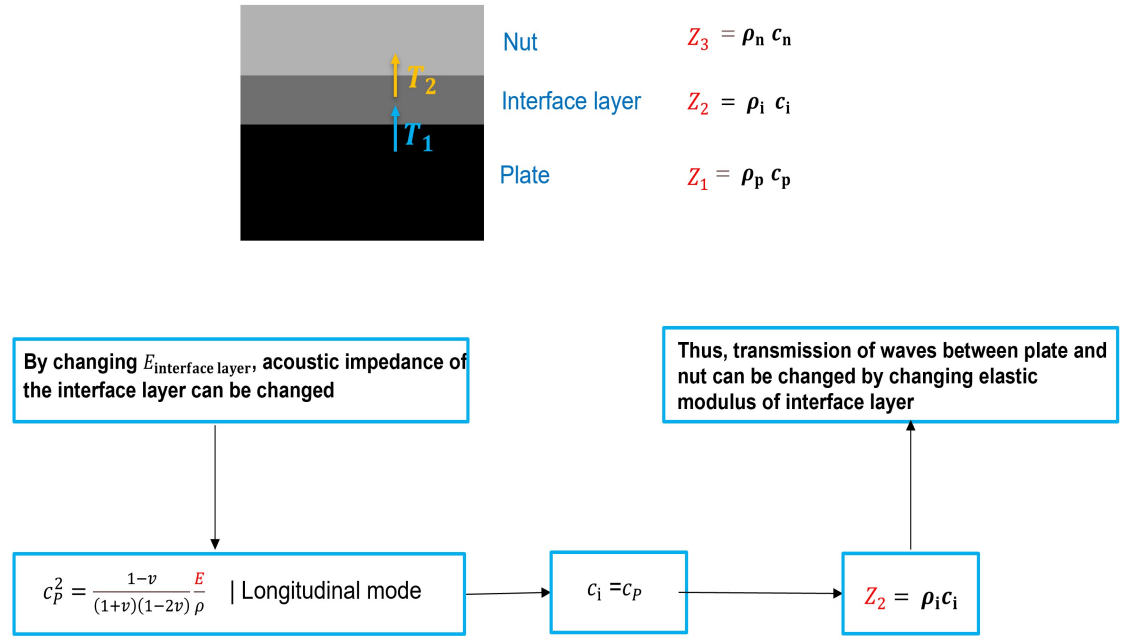

Figure 6-6: *Schematic representation of the assumed wave propagation and the outline of the approach.*

The acoustic impedance of each material can be calculated using Equation 2-3. The acoustic impedance of the interface layer can be adjusted by adjusting the velocity of the wave in the layer. In addition, the velocity of the wave (longitudinal mode[1] is considered) can be changed by adjusting Young's modulus of the interface layer. Thus, adjusting Young's modulus of interface layer can control the transmission of the waves across it.

Using Equation 6-4, the wave transmission across the plate and interface layer (T_1) is calculated. Then, the wave transmission across the interface layer and the nut is calculated (T_2). Then the total transmission from the plate to the nut is calculated by multiplying the transmission coefficient T_1 and T_2. Similarly, the total transmission is calculated for varying acoustic impedance of the interface layer. Figure 6-7 shows the total transmission coefficient calculated by the analytical approach for varying Young's modulus of the interface layer. Thus by changing the interface layer stiffness, the wave transmission across the interface can be varied. Therefore, the influence of surface roughness for varying preload can be simulated in the numerical simulation by changing Young's modulus of the introduced interface layer.

[1]Longitudinal mode is the fastest and the first arriving mode in solids.

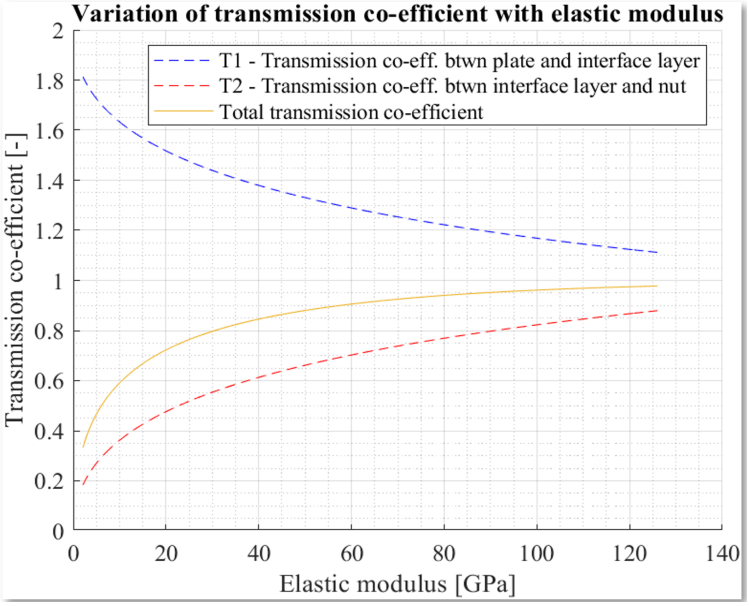

Figure 6-7: *Analytical total transmission of wave between the plate and nut for varying interface property.*

Numerical verification

The analytical approach showed the variation of wave transmission by changing the interface layer property. However, the analytical transmission did not consider the interface layer thickness. Therefore, the numerical simulation is performed to verify the analytical approach and check the influence of interface layer thickness. The model considered for the numerical verification is shown in Figure 6-8. The source and sensor are positioned next to the interface layer in the plate and the nut region to measure only the influence of interface thickness. The source used for the experiments is utilised for the numerical simulation. Mesh convergence for the model is achieved at the element size 2mm and second-order polynomial. Also, the model was converged for 4mm and fourth-order polynomial.

The transmission coefficient of the signal is determined by taking a ratio of the peak amplitude of the signal received after propagating through the interface layer (S2) to the peak amplitude of the base signal[2] (S1). Figure 6-9 shows the signal (S2) collected by the sensor for different Young's modulus of the interface layer. The transmission of the wave to nut decreases as Young's modulus of the interface layer is decreased.

$$T_{\text{Numerical}} = \frac{\widehat{P}_{(S_2)}}{\widehat{P}_{(S_1)}} \tag{6-5}$$

where $T_{\text{Numerical}}$ is the total transmission coefficient, $\widehat{P}_{(S_2)}$ is the peak value of the signal transmitted through the interface layer and $\widehat{P}_{(S_1)}$ is the peak value of the base signal received

[2]Base signal was collected by assuming the entire domain as a plate material with the same source and sensor location.

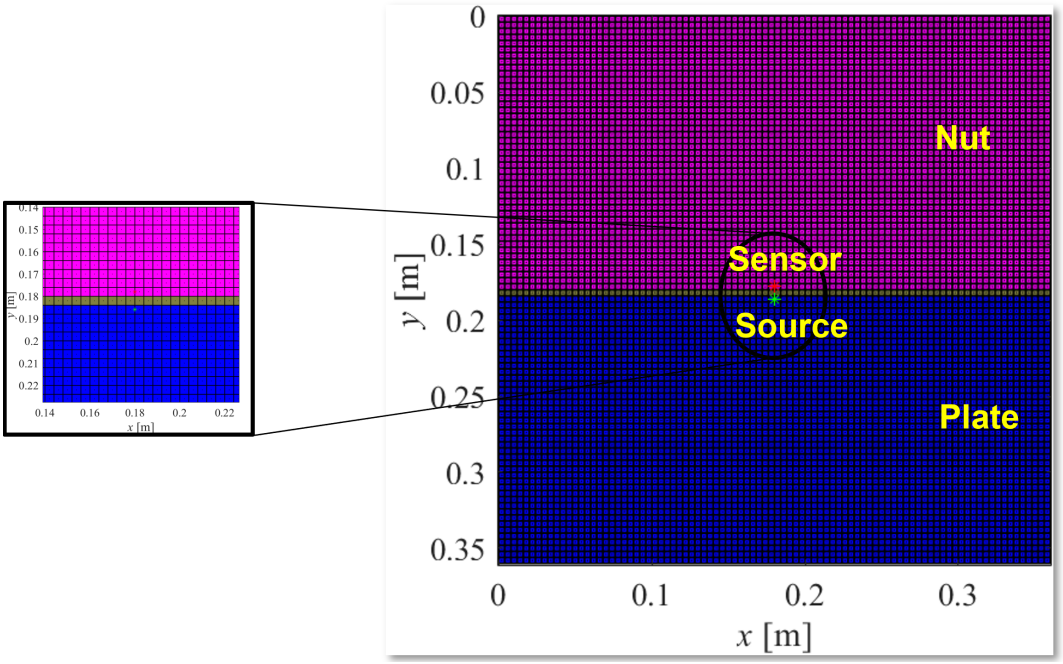

Figure 6-8: *Model considered for the numerical verification.*

by considering the entire domain as a plate mateiral.

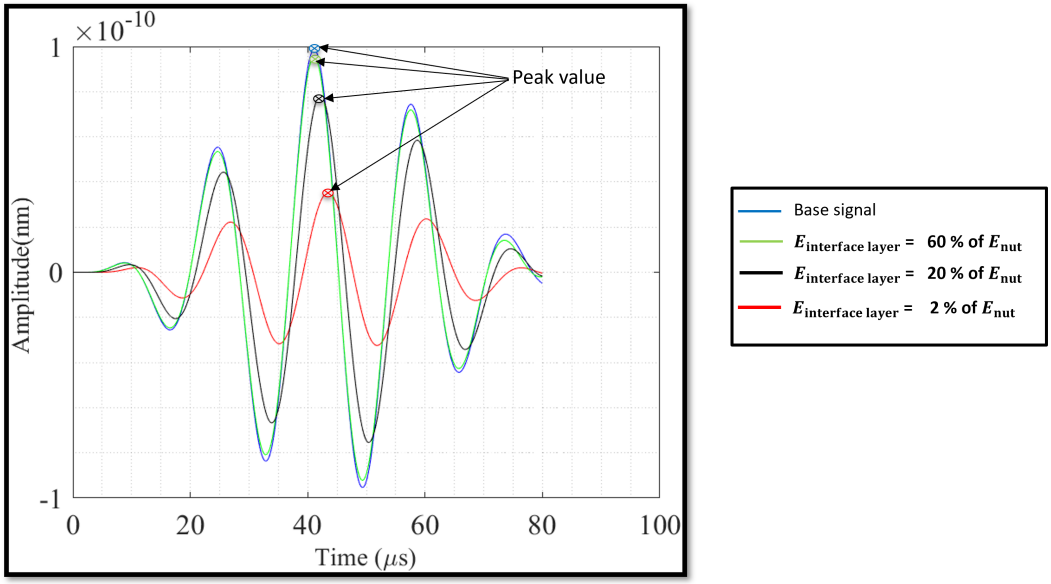

Figure 6-9: *Signal collected by the sensor for different Young's modulus of interface layer.*

Figure 6-10 shows the total transmission coefficient of numerical simulation in comparison to the total analytical transmission coefficient. The trend of the analytical and numerical transmission coefficients is the same. However, there is a slight difference in the trend, which could be due to considered interface layer thickness. For numerical simulation, the total transmission coefficient was calculated for mesh size of 2mm and second-order polynomial and as well as for 4mm and fourth-order polynomial. Again, the difference in the trend can be seen because of the interface layer thickness.

Moreover, the values for numerical transmission coefficient are obtained only for the ten different interface layer Young's modulus and plotted correspondingly. In contrast, the analytical trend was made as a continuous plot. It is also observed that as the thickness of the interface layer increases, the transmission coefficient decreases. Based on the mesh convergence of the main model without interface layer as discussed in Section 6-2-4, 2mm element size and second-order polynomial are considered for the interface layer thickness. Therefore, the main simulation is run by considering the interface layer thickness as 2mm and adjusting Young's modulus to represent different preloads.

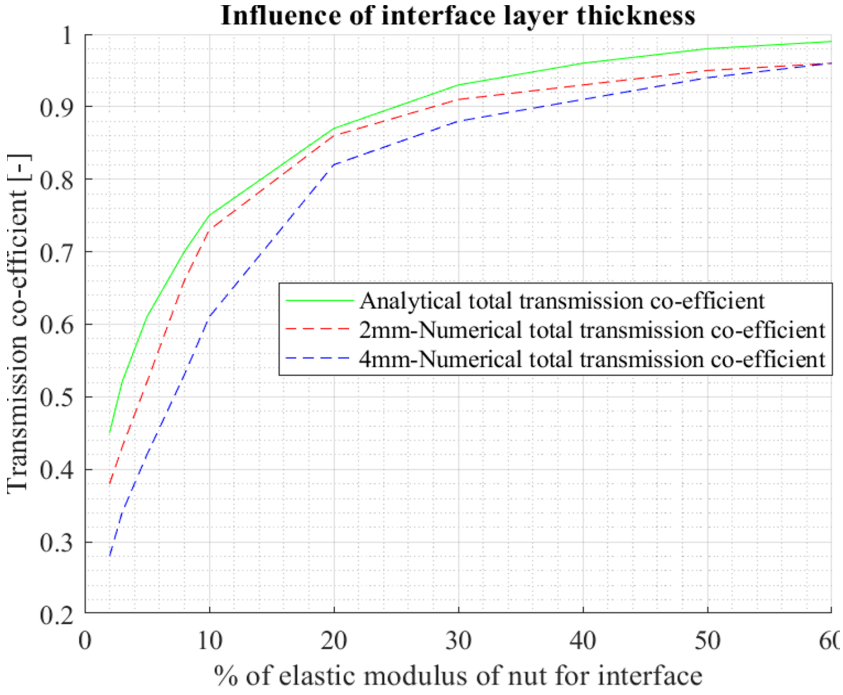

Figure 6-10: *Total transmission of numerical simulation in comparison to the analytical total transmission.*

6-2-3 Mesh refinement

A mesh refinement study was done to determine an optimum element size and polynomial order. The study was done by transmitting a signal from the source node, and the corresponding responses were collected from the sensor nodes. The received responses for each element size and polynomial order were compared. The zero-lag cross-correlation value was used as a parameter to check the mesh convergence. Figure 6-11 shows the results of mesh refinement. Finally, an element size of 2mm and a second-order polynomial was considered for the entire domain. The element size was not decreased below 2mm to avoid a huge computational time.

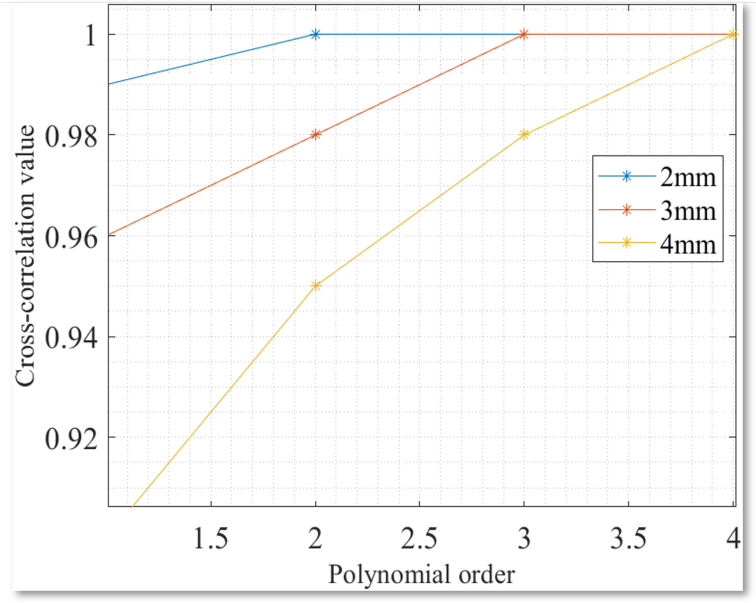

Figure 6-11: *Mesh refinement study showing a convergence from element size of 2mm and polynomial order 2.*

6-2-4 Simulation results

The simulation was run in the main model with the interface layer and the element size of 2mm, second-order polynomial. The sensors on the plate and the top end of the bolt measure the responses to the given 40kHz source. Since the experimental preloads cannot be directly translated into a particular value of interface Young's modulus, six different Young's modulus of the interface layer is used in the simulation. The methodology and hypothesis verification procedure are the same as discussed in Chapter 5-1-3. Results obtained from the simulation are shown in Figure 6-12 and 6-13. The simulation results show a similar energy and power ratio trend compared to experimental results (bolt 1- VS600-Z1). Thus the proposed methodology and hypotheses are confirmed independent of sensors, couplant and other environmental factors.

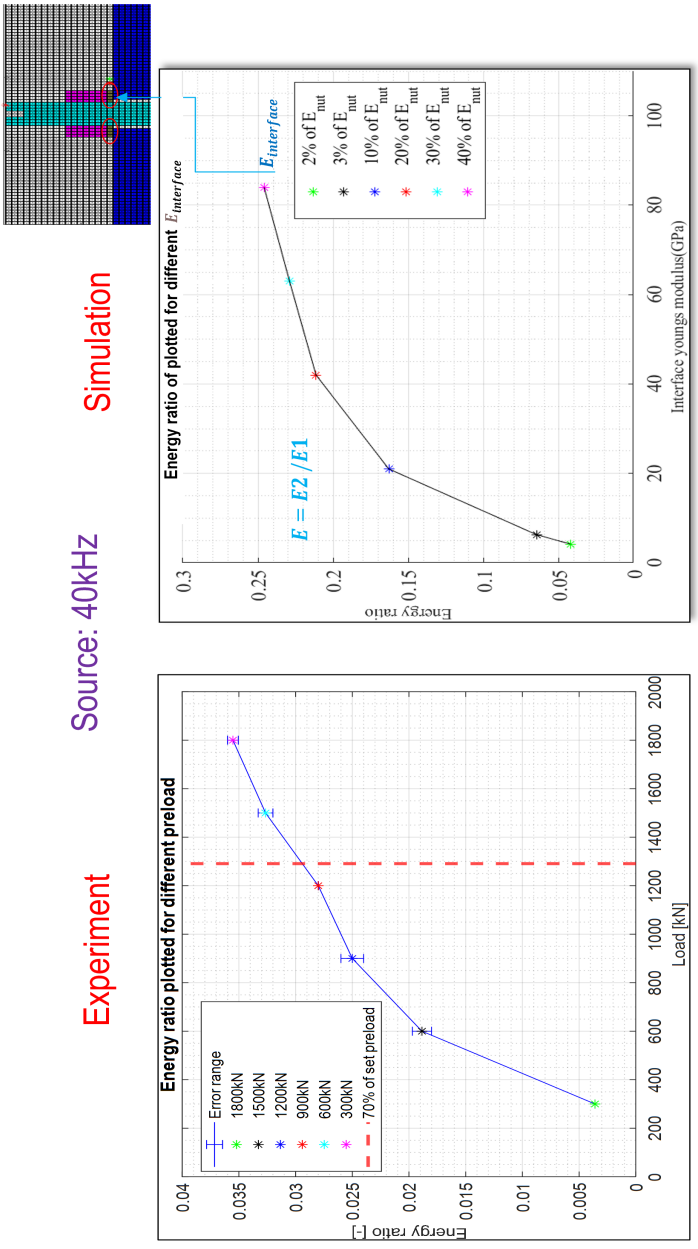

Figure 6-12: *Energy ratio plotted for experimental(bolt 1 - VS600) and numerical simulation output.*

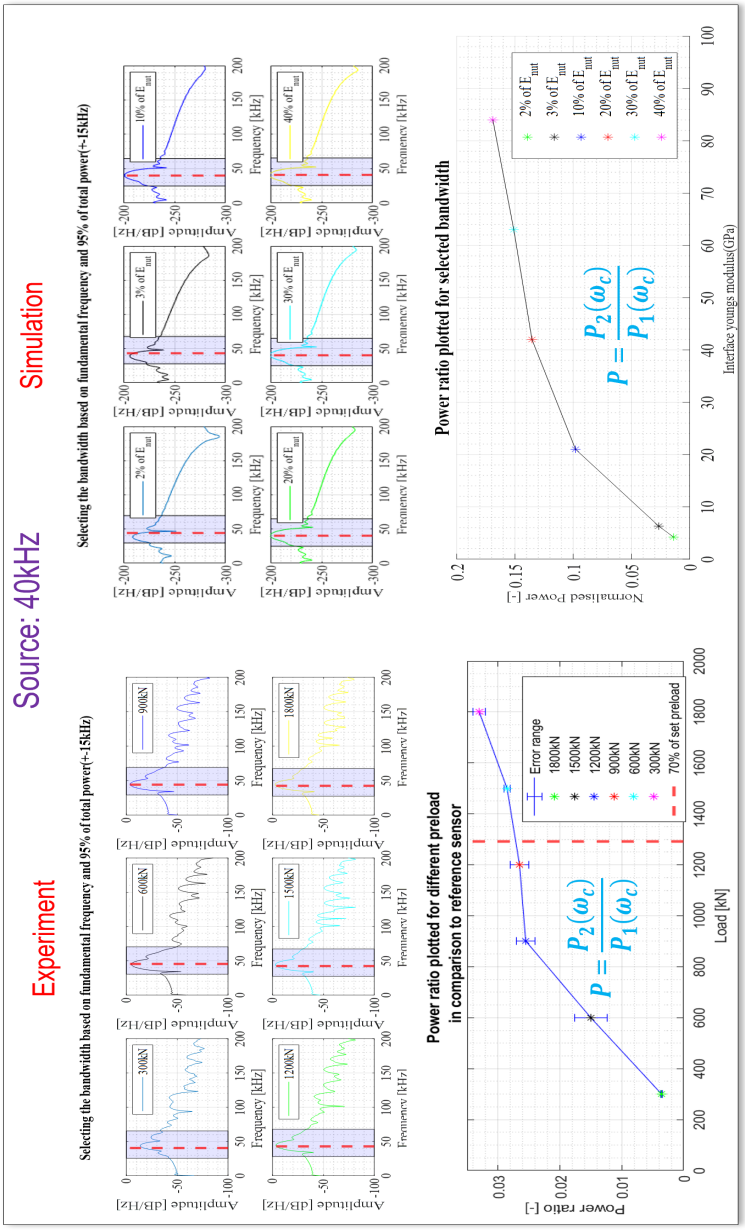

Figure 6-13: *Power ratio plotted for experimental(bolt 1 - VS600) and numerical simulation output.*

Passive preload monitoring

So far, all the experiments and simulations considered the active source near the plate-nut interface for determining the preload. To check the feasibility of passive preload monitoring, signals from the outside environment for preload estimation are conducted. Figure 6-14 shows the concept for passive preload monitoring.

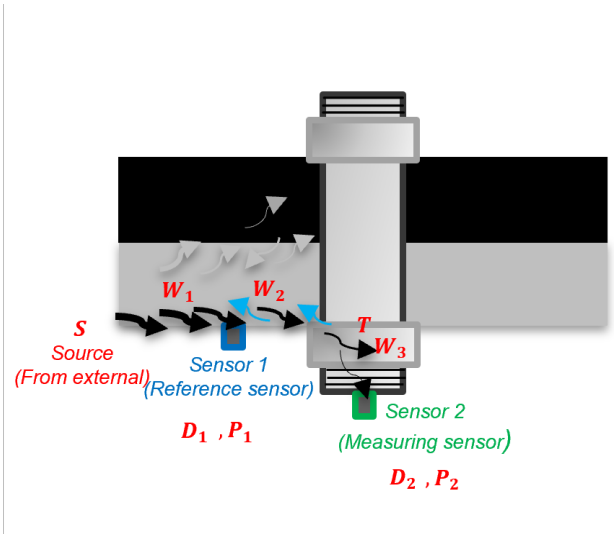

Figure 6-14: *Representation of passive preload monitoring.*

The source location in the numerical simulation was adjusted to evaluate the passive preload monitoring. Figure 6-15 shows the source location used. Figure 6-16 shows the energy ratio obtained from the simulation for the feasibility of passive monitoring. The results of the changed source location also follow the proposed hypothesis with a similar energy and power ratio trend. Therefore, the feasibility of passive preload monitoring is considered verified, and the same methodology and hypotheses can be extended. The source used at the chosen location for simulation was the 40kHz signal. However, the signals from the environment can be random, and the validity for the random signals is not explored in this feasibility study.

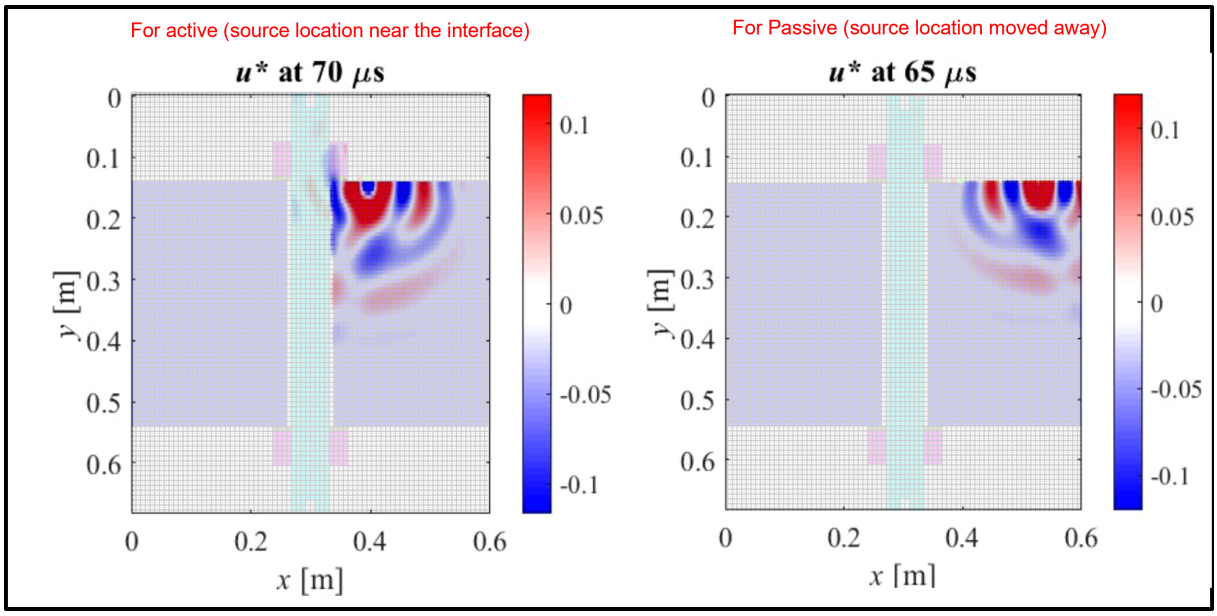

Figure 6-15: *Source location in numerical simulation for active and passive feasibility study.*

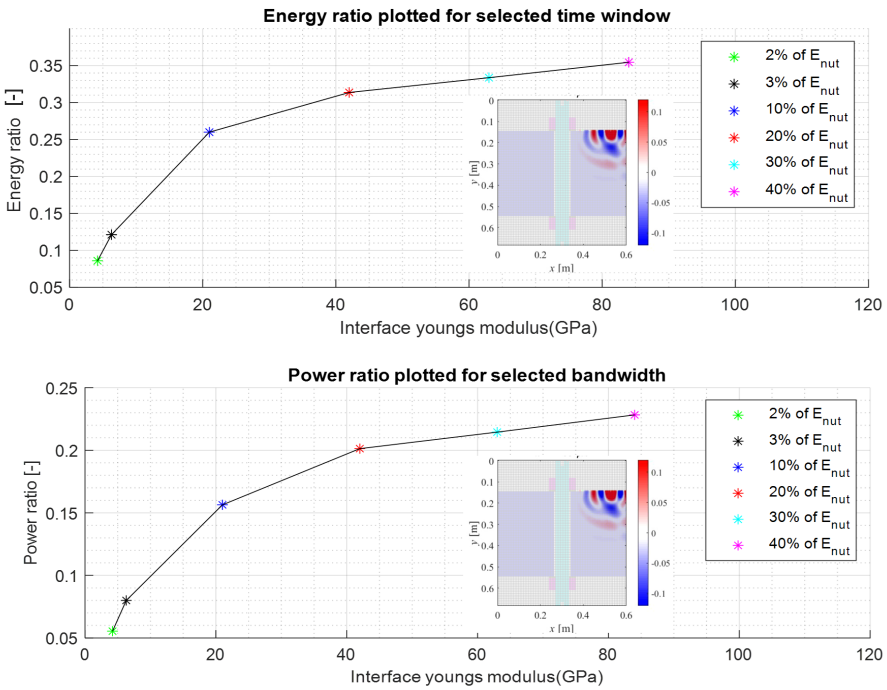

Figure 6-16: *Energy ratio from the simulation result of passive preload monitoring.*

6-2-5 Simulation conclusion

- SEM was used for the simulation of wave propagation in bolted joints.
- The knowledge gap on the influence of surface roughness in the numerical simulation was bridged by introducing a concept of the interface layer and tuning its stiffness.
- The validity of the proposed methodology and hypotheses were verified from the simulation results. The verification was done by performing numerical simulations with six chosen Young's modulus of the interface layer and comparing the obtained trend with the experimental observations.
- Feasibility of extending the proposed methodology and hypotheses for passive preload monitoring was examined. The simulation results suggest that the source from a distance may also be used for preload estimation. However, this study did not verify the validity of random source signals.

Chapter 7

Conclusions and recommendations

7-1 Conclusions

The main research question in this study was:

> *'Can ultrasonic waves be utilized for monitoring of individual bolts in a multi-bolted joint independent of its size and length ?'*

A summary of the conclusions is provided in relation to the research subquestions.

Preload detection

From the analysis of the knowledge gap in the literature, it is clear that most of the published investigations were limited to flat lap joints with a single bolt. In addition, the sensor positions used in the experimental setup could not track individual bolt preload in a multi-bolted joint and were baseline-dependent. Moreover, the previous studies had a knowledge gap on the time window selection of the sensor responses and the applicability of the method for larger bolt sizes.

Hence, in this research, an analytical framework and methodology were formulated based on the proposed preliminary experimental setup to check for the feasibility of preload detection using ultrasonic waves. In addition, two research hypotheses were proposed based on the principle of an increase in the true contact area with an increase in preload. Finally, small- and large-scale experiments were conducted to check for the validity of the proposed hypotheses and methodology.

The small-scale experiment on M12 bolts indicated that the energy and power ratio increases as the preload is increased. Also, the results indicate that the source frequencies have a significant influence on the proposed methodology. Furthermore, the results showed that the methodology could be applicable better to lower source frequency (50kHz) than very high

frequency (600kHz). Based on the small-scale experimental observations, large-scale experiments on M64 bolts were conducted to ensure that the methodology and hypotheses are independent of bolt size and length. The experiment results validated the proposed methodology and hypotheses. However, the validity was not proved for all the source frequencies. This discrimination of the validity could be partly due to the small wavelength at higher frequencies and the increased scattering, and partly due to the use of resonant type sensors for the experiments.

Moreover, large-scale experiments conducted were only with two diagonal bolts. Therefore, the influence of the adjacent bolt pretension was not investigated in this research. However, the proposed methodology depends on the local change in the true contact area of the plate-nut interface. Hence, the results are expected only to change when there is a change in the contact of the interface asperities and not influenced notably by the adjacent bolts. Therefore, the proposed sensor positions, methodology and hypotheses can be extended to every individual bolt in a multi-bolted joint to estimate the preload present.

Numerical simulation was performed to check the validity of the proposed methodology and the hypothesis without the influence of sensors and coupling. A novel approach was introduced to implement the change in wave transmission due to preload change. The proposed approach successfully validated the hypotheses and obtained results with a similar trend of experiment results. The feasibility study on extending the proposed methodology and hypotheses to passive preload monitoring suggest that the source from a distance can be used for preload estimation. However, the applicability of methodology and hypotheses for random noise was not evaluated in this research.

This research suggests that individual bolt preload monitoring, independent of bolt dimension, is feasible using the proposed methodology and the hypotheses. However, further research on sensor selection, source frequency, and the influence of other environmental factors is required to increase the reliability and accuracy of the methodology and hypotheses. In addition, Section 7-2 gives some recommendations for the future research.

Crack detection

This feasibility research investigated whether the same experimental setup for preload detection can be used for crack monitoring. In the scope of this research, this study was limited to the feasibility of crack detection. Therefore, experiments were conducted by simulating cracks in the first engaging bolt thread. The Hsu-Nielsen source was used to simulate cracks in bolts for this research. The results showed that the sensors in the setup could pick up the signals from the simulated cracks. Moreover, the results suggested that the response of the sensor attached to the bolt end could be preferred for further analysis of crack tracking since the wave does not have to undergo amplitude loss by propagating through any interface. Based on this observation, it is clear that the acoustic emission from the crack initiation or growth in each bolt can be identified by the sensor attached to the corresponding bolt. The acoustic emission from the adjacent bolts is expected to be weaker due to the transmission of waves through multiple interfaces. The feasibility of measuring these signals was not investigated in this research.

7-2 Recommendations

Preload monitoring

External loads and noise - The experiments in this research were conducted in a laboratory environment with controlled pretension without any external loads acting on the bolts. Experiments can be conducted by exposing the bolted joints to axial or shear loads for future research. Moreover, experiments can be performed in an offshore environment to assess the influence of external noise.

Surface roughness - While the feasibility research suggested that the proposed hypotheses are independent of bolt dimension, their applicability across a range of surface roughness levels must be tested. Therefore, multiple experiments should be conducted on geometries (connecting flange and nut) of different surface roughness to establish the optimum criteria required for the hypotheses to be true.

Sensor selection - All the sensors used in this experiment were resonant frequency sensors. Moreover, the results obtained have shown some issues for specific source frequencies based on the type of sensor used. Therefore, it is suggested that broadband sensors could be used along with resonant type sensors to get better clarification on the influence of source frequency responses.

Passive preload monitoring - In order to check for the feasibility of passive preload monitoring, experiments can be conducted by having a known source from a distance similar to a numerical simulation performed in this study. Later, the known source can be extended to an unknown excitation.

In-situ monitoring - To achieve the main objective of in-situ monitoring, a proper trend between the preload and the introduced energy or power ratio needs to be established. A proper trend can be achieved by performing multiple experiments using the appropriate sensor and source types for the selected bolt size and surface roughness. Once the relationship is established, a calibration procedure can be formulated for all the bolt sizes. Additionally, further hardware development for in-situ monitoring is necessary, including wireless transmission and the ability to withstand loads operating on the bolted joints.

Crack detection

The simulated crack experiments performed were not polluted with any external noise. Hence, clear sensor responses were received, and the peak amplitude of the received simulated crack response was around 60dB. However, external noise has the possibility to mask the actual acoustic signals from the bolt crack initiation or growth in practical offshore applications. Fatigue tests can be conducted to check the actual intensity of the acoustic waves generated and the possible crack detection range in the real environment. Along with crack detection, the crack tracking approach can be developed as discussed in Chapter 1-5-3.

Numerical simulation

Geometry - This research employed a 2D representation of the geometry of the experimental setup for numerical simulation. Therefore, a detailed evaluation could be made by performing a full 3D simulation of the situation.

Source definition - The source and sensor were defined as nodal points in the numerical simulation performed. However, the propagating wavefront will change when the source definition changes according to the real geometry of the sensor. Hence, based on the type of sensor used, the definition of the source could be changed and verified.

Interface layer - The proposed methodology for the interface layer was based on the change in acoustic impedance of the plate-nut interface for different preload. As a result, the wave transmissibility over the plate-nut interface determines the interface stiffness. However, the same can also be verified using an electrical impedance. Thus, experiments can be conducted to validate and establish the required interface stiffness for a given bolt corresponding to its preloads.

7-3 Final goal

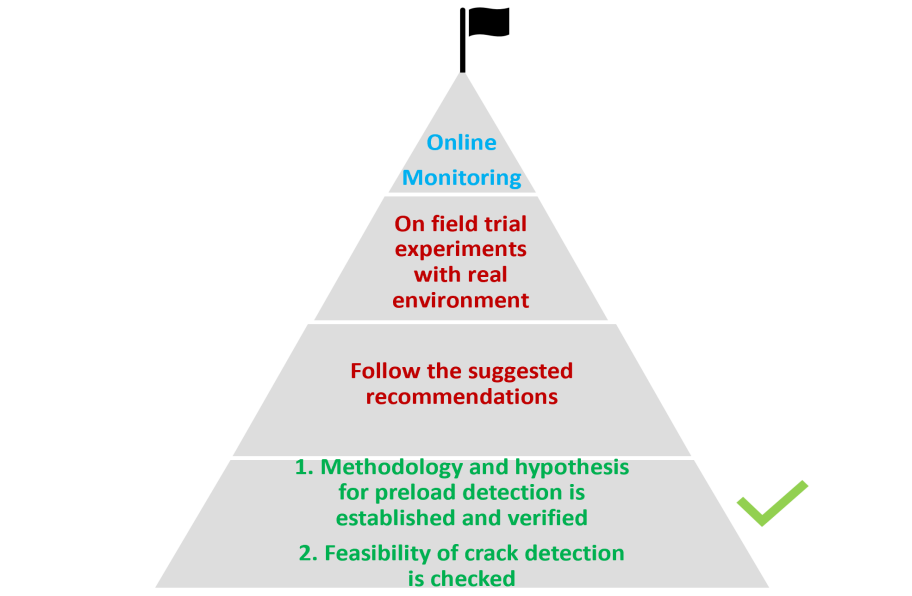

Figure 7-1: *What to achieve finally ?.*

Appendix A

Static preload analysis

A-1 Preliminary experimental setup

Earlier studies on preload detection used single bolted lap joints with actuators and sensors on the top and bottom plates. However, the sensor setup used in the previous researches cannot track individual bolt preload in multi bolted structures. The basic principle of the chosen preload detection method for this feasibility study is based on the change of true contact area. The study by Marshall et al. [116], and Stephen et al. [117] showed that the change in the true contact area is proportional to the preload contact pressure. Therefore, a static preload analysis was performed in ansys to check the extent of pressure distribution in the plates for bolt preload. Determining the extent of pressure distribution will assist in positioning the sensor and actuator appropriately. Considerations taken for the analysis are as follows.

Considerations for static preload analysis:

Geometry - The small scale experiment design described in chapter 4 was used to perform static preload analysis. Figure A-1 shows the slotted plates of dimension 100mm X 100mm X 20mm fastened with M12 bolt considered for the analysis. A cylinder with a nut was considered for the bolt geometry. Both plate and bolt material was considered as structural steel.

Contacts - The contact between the inside surface of the nut and bolt was considered as bonded. The interface of the plates was defined as a rough contact. Similarly, the bottom face of the nut and the plate was considered as rough contact.

Boundary condition - The two sides of the plates were fixed.

Mesh - Global mesh size of 3mm (mesh refinement check was performed based on the peak pressure value) was considered for the analysis, with 61506 nodes and 80426 elements in total. Element type considered for the analysis is SOLID185.

Load - Preload of 50kN corresponding to M12 - 8.8 grade bolt was applied in two steps

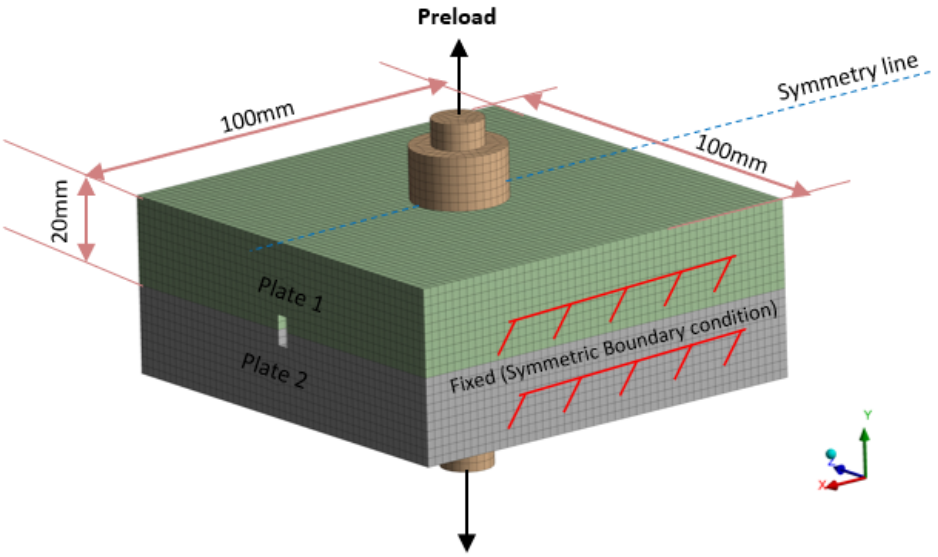

Figure A-1: *Model used for static preload analysis.*

(25kN and 50kN).

Figure A-2 shows the extend of pressure distribution in the plate obtained for the preload applied. Analysis showed that the applied preload generated a local pressure distribution in the plate-nut and plate-plate interfaces. The local pressure distribution changed with preload, indicating a change in the contact area. Therefore, the actuator and sensor positions are considered near the bolted joint interface for the analytical framework. The proposed sensor and actuator positions are expected to have better sensitivity for the preload change. Figure A-1 shows the considered preliminary experimental setup for the analytical framework. The sensor is attached to the top of the bolt, and the actuator is positioned near the plate and nut interface. In addition, a reference sensor is placed in between the actuator and the interface to ensure that the methodology is independent of baseline measurement.

Figure A-2 shows the extend of pressure distribution in the plate obtained for the preload applied. Analysis showed that the applied preload generated a local pressure distribution in the plate-nut and plate-plate interfaces. The local pressure distribution changed with preload, indicating a change in the contact area. Therefore, the actuator and sensor positions are considered near the bolted joint interface for the analytical framework.

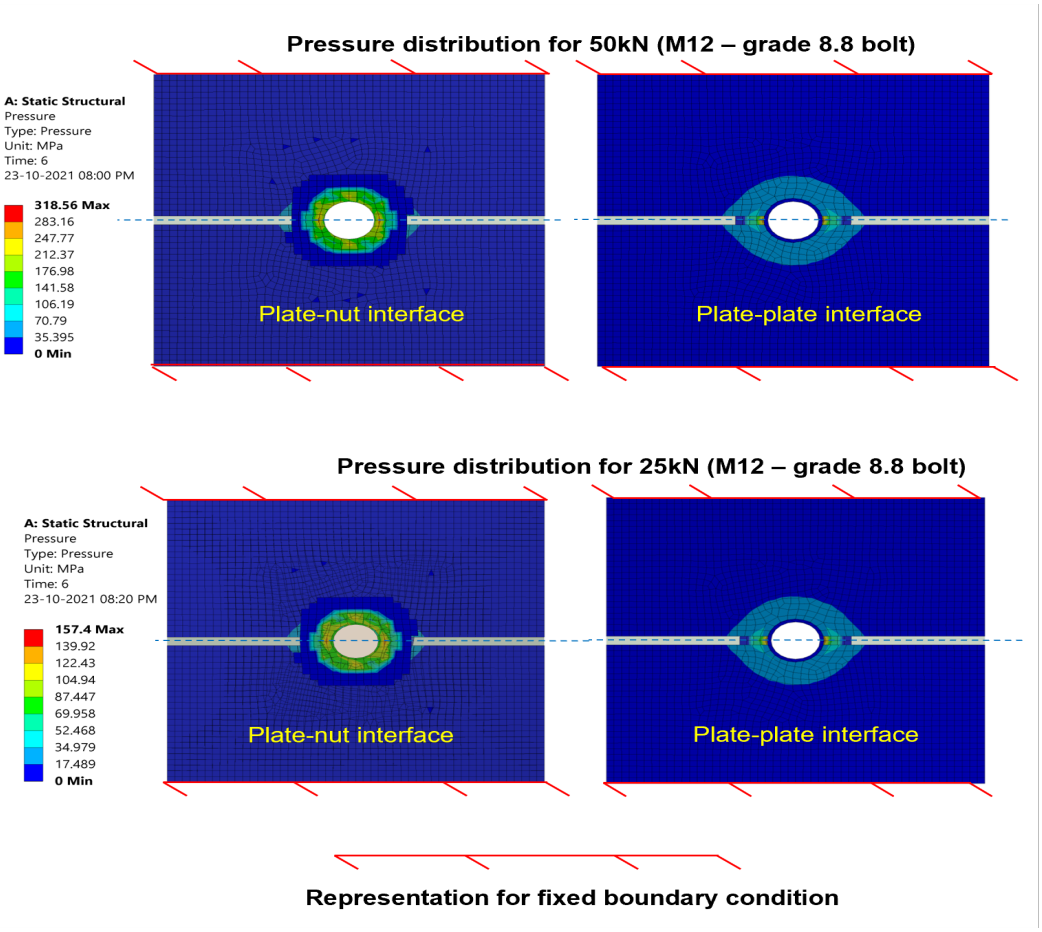

Figure A-2: *Pressure distribution on plate for preload of 50kN and 25kN. The extend of pressure distribution is found to be a local effect with increase in magnitude for increasing preload.*

Bibliography

[1] J. Bickford, *"Handbook of bolts and bolted joints"*. CRC press, 1998.

[2] J. H. Bickford, *Introduction to the design and behavior of bolted joints: non-gasketed joints*. CRC press, 2007.

[3] R. G. Budynas and J. K. Nisbett, *"Shigley's mechanical engineering design"*. Mc Graw Hill, 2015.

[4] K. P. Fischer, "A review of offshore experiences with bolts and fasteners," in *Corrosion*, OnePetro, 2003.

[5] O. Standard, "Design of offshore steel structures," tech. rep., DNV-OS-C101, 2019.

[6] P. Schaumann and R. Eichstädt, "Fatigue assessment of high-strength bolts with very large diameters in substructures for offshore wind turbines," in *The Twenty-fifth International Ocean and Polar Engineering Conference*, OnePetro, 2015.

[7] "Data sheet glas dowr." https://www.bluewater.com/wp-content/uploads/2013/03/Glas-Dowr_rev.pdf. (Accessed on 07/24/2021).

[8] S. Lochan, A. Mehmanparast, and J. Wintle, "A review of fatigue performance of bolted connections in offshore wind turbines," *Procedia Structural Integrity*, vol. 17, pp. 276–283, 2019.

[9] J. Bäckstrand and A. Hurtig, "Accident with a wind turbine in Lemnhult," *Swedish Accident Investigation Authority*, 2017. https://www.havkom.se/en/investigations/vaegtrafik-oevrigt/olycka-med-vindkraftverk-i-lemnhult.

[10] Y. Ma, P. Martinez-Vazquez, and C. Baniotopoulos, "Wind turbine tower collapse cases: a historical overview," *Proceedings of the Institution of Civil Engineers-Structures and Buildings*, vol. 172, no. 8, pp. 547–555, 2019.

[11] B. B. Ajaei and S. Soyoz, "Effects of preload deficiency on fatigue demands of wind turbine tower bolts," *Journal of Constructional Steel Research*, vol. 166, p. 105933, 2020.

[12] R. A. I. Branch, "Progress report: Derailment at grayrigg," *Cumbria, Department of Transport*, 2007.

[13] V. Kaminskaya and A. Lipov, "Self-loosening of bolted joints in machine tools during service," *Soviet Engineering Research*, vol. 10, no. 8, pp. 81–85, 1990.

[14] Y. Shoji and T. Sawa, "Analytical research on mechanism of bolt loosening due to lateral loads," in *ASME Pressure Vessels and Piping Conference*, vol. 41871, pp. 59–65, 2005.

[15] R. Yan, X. Chen, and S. C. Mukhopadhyay, *"Structural health monitoring"*. Springer, 2017.

[16] H. Sohn, C. R. Farrar, F. M. Hemez, and J. J. Czarnecki, "A review of structural health review of structural health monitoring literature 1996-2001.," 2002.

[17] A. Lee, G. Wang, S. Ternowchek, and S. F. Botten, "Structural health monitoring on ships using acoustic emission testing," in *Proceedings of the Ship Structure Committee Symposium: Vessel Safety & Longevity through Ship Structure Research, Linthic, MD, USA*, pp. 18–20, 2014.

[18] L. Pahlavan, "Wave propagation in thin-walled composite structures: Application to structural health monitoring," 2012.

[19] C. Kralovec and M. Schagerl, "Review of structural health monitoring methods regarding a multi-sensor approach for damage assessment of metal and composite structures," *Sensors*, vol. 20, no. 3, p. 826, 2020.

[20] A. Rytter, "Vibrational based inspection of civil engineering structures," 1993.

[21] S. M. Parvasi, S. C. M. Ho, Q. Kong, R. Mousavi, and G. Song, "Real time bolt preload monitoring using piezoceramic transducers and time reversal technique—a numerical study with experimental verification," *Smart Materials and Structures*, vol. 25, no. 8, p. 085015, 2016.

[22] J. H. Bickford, *Introduction to the design and behavior of bolted joints: non-gasketed joints*. CRC press, 2007.

[23] N. Motosh, "Development of design charts for bolts preloaded up to the plastic range," 1976.

[24] S. M. Y. Nikravesh and M. Goudarzi, "A review paper on looseness detection methods in bolted structures," *Latin American Journal of Solids and Structures*, vol. 14, pp. 2153–2176, 2017.

[25] S. W. Doebling, C. R. Farrar, M. B. Prime, *et al.*, "A summary review of vibration-based damage identification methods," *Shock and vibration digest*, vol. 30, no. 2, pp. 91–105, 1998.

[26] W. Xu, "Effect of bolted joint preload on structural damping," 2013.

[27] M. Todd, J. Nichols, C. Nichols, and L. Virgin, "An assessment of modal property effectiveness in detecting bolted joint degradation: theory and experiment," *Journal of sound and vibration*, vol. 275, no. 3-5, pp. 1113–1126, 2004.

[28] V. Caccese, R. Mewer, and S. S. Vel, "Detection of bolt load loss in hybrid composite/metal bolted connections," *Engineering structures*, vol. 26, no. 7, pp. 895–906, 2004.

[29] C. Butner, D. Adams, and J. R. Foley, "Simplified nonlinear modeling approach for a bolted interface test fixture," in *Topics in Nonlinear Dynamics, Volume 3*, pp. 71–82, Springer, 2012.

[30] C. Butner, D. Adams, and J. Foley, "Understanding the effect of preload on the measurement of forces transmitted across a bolted interface," in *Modal Analysis Topics, Volume 3*, pp. 567–578, Springer, 2011.

[31] W. Xu, "Effect of bolted joint preload on structural damping," 2013.

[32] S. M. Sah, J. J. Thomsen, M. Brøns, A. Fidlin, and D. Tcherniak, "Estimating bolt tightness using transverse natural frequencies," *Journal of Sound and Vibration*, vol. 431, pp. 137–149, 2018.

[33] F. Du, C. Xu, H. Ren, and C. Yan, "Structural health monitoring of bolted joints using guided waves: a review," *Struct. Health Monit. Sens. Process*, vol. 8, pp. 163–180, 2018.

[34] G. Park and D. J. Inman, "Structural health monitoring using piezoelectric impedance measurements," *Philosophical Transactions of the Royal Society A: Mathematical, Physical and Engineering Sciences*, vol. 365, no. 1851, pp. 373–392, 2007.

[35] C. Liang, F. P. Sun, and C. A. Rogers, "Coupled electro-mechanical analysis of adaptive material systems-determination of the actuator power consumption and system energy transfer," *Journal of intelligent material systems and structures*, vol. 8, no. 4, pp. 335–343, 1997.

[36] S. Ritdumrongkul, M. Abe, Y. Fujino, and T. Miyashita, "Quantitative health monitoring of bolted joints using a piezoceramic actuator–sensor," *Smart materials and structures*, vol. 13, no. 1, p. 20, 2003.

[37] S. Ritdumrongkul and Y. Fujino, "Identification of the location and level of damage in multiple-bolted-joint structures by pzt actuator-sensors," *Journal of Structural Engineering*, vol. 132, no. 2, pp. 304–311, 2006.

[38] J. Shao, T. Wang, H. Yin, D. Yang, and Y. Li, "Bolt looseness detection based on piezoelectric impedance frequency shift," *Applied Sciences*, vol. 6, no. 10, p. 298, 2016.

[39] L. Huo, D. Chen, Y. Liang, H. Li, X. Feng, and G. Song, "Impedance based bolt preload monitoring using piezoceramic smart washer," *Smart Materials and Structures*, vol. 26, no. 5, p. 057004, 2017.

[40] J. R. Wait, G. Park, and C. R. Farrar, "Integrated structural health assessment using piezoelectric active sensors," *Shock and Vibration*, vol. 12, no. 6, pp. 389–405, 2005.

[41] Y.-K. An and H. Sohn, "Integrated impedance and guided wave based damage detection," *Mechanical Systems and signal processing*, vol. 28, pp. 50–62, 2012.

[42] R. Miao, R. Shen, S. Zhang, and S. Xue, "A review of bolt tightening force measurement and loosening detection," *Sensors*, vol. 20, no. 11, p. 3165, 2020.

[43] S. Tang, "Wave propagation in initially-stressed elastic solids," *Acta Mechanica*, vol. 4, no. 1, pp. 92–106, 1967.

[44] K.-Y. Jhang, H.-H. Quan, J. Ha, and N.-Y. Kim, "Estimation of clamping force in high-tension bolts through ultrasonic velocity measurement," *Ultrasonics*, vol. 44, pp. e1339–e1342, 2006.

[45] G. C. Johnson, A. C. Holt, and B. Cunningham, "An ultrasonic method for determining axial stress in bolts," *Journal of Testing and Evaluation*, vol. 14, no. 5, pp. 253–259, 1986.

[46] J. R. Meisterling, "Joint integrity monitoring using permanent ultrasonic bolt load transducers," in *Power Conference*, vol. 49354, pp. 319–324, 2010.

[47] T. Wang, G. Song, S. Liu, Y. Li, and H. Xiao, "Review of bolted connection monitoring," *International Journal of Distributed Sensor Networks*, vol. 9, no. 12, p. 871213, 2013.

[48] G. C. Johnson, A. C. Holt, and B. Cunningham, "An ultrasonic method for determining axial stress in bolts," *Journal of Testing and Evaluation*, vol. 14, no. 5, pp. 253–259, 1986.

[49] H. Yasui and K. Kawashima, "Acoustoelastic measurement of bolt axial load with velocity ratio method," in *Proceedings of the 15th World Conference on Non-Destructive Testing, Rome, Italy*, pp. 15–21, 2000.

[50] N. Kim and M. Hong, "Measurement of axial stress using mode-converted ultrasound," *Ndt & E International*, vol. 42, no. 3, pp. 164–169, 2009.

[51] Q. Pan, R. Pan, C. Shao, M. Chang, and X. Xu, "Research review of principles and methods for ultrasonic measurement of axial stress in bolts," *Chinese Journal of Mechanical Engineering*, vol. 33, no. 1, pp. 1–16, 2020.

[52] B. Drinkwater, R. Dwyer-Joyce, and P. Cawley, "A study of the interaction between ultrasound and a partially contacting solid—solid interface," *Proceedings of the Royal Society of London. Series A: Mathematical, Physical and Engineering Sciences*, vol. 452, no. 1955, pp. 2613–2628, 1996.

[53] F. Amerini and M. Meo, "Structural health monitoring of bolted joints using linear and nonlinear acoustic/ultrasound methods," *Structural health monitoring*, vol. 10, no. 6, pp. 659–672, 2011.

[54] S. Biwa, S. Nakajima, and N. Ohno, "On the acoustic nonlinearity of solid-solid contact with pressure-dependent interface stiffness," *J. Appl. Mech.*, vol. 71, no. 4, pp. 508–515, 2004.

[55] F. Amerini, E. Barbieri, M. Meo, and U. Polimeno, "Detecting loosening/tightening of clamped structures using nonlinear vibration techniques," *Smart materials and structures*, vol. 19, no. 8, p. 085013, 2010.

[56] J. Yang, F.-K. Chang, and M. M. Derriso, "Design of a built-in health monitoring system for bolted thermal protection panels," in *Nondestructive Evaluation and Health Monitoring of Aerospace Materials and Composites II*, vol. 5046, pp. 59–70, International Society for Optics and Photonics, 2003.

[57] J. Yang and F.-K. Chang, "Detection of bolt loosening in c–c composite thermal protection panels: I. diagnostic principle," *Smart Materials and Structures*, vol. 15, no. 2, p. 581, 2006.

[58] D. Doyle, A. Zagrai, B. Arritt, and H. Çakan, "Damage detection in bolted space structures," *Journal of Intelligent Material Systems and Structures*, vol. 21, no. 3, pp. 251–264, 2010.

[59] T. Wang, G. Song, Z. Wang, and Y. Li, "Proof-of-concept study of monitoring bolt connection status using a piezoelectric based active sensing method," *Smart Materials and Structures*, vol. 22, no. 8, p. 087001, 2013.

[60] R. Kędra and M. Rucka, "Research on assessment of bolted joint state using elastic wave propagation," in *Journal of Physics: Conference Series*, vol. 628, p. 012025, IOP Publishing, 2015.

[61] H. Yin, T. Wang, D. Yang, S. Liu, J. Shao, and Y. Li, "A smart washer for bolt looseness monitoring based on piezoelectric active sensing method," *Applied Sciences*, vol. 6, no. 11, p. 320, 2016.

[62] M. Fink, "Time reversal of ultrasonic fields. i. basic principles," *IEEE transactions on ultrasonics, ferroelectrics, and frequency control*, vol. 39, no. 5, pp. 555–566, 1992.

[63] W. Tao, L. Shaopeng, S. Junhua, and L. Yourong, "Health monitoring of bolted joints using the time reversal method and piezoelectric transducers," *Smart Materials and Structures*, vol. 25, no. 2, p. 025010, 2016.

[64] F. Du, C. Xu, and J. Zhang, "A bolt preload monitoring method based on the refocusing capability of virtual time reversal," *Structural Control and Health Monitoring*, vol. 26, no. 8, p. e2370, 2019.

[65] I. Y. Solodov, "Ultrasonics of non-linear contacts: propagation, reflection and nde-applications," *Ultrasonics*, vol. 36, no. 1-5, pp. 383–390, 1998.

[66] J. Chen, D. Zhang, Y. Mao, and J. Cheng, "Contact acoustic nonlinearity in a bonded solid–solid interface," *Ultrasonics*, vol. 44, pp. e1355–e1358, 2006.

[67] Y. Yang, C.-T. Ng, and A. Kotousov, "Bolted joint integrity monitoring with second harmonic generated by guided waves," *Structural Health Monitoring*, vol. 18, no. 1, pp. 193–204, 2019.

[68] Z. Zhang, H. Xu, Y. Liao, Z. Su, and Y. Xiao, "Vibro-acoustic modulation (vam)-inspired structural integrity monitoring and its applications to bolted composite joints," *Composite Structures*, vol. 176, pp. 505–515, 2017.

[69] J. J. Meyer and D. E. Adams, "Theoretical and experimental evidence for using impact modulation to assess bolted joints," *Nonlinear Dynamics*, vol. 81, no. 1, pp. 103–117, 2015.

[70] E. H. Clayton, M. B. Kennel, T. R. Fasel, M. D. Todd, M. C. Stabb, and B. J. Arritt, "Active ultrasonic joint integrity adjudication for real-time structural health monitoring," in *Health Monitoring of Structural and Biological Systems 2008*, vol. 6935, p. 69350M, International Society for Optics and Photonics, 2008.

[71] D. Doyle, W. Reynolds, B. Arritt, and B. Taft, "Computational setup of structural health monitoring for real-time thermal verification," in *Smart Materials, Adaptive Structures and Intelligent Systems*, vol. 54723, pp. 447–453, 2011.

[72] J. Bao, Y. Shen, and V. Giurgiutiu, "Linear and nonlinear finite element simulation of wave propagation through bolted lap joint," 54th AIAA/ASME/ASCE/AHS/ASC Structures, Structural Dynamics, and Materials ..., 2013.

[73] S. Marburg, "Discretization requirements: How many elements per wavelength are necessary?," in *Computational Acoustics of Noise Propagation in Fluids-Finite and Boundary Element Methods*, pp. 309–332, Springer, 2008.

[74] S. Gopalakrishnan, A. Chakraborty, and D. R. Mahapatra, *Spectral finite element method: wave propagation, diagnostics and control in anisotropic and inhomogeneous structures*. Springer Science & Business Media, 2007.

[75] M. Khan, "Non-destructive testing applications in commercial aircraft maintenance," *Journal of Nondestructive Testing*, 1999.

[76] A. Uludag, "The magnetic particle inspection examination of aircraft propeller mounting bolts," *Journal of Multidisciplinary Engineering Science and Technology*, vol. 3, pp. 1–5, 2016.

[77] M. Willcox and G. Downes, "A brief description of ndt techniques," *Toronto: NDT Equipment Limited*, 2003.

[78] D. M. Suh and W. W. Kim, "A new ultrasonic technique for detection and sizing of small cracks in studs and bolts," *Journal of nondestructive evaluation*, vol. 14, no. 4, pp. 201–206, 1995.

[79] M. Moles and R. Ginzel, "Phased arrays for detecting cracking in bolts," in *6th International Conference on NDE for Structural Integrity for Nuclear and Pressurized Components, Budapest, Hungary*, pp. 8–10, 2007.

[80] F. Mevissen and M. Meo, "A nonlinear ultrasonic modulation method for crack detection in turbine blades," *Aerospace*, vol. 7, no. 6, p. 72, 2020.

[81] D. Granata, P. Kulowitch, W. Scott, and J. Talia, "Acoustic emission waveform acquisition during fatigue crack growth," in *Review of Progress in Quantitative Nondestructive Evaluation*, pp. 2183–2190, Springer, 1993.

[82] D. Yoon, J. Jung, K. Kim, P. Park, and S. Lee, "Ae parameter analysis for fatigue crack monitoring," in *the 15th World Conference on Nondestructive Tesfing*, 2000.

[83] M. Bassim, "Detection of the onset of fatigue crack growth in rail steels using acoustic emission," *International Journal of Fatigue*, vol. 4, no. 17, p. 307, 1995.

[84] N. Pugno, M. Ciavarella, P. Cornetti, and A. Carpinteri, "A generalized paris' law for fatigue crack growth," *Journal of the Mechanics and Physics of Solids*, vol. 54, no. 7, pp. 1333–1349, 2006.

[85] Z. Gong, E. Nyborg, and G. Oommen, "Acoustic emission monitoring of steel railroad bridges," *Materials evaluation*, vol. 50, no. 7, 1992.

[86] J. Yu, P. Ziehl, B. Zárate, and J. Caicedo, "Prediction of fatigue crack growth in steel bridge components using acoustic emission," *Journal of Constructional Steel Research*, vol. 67, no. 8, pp. 1254–1260, 2011.

[87] A. Keshtgar and M. Modarres, "Detecting crack initiation based on acoustic emission," *Chemical engineering*, vol. 33, 2013.

[88] A. Urbahs, K. Carjova, and J. Fescuks, "Analysis of the results of acoustic emission diagnostics of a structure during helicopter fatigue tests," *Aviation*, vol. 21, no. 2, pp. 64–69, 2017.

[89] J. Pascoe, D. Zarouchas, R. Alderliesten, and R. Benedictus, "Using acoustic emission to understand fatigue crack growth within a single load cycle," *Engineering Fracture Mechanics*, vol. 194, pp. 281–300, 2018.

[90] J. Berenbak, "Evaluation tightening preloaded bolt assemblies according to en 1090-2," *CEN/TC135WG2*, 2012.

[91] M. P. Nijgh, *"Loss of preload in pretensioned bolts"*. TU Delft, 2016.

[92] M. D'Antimo, M. Latour, G. F. Cavallaro, J.-P. Jaspart, S. Ramhormozian, and J.-F. Demonceau, "Short-and long-term loss of preloading in slotted bolted connections," *Journal of Constructional Steel Research*, vol. 167, p. 105956, 2020.

[93] N. Fric, M. Veljković, Z. Mišković, and D. Buđevac, "Experimental investigation of preload losses in high strength bolts under cyclic loading," *GRADEVINAR*, vol. 73, no. 5, p. 453, 2021.

[94] G. Meyer and D. Strelow, "How to calculate preload loss due to permanent set in bolted joints," *Assembly Engineering*, 1972.

[95] I. B. D. van Hove and J. J. van Loon, "Preload loss of stainless (steel) bolts in aluminium/steel joints,"

[96] J. Goodier, "Loosening by vibration of threaded fastenings, mech," *Engg.*, vol. 67, p. 798, 1945.

[97] G. H. Junker, "New criteria for self-loosening of fasteners under vibration," *Sae Transactions*, pp. 314–335, 1969.

[98] Y. Jiang, M. Zhang, T.-W. Park, and C.-H. Lee, "An experimental investigation on self-loosening of bolted joints," in *ASME Pressure Vessels and Piping Conference*, vol. 16982, pp. 17–22, 2003.

[99] J. Bannantine, J. Comer, and J. Handrock, *"Fundamentals of metal fatigue analysis"*. 1990.

[100] M. P. Szolwinski and T. N. Farris, "Observation, analysis and prediction of fretting fatigue in 2024-t351 aluminum alloy," *Wear*, vol. 221, no. 1, pp. 24–36, 1998.

[101] J. Schijve, *"Fatigue of structures and materials"*. Springer Science & Business Media, 2001.

[102] R. S. Charlton, "Threaded fasteners: Part 1-failure modes and design criteria of connections," in *Corrosion 2011*, OnePetro, 2011.

[103] S. Hashimura and D. F. Socie, "A study of loosening and fatigue of bolted joints under transverse vibration," *SAE transactions*, pp. 630–640, 2005.

[104] L. Mordfin, *Some Problems of Fatigue of Bolts and Bolted Joints in Aircraft Applications*, vol. 136. US Department of Commerce, National Bureau of Standards, 1962.

[105] W. Fisher, R. Cross, and G. Norris, "Pre-tensioning for preventing fatigue failure in bolts: Simple theory and an account of experiments carried out at the rae," *Aircraft Engineering and Aerospace Technology*, 1952.

[106] V. Giurgiutiu, *"Structural health monitoring: with piezoelectric wafer active sensors"*. Elsevier, 2007.

[107] J. T. Stephen, *Condition monitoring of bolted joints*. PhD thesis, University of Sheffield, 2015.

[108] J. Krautkrämer and H. Krautkrämer, *Ultrasonic testing of materials*. Springer Science & Business Media, 2013.

[109] F. Zhang, "Evaluation of acoustic emission monitoring of existing concrete structures," 2017.

[110] D. Angelis, C. Grosse, O. Masayasu, and T. Shiotani, "Acoustic emission testing: Basics for research-appllication in civil engineering," 2018.

[111] M. G. Sause, "Investigation of pencil-lead breaks as acoustic emission sources," 2011.

[112] N. Hsu and B. FR, "Characterization and calibration of acoustic emission sensors," 1981.

[113] D. Komatitsch and J. Tromp, "Introduction to the spectral element method for three-dimensional seismic wave propagation," *Geophysical journal international*, vol. 139, no. 3, pp. 806–822, 1999.

[114] K. Kendall and D. Tabor, "An utrasonic study of the area of contact between stationary and sliding surfaces," *Proceedings of the Royal Society of London. A. Mathematical and Physical Sciences*, vol. 323, no. 1554, pp. 321–340, 1971.

[115] R. Dwyer-Joyce, B. Drinkwater, and A. Quinn, "The use of ultrasound in the investigation of rough surface interfaces," *J. Trib.*, vol. 123, no. 1, pp. 8–16, 2001.

[116] M. Marshall, R. Lewis, and R. Dwyer-Joyce, "Characterisation of contact pressure distribution in bolted joints," *Strain*, vol. 42, no. 1, pp. 31–43, 2006.

[117] J. Stephen, M. Marshall, and R. Lewis, "An investigation into contact pressure distribution in bolted joints," *Proceedings of the Institution of Mechanical Engineers, Part C: Journal of Mechanical Engineering Science*, vol. 228, no. 18, pp. 3405–3418, 2014.

Glossary

List of Acronyms

SHM	Structural Health Monitoring
NDT	Non-Destructive Technique
DTI	Direct tension indicator
TOF	Time Of Flight
CAN	Contact Acoustic Non-linearity
FEM	Finite Element Method
SEM	Spectral Finite Element Method
AE	Acoustic Emission
DAQ	Data Acquisition System
PLB	Pencil-Lead Breaks
STFT	Short Term Fourier Transform